REPUBLIQUE ALGERIENNE DEMOCRATIQUE ET POPULAIRE
MINISTERE DE L'ENSEIGNEMENT SUPERIEUR ET DE LA RECHERCHE SCIENTIFIQUE



UNIVERSITE YAHIA FARES DE MEDEA
FACULTE DE TECHNOLOGIE
DEPARTEMENT DE GENIE ELECTRIQUE

THESE

Présentée pour l'obtention du diplôme Doctorat LMD

Spécialité : Automatique des systèmes

Par
SABRI NASSIM

CONTRIBUTION AU DÉVELOPPEMENT DE PROCÉDURES MONITORING TEMPS RÉELS DE DIAGNOSTIC ET DE DÉTECTION DES PANNES DANS LES SYSTÈMES PHOTOVOLTAÏQUES

Soutenue le …/…/…

Devant le jury :

Chiba Younes	MCA, Université de Médéa	Président
Kouzou Abdellah	Professeur, Université de Djelfa	Examinateur
Laroussi Kouider	MCA, Université de Djelfa	Examinateur
Tlemçani Abdelhalim	Professeur, Université de Médéa	Directeur de thèse
Chouder Aissa	Professeur, Université de M'sila	Co-Directeur de thèse

Acknowledgement

First of all, I would like to express my deepest appreciation to my supervisors, Prof. Abdelhalim Tlemçani, and Prof. Aissa Chouder, who gave me this great research opportunity. I am extremely grateful to my supervisor Prof. Abdelhalim Tlemçani for his invaluable advice, continuous support, and patience during my PhD study. His plentiful experience, confidence, and trust in my work have encouraged me in all the time of my academic research and daily life.

I would like also to show gratitude to Prof. Aissa Chouder for his knowledge, assistance, and help during my PhD study.

I would like to thank my examiners, Dr. Younes Chiba, Prof. Abdellah Kouzou, and Dr. Kouider Laroussi, for their valuable suggestions and insightful comments.

I am heartily thankful to Mr. Walid Merrouche from Centre de Développement des Energie Renouvelables, who offered me great support, and help about the battery of the solar photovoltaic.

I would like to thank all my friends and all colleagues that I met during my graduate studies.

Finally, I am infinitely grateful to my parents, who always believing in me and encouraging me. Their constant love, support, and sacrifices are the reason behind this work.

ملخص

تتسبب الأعطاب في الأنظمة الكهروضوئية المستقلة في فقدان كبير للطاقة و تضع النظام في مواقف حرجة و خطرة. لجلب مزيد من ميزات السلامة ورفع كفاءة النظام وموثوقيته وعمر المكونات، تهدف هذه الأطروحة إلى اقتراح طرق جديدة للكشف عن الأعطاب وتصنيفها في الأنظمة الكهروضوئية المستقلة والبطارية. ستعمل هذه الطرق على إزالة

القيود الموجودة في تحليل الأعطال و القصور الموجود في أجهزة الحماية الكهربائية مثل الصمامات. سلطت هذه الأطروحة الضوء على نوعين من الأعطاب الوحيدة في الأنظمة الكهروضوئية المستقلة، الأعطاب التي تحدث في الوحدات الكهروضوئية و الأعطاب التي تتطورما بين خلايا البطارية والتي لم تتم دراستها في المراجع. يشجع حجم البيانات المتوفرة من النظام وكذلك الإهتمام المتزايد بتقنيات التعلم الآلي على تطبيق هذه الطرق في الكشف عن الأعطاب في النظام الكهروضوئي المستقل. حيث تم إعتماد العديد من التقنيات للكشف عن الأعطاب وتصنيفها مثل الشبكة العصبية الاصطناعية، وكشف الشذوذ، وآلية الفواصل الواسعة. و قد تم التحقق من صحة أدائها بإستخدام البيانات من المحاكاة و التجربة. لهذا الغرض، تم تطويربرنامج محاكاة ملائم لدراسة الأعطاب في نظام الكهروضوئي المستقل، كما تم إعداد نضام معياري لتجربة الأعطاب في ظروف العمل الحقيقية. أظهرت نتائج الاختبار جدوى طرق التعلم الآلي المقترحة للكشف عن الأعطاب وتصنيفها في النظام الكهروضوئي المستقل و التي يمكن توجيهها نحو التطبيق العملي.

الكلمات الرئيسية : الأنظمة الكهروضوئية المستقلة ؛ البطارية ؛ الكشف عن الأعطاب ؛ البيانات ؛ التعلم الآلي.

Resumé

Les défauts dans les systèmes photovoltaïques autonomes provoquent une perte de puissance significative et mettent le système dans des situations critiques et dangereuses. Afin d'apporter plus de sécurité et d'augmenter l'efficacité, la fiabilité et la durée de vie des composants du système, cette thèse vise à proposer de nouvelles méthodes de détection et de classification des défauts dans les systèmes photovoltaïques autonomes et les batteries. Ces méthodes permettraient de surmonter

les limites des analyses de défauts existantes ainsi que les lacunes des dispositifs de protection électrique tels que les fusibles. Deux types de défauts uniques sont traités dans cette thèse, celui qui se produit dans les modules PV et celui qui évolue dans les cellules de la batterie, qui n'ont pas été étudiés dans la littérature. La quantité de données disponibles du système ainsi que l'intérêt croissant pour les techniques d'apprentissage automatique encouragent l'application de ces méthodes comme détection de défauts dans les systèmes photovoltaïques autonomes. Plusieurs techniques sont adoptées pour la détection et la classification des défauts, telles que le réseau neuronal artificiel, la détection d'anomalies et la machine à vecteurs de support. Leurs performances ont été validées en utilisant des données provenant de plateformes de simulation et expérimentales. À cette fin, une simulation adéquate a été développée pour la recherche de défauts dans un système photovoltaïque autonome, et un système de référence a été mis en place pour expérimenter les défauts dans des conditions de travail réelles. Les résultats des tests démontrent la faisabilité des méthodes d'apprentissage automatique proposées pour détecter et classer les défauts dans les systèmes photovoltaïques autonomes qui pourraient être orientés vers une application pratique.

Mots clés : systèmes photovoltaïques autonomes ; batterie ; détection des défauts ; données ; apprentissage automatique.

Abstract

Faults in the stand-alone photovoltaic systems cause a significant power loss and put the system in critical and hazardous situations. To bring more safety features and increase the system efficiency, reliability, and lifetime of the components, this thesis aims to propose new fault detection and classification methods in the stand-alone photovoltaic systems as well as battery. These methods

would overcome the limitations of existing fault analysis as well as the shortcoming of electrical protection devices such as a fuse. Two types of unique faults are treated in this thesis, the one that occurs in PV modules and those that evolve in battery cells, which have not been studied in the literature. The amount of data available from the system as well as the growing interest in machine learning techniques encourages the application of these methods as fault detection in stand-alone photovoltaic systems. Several techniques are adopted for fault detection and classification such as Artificial Neural Network, Anomaly detection, and Support Vector Machine. Their performance has been validated using data from both simulation and experimental platforms. For this purpose, an adequate simulation has been developed for fault investigation in a stand-alone photovoltaic system, and a benchmark system has been set up to experiment the faults in real working conditions. The test results demonstrate the feasibility of the proposed machine learning methods to detect and classify the faults in stand-alone photovoltaic systems which could be directed toward practical application.

Keywords: stand-alone photovoltaic system; battery; fault detection; data; machine learning.

Table des matières

Acknowledgement.....ii

ملخص ii
Resumé iii
Abstract iv
Table des matières v
List of figures ix
List of tables xi
List of Acronyms xi
General Introduction 1
Chapter: 1 Litterature review 5
1.1 Introduction 5
1.2 Typical fault in SAPV system 5
1.3 Faults on PV side 7
1.4 Faults on Battery side 7
1.5 Visual inspection of PV modules 8
1.5.1 Yellowing and browning 8
1.5.2 Delaminations 9
1.5.3 Bubbles 10
1.5.4 Cracks in cells 11
1.5.5 Defect in anti-reflective coating (ARC) 12
1.5.6 Hot spot 12
1.6 Performance evaluation of SAPV system based on power loss parameters 13
1.6.1 Reference yield 14
1.6.2 Array yield 14
1.6.3 Final yield 14
1.6.4 Capture losses 14
1.6.5 System losses 15
1.6.6 Performance ratio 15
1.6.7 Limitations of power loss fault analysis 15
1.7 A literature fault detection and diagnosis 16
1.7.1 Pv system case 16
1.7.2 Battery case 19
1.8 Manual troubleshooting of SAPV system 22
1.9 Conclusion 23
Chapter: 2 Stand-Alone Photovoltaic System: Generalities, Modelling and Simulation 26

2.1 Introduction 26
2.2 Stand-Alone photovoltaic system 26
2.3 Basic Elements for Stand-Alone photovoltaic system 27
2.3.1 PV system 27
2.3.2 Static characteristic of PV module 29
2.3.3 The Battery 30
2.3.4 Battery type 31
2.3.5 Charge and discharge Curve 33
2.4 The charge regulator 34
2.4.1 Series regulation 34
2.4.2 Shunt regulation 35
2.4.3 PWM regulation 35
2.5 Modeling of Stand-alone photovoltaic system 36
2.5.1 Model for PV cells 36
2.5.2 Lead-acid battery modeling 38
2.5.3 Load representation 39
2.6 Simulation in Matlab/Simulink 39
2.6.1 SAPV benchmark system 40
2.6.2 SAPV system validation model 42
2.7 Conclusion 44
Chapter: 3 Battery Internal Fault Monitoring 45
3.1 Introduction 45
3.2 Lead-acid battery constitution 46
3.3 Causes of internal short-circuit 46
3.3.1 Corrosion 46
3.3.2 Mossing 47
3.3.3 Lead drop 47
3.3.4 Mechanical failure 47
3.4 Key Factors 47
3.5 Limitations of the electrical protection device 48
3.6 Battery model considerations 49
3.7 Proposed battery fault detection 52
3.7.1 Anomaly detection 52
3.7.2 Proposed battery fault classification 57
3.7.3 SVM algorithm 57

3.8 Conclusion 62
Chapter: 4 Fault diagnosis in stand-alone photovoltaic system using Artificial Neural Network 63
4.1 Introduction 64
4.2 ANN and the brain (motivation) 64
4.3 The basic concept of ANN 65
4.3.1 Single neuron Perceptron 65
4.3.2 Multi layer perceptron 67
4.3.3 Backpropagation Training algorithm 68
4.3.4 Levenberg-Marquardt algorithm 69
4.4 Application of ANN for FDD in SAPV system 70
4.4.1 Data acquisition 71
4.4.2 Data pre-processing 74
4.4.3 ANN Configuration 74
4.4.4 Training, and Test results 77
4.4.5 Matlab GUI Integration with the system 80
4.5 Enhacement of power losses analysis by ANN 82
4.5.1 Background 82
4.5.2 Methodology 83
4.5.3 Structure design 84
4.5.4 Network selection 85
4.5.5 Online MLP test 88
4.6 Conclusion 95
General Conclusion 96
References 98
Lists of Publications and Conference papers 107

List of figures

Figure 1.1 Basic Configuration of SAPV system. 5
Figure 1.2 Common faults in SAPV system....6
Figure 1.3 Effects of internal battery resistance [8]....8
Figure 1.4 browning effect on a PV cell 9
Figure 1.5 Delamination default of a PV module [12]....9
Figure 1.6 Bubbles on the front and the back side of PV module....11
Figure 1.7 Cracks in a PV cell [13] 11
Figure 1.8 discoloring effect due to a change of ARC [12] 12
Figure 1.9 Hot spot damage on PV cell 13
Figure 1.10 Scheme of getting energy parameters....13
Figure 1.11 Diverse daily indices of performance.....15
Figure 1.12 The IV characteristic affected by different classes [21]. 16
Figure 1.13 Overview system of PV fault detection using power comparison [18]. 17
Figure 1.14 Infrared thermal image of short-circuited PV cell [26] 18
Figure 1.15 Battery voltage scenarios [37]. 19
Figure 1.16 State of charge (SOC) with different internal resistance values [38]....20
Figure 1.17 Battery voltage curves comparison of normal and overcharges effect [38]....21
Figure 1.18 Battery state of charge comparison of normal and overcharges effect [38]....22
Figure 1.19 Troubleshooting guidance [39]. 25
Figure 2.1 Typical SAPV system 26
Figure 2.2 Basic structure of PV system....27
Figure 2.3 I-V curve of a PV module....29
Figure 2.4 Irradiance effect on I_V and P_V characteristics....30
Figure 2.5 Temperature effect on I_V and P_V characteristics 30
Figure 2.6 Basic SAPV system element 31
Figure 2.7 Charge curve....33
Figure 2.8 Discharge curve....33
Figure 2.9 Series type charge regulator....34
Figure 2.10 Shunt type charge regulator....35
Figure 2.11 PWM type charge regulator....36
Figure 2.12 Equivalent circuit for one diode model 36
Figure 2.13 Equivalent circuit for battery model 38
Figure 2.14 SimPowerSystem based model of SAPV system....40
Figure 2.15 SAPV system experimental set-up at CDER, Bouzareah, Algeria 41
Figure 2.16 Captured profile of solar irradiance and ambient temperature 42
Figure 2.17 (a),(b) Simulated with measured PV and battery current, (c) battery voltage ..43
Figure 2.18 Simulated versus experiment of load power....44
Figure 3.1 The internal structure of a flooded lead-acid battery [1] 46
Figure 3.2 Corroded plate of lead-acid battery....47
Figure 3.3 Battery protection using : (a) terminal protection fuse, (b) midpiont fuse 49
Figure 3.4 Battery cells configuration for fault analysis 50
Figure 3.5 Simulation of the battery under short-circuit cell condition 51
Figure 3.6 Illustration of Gaussian distribution with data....53

Figure 3.7 Flowchart of the procedure to select the threshold ε....55
Figure 3.8 Captured irradiance and temperature profile 55
Figure 3.9 Test result : N 56
Figure 3.10 Test result : F3....56
Figure 3.11 Test result: F2....56
Figure 3.12 Test result: F2 with (R≈0)....56
Figure 3.13 Test result: F4....56
Figure 3.14 Test result: F5....56
Figure 3.15 Schematic of separating binary class by svm 57
Figure 3.16 Irradiance and Temperature profile 58
Figure 3.17 Flowchart of the proposed fault diagnosis process 59
Figure 3.18 AD Test result : N....60
Figure 3.19 SVM Test result : N....60
Figure 3.20 AD Test result : F1 61
Figure 3.21 SVM Test result : F1 61
Figure 3.22 AD Test result : F3 61
Figure 3.23 SVM Test result : F3 61
Figure 3.24 AD Test result: F6 62
Figure 3.25 SVM Test result: F6 62
Figure 4.1 Schematic of a biological neuron....65
Figure 4.2 Neuron perceptron model 66
Figure 4.3 Decision boundary for two input....67
Figure 4.4 Three layer Network....67
Figure 4.5 Steps to develop ANN prediction model....71
Figure 4.6 Small SAPV System....71
Figure 4.7 Faults Created in SAPV system 72
Figure 4.8 Data aquisition facilities from SAPV system 73
Figure 4.9 Experiment facilities at LREA, Médéa University (Algeria)....74
Figure 4.10 ANN structure for fault detection 75
Figure 4.11 ANN structure for fault diagnosis....76
Figure 4.12 Learning curve of ANN fault detection....78
Figure 4.13 Learning curve of ANN fault diagnosis 78
Figure 4.14 Confusion matrix of test ANN detection model....79
Figure 4.16 General accuracy of ANN detection model....79
Figure 4.15 Confusion matrix of test ANN diagnosis model 79
Figure 4.17 General accuracy of ANN diagnosis model 80
Figure 4.18 Computer implementation of GUI matlab 81
Figure 4.19 Flowchart for fault detection and diagnosis by ANN 82
Figure 4.20 Block diagram of construction improved faults daignosis....83
Figure 4.21 ANN structure for : (a) MLP network, (b) PNN network , (c) RBFN network85
Figure 4.22 Observed, Predicted quality indices for MLP network 87
Figure 4.23 Observed, Predicted quality indices for PNN....88
Figure 4.24 Observed, Predicted quality indices for RBFN 88
Figure 4.25 Online F1 test (a) Lc variation, (b) ANN output....90
Figure 4.26 Online F2 test (a) Ls variation, (b) ANN output 92

Figure 4.27 Online F3 test (a) Ls variation, (b) ANN output 94

List of tables

Tableau 2-1 Solar cell technologies comparison [7]–[11].....28
Tableau 2-2Main battery technologies comparaison [50], [51]. 31
Tableau 2-3 Electrical parameters of main component SAPV system and acquisition system 41
Tableau 3-1 Electrical characteristics of SAPV system component.....50
Tableau 3-2 Faults notation in battery.....51
Tableau 3-3 Main training parameters for AD and SVM 59
Tableau 3-4 Individual class accuracy with AD and SVM algorithm. 62
Tableau 4-1 Electrical Characteristics of experimental SAPV System 72
Tableau 4-2 Output vector of ANN fault detection 76
Tableau 4-3 Output vector of ANN fault diagnosis.....76
Tableau 4-4 Different faults created in simulation environement.....84
Tableau 4-5 Test accuracy for MLP, PNN and RBFN network.....86

List of Acronyms

AC	Alternative Current
AD	Anomaly detection
ANN	Artificial Neural Network
ARC	Anti Reflective Coating
BNN	Beysian Neural Network
BP	Back Propagation
BPLM	Back Propagation Levenberg-Marquardt
CDER	Centre de Développement des Energies Renouvelable
DC	Direct Current
EVA	Ethylene Vinyl Acetate
FDD	Fault Detection and Diagnosis
GUI	Graphical User Interface
HMM	Hidden Markov Model

I-V	Current-Voltage
IR	Internal Resistance
MLP	Multi Layer Perceptron
MPP	Maximum Power Point
MPPT	Maximum Power Point Tracking
OCPD	Overcurrent Protection Device
OVPD	Overvoltage Protection Device
PDF	Probability Density Function
PNN	Probabilistic Neural Network
PR	Performance Ratio
PV	Photovoltaic
PWM	Pulse Width Modulation
RBFN	Radial Basis Function Network
RCD	Residual Current Detector
SAPV	Stand Alone Photovoltaic
SOC	State of Charge
STC	Standard Test Condition
SVM	Support Vector Machine
TDR	Time Domain Reflectometry
UV	Ultraviolet

General Introduction

Numerous key challenges facing PV systems to become a major source of electricity around the world: lowering the cost, improve the PV system reliability, integration challenges with the grid, and political decisions. Nevertheless, PV systems keep growing in most countries due to a number of advantages such as emission-free energy, low maintenance required and constitutes an alternative energy source in places where grids are not yet developed [1].

PV systems can be classified into three main categories: grid-connected system, stand-alone photovoltaic system, and hybrid system. A grid-connected system is designed to feed the DC energy of PV modules into the grid via the inverter, this category is the most dominated in the PV market [2]. A Stand-alone photovoltaic system works independently from the grid, it is used together with the storage battery element to feed a specified load and bring electricity to people having difficult access to the grid. A hybrid system combines the advantage of both PV systems and additional electrical generator sources such as diesel generators, wind turbines, etc. It is used to supply a large varied load. In this thesis, different operational issues related to the stand-alone photovoltaic system will be considered as well as fundamental approaches addressing them.

Despite the fact that stand-alone photovoltaic systems provide flexible use and require a little maintenance, they are still subject to various faults along with a PV system, battery, wiring, power conditioning units, etc. Faults in stand-alone photovoltaic systems influence the output power performance by a large amount of power lost as well as lead to critical situations and potential safety issues such as fire hazard, DC arcs, electrical shock hazard, and battery explosion. To avoid these damages, this thesis proposes fault detection and classification in stand-alone photovoltaic systems, where it is considered that the PV modules and battery are the only sources of the fault.

Fault detection and isolation have an important role to increase the system's reliability, efficiency, availability, and safety, furthermore, it reduces the maintenance and replacement cost. As the PV system output change according to the environmental condition (irradiance level and temperature), fault in the PV system under low irradiance may not produce a large enough current to blow the fuse sized at 1.56 I_{SC} [3] to protect the PV modules and conductors. In this case, the fault remains undetected and leads to unexpected problems. The other safety concern is situated in the battery, this last represents the higher risk since the battery fault may not be detected by conventional protection devices due to the complexities in selecting the right sizing fuse and the

problem of its location [4]. Moreover, fault detection in Stand-alone photovoltaic systems has not been enough reported in the literature before.

Nowadays, most installed PV systems include a data logger board, thus various data are becoming available from PV modules, battery, charge regulator, weather station, etc. The excessive data enable the evaluation and calculation of power losses over a long period of time. Hence, the new proposed fault detection algorithm will be developed using historical data readily available from a stand-alone photovoltaic system, in which machine learning approach is one of the best ways to identify the fault types. In addition, machine learning methods have been widely used for fault detection and diagnosis for grid-connected PV systems [5].

The proposed machine learning algorithm for fault classification has the potential to provide accurate results, more generalization features, and easy hardware implementation. Furthermore, it only uses readily available measurements such as voltage and current of PV modules, battery, and load without requiring additional sensing circuits. Machine learning algorithms extract information from a data set, where this data contains a number of instances that refer to the measurements. Each instance contains certain variables (features or attributes) that characterize an instance, and have a class label that determines which category belongs (Normal or Faults). In summary, a data set with a class label is called labeled data, and the learning using completely this data is supervised. Otherwise, it is unlabeled data and the learning with only unknown classes is unsupervised.

Artificial Neural Network has been proposed as supervised machine learning fault detection and classification in a stand-alone photovoltaic system. To demonstrate their effectiveness, some typical fault has been considered such as short-circuit of PV module, open circuit PV module and external battery short-circuit. The proposed method has been validated using both data of experimental and simulation, in which the effect of maximum power point tracker on the fault has not been considered. Two small-scale experimental stand-alone photovoltaic benchmark system is studied in this thesis. The first system has been set up in Centre de Développement des Energies Renouvelable (CDER), whereas the second system is developed at the University of Médéa.

Battery internal faults have been addressed in this work as part of fault detection in a stand-alone photovoltaic system. The study of battery fault may be complex due to the difficulty of obtaining the labeled fault data. For this reason, Anomaly detection has been proposed as an unsupervised machine learning algorithm for internal fault detection in the battery. The algorithm uses only Normal data to build up the fault prediction model. Also, this thesis proposes internal fault identification using Support Vector Machine algorithm that requires a few numbers of labeled

fault data. The performance of fault detection and identification has been validated using simulation data.

The thesis is organized as follows:

Chapter 1 presents the results of the literature review. Chapter 2 focuses on the modeling, development, and simulation of a stand-alone photovoltaic system. Chapter 3 discusses the internal short detection and identification in the battery using the learning algorithm: Anomaly detection (AD) and Support Vector Machine (SVM) respectively. Chapter 4 develops the proposed fault diagnosis in the stand-alone photovoltaic system using a supervised Artificial Neural Network (ANN).

Chapter 1 : Literature review

- Overview on previous literature work in fault evaluation for PV system, specifically for stand-alone photovoltaic system.
- Show the advantages and inconveniences of existing fault detection approaches.

Chapter 2: Stand-Alone Photovoltaic System: Generalities, Modelling, and Simulation.

- Development of the simulation platform able to use irradiance level and ambient temperature as input to predict the system output, as well as it is applicable to predict the interconnection of PV modules and battery under fault scenarios.
- The simulation model output is verified with the real measurement of a small-scale benchmark stand-alone photovoltaic system for proof of model validity.

Chapter 3: Battery Internal Fault Monitoring.

- Simulation of battery fault behavior using the basic configuration of series assembled battery cells, in which the battery cell is represented by a battery unit due to the modularity and flexibility of simulated battery block.
- Development of appropriate internal short detection and identification methods in the battery using respectively Anomaly detection and Support Vector Machine algorithm.
- Based on simulation data, test validity is performed to verify the effectiveness of proposed methods to correctly detect and identify the internal fault.

Chapter 4: Fault diagnosis in stand-alone photovoltaic system using Artificial Neural Network.

- The fundamental mathematical approach of fault diagnosis based ANN is given in detail.
- An experiment of typical fault has been carried out in a small-scale benchmark stand-alone photovoltaic system for collecting the labeled fault data.

- The development of fault classification model based on ANN and using real data, the proposed approach is integrated with the benchmark system using Graphical User Interface (GUI) Matlab.
- Enhancement of fault analysis by using ANN and power loss parameters as inputs to better predict the performance of the stand-alone photovoltaic systems.
- In addition, to overcome the limitations of having labeled data for supervised ANN, the simulation environment developed in chapter 2 is used to generate the different faulty data, whereas the steady-state is obtained from the real working condition.

Chapter: 1 Litterature review

1.1 Introduction

One of the biggest problems facing a SAPV system is the detection and isolation of faults occurring during its operation. These faults may have undetectable by electrical protection devices (OCPD and OVPD), and cause a large amount of energy loss that reduces its efficiency and profitability. In addition to affecting the whole system performance, the effects of faults could be devastating as the risk of fire hazards and explosion is increased and therefore the system reliability and security is reduced. This chapter explores the main typical faults in the SAPV system as well as a literature review for different fault detection and diagnosis approaches in a PV system, battery, and whole SAPV systems. The chapter ends with troubleshooting guidance given by Sandia Laboratory for finding problems in the SAPV system.

1.2 Typical fault in SAPV system

The standard configuration of the SAPV system is shown in Figure 1.1, it includes mainly PV modules, battery, load as well as a charge regulator. Plenty of electrical faults can occur in the SAPV system as given in Figure 1.2, where these faults are situated on the PV system side as well as a battery side. These faults are mainly due to corrosion, delamination, and manufacturing defects within a PV module or battery. In this thesis, some faults have been examined such as short-circuit and open-circuit of PV module as well as short-circuit and increasing internal resistance of the battery. Note that, the effect of MPPT has not been considered in this work.

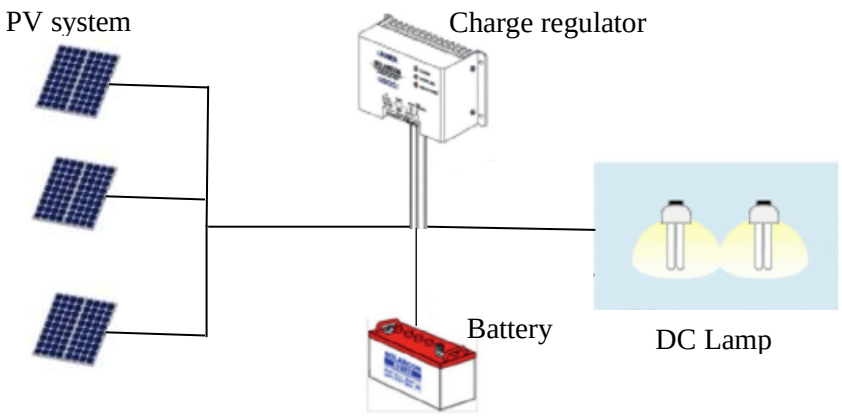


Figure 1.1 Basic Configuration of SAPV system.

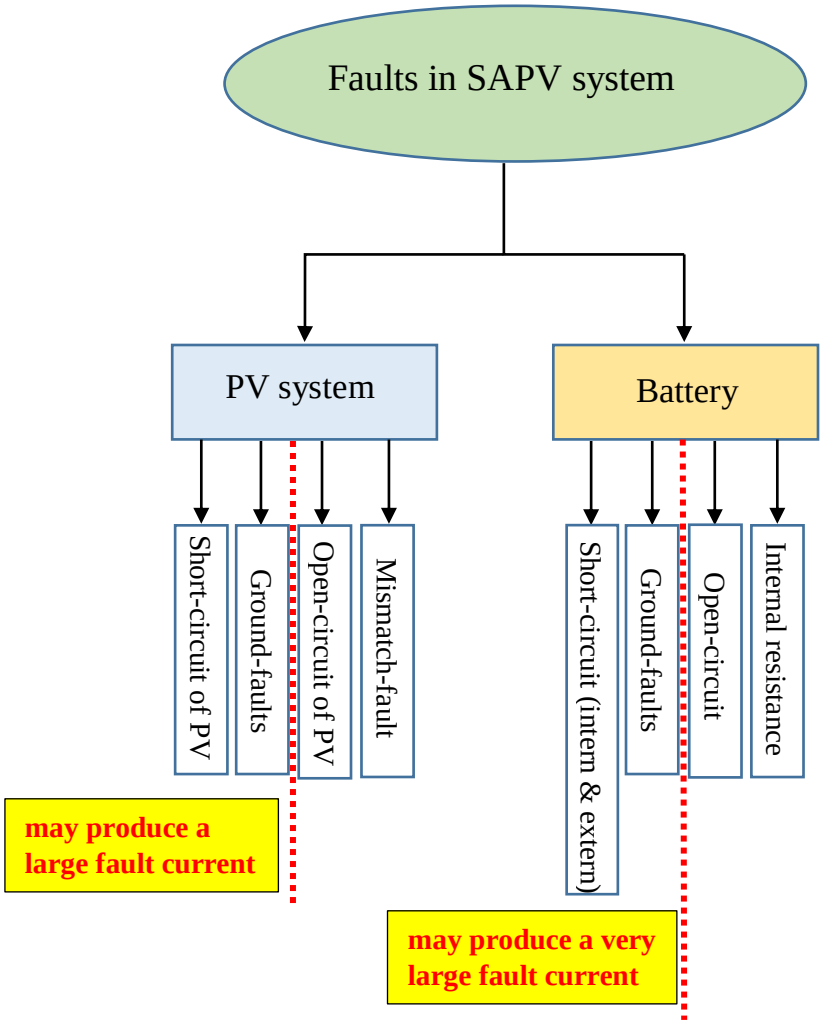


Figure 1.2 Common faults in SAPV system.

1.3 Faults on PV side

Mismatch fault such as partial shading, hot spot, etc is the most frequent fault in a PV system, this fault occurs when the expected PV power of one PV module differs from the rest of PV modules due to the environmental conditions (irradiance and temperature). Mismatch fault causes local heating on the PV module (hot spot) and could lead to irreparable damage as well as a large power loss. Bypass diodes can be placed on each PV module to prevent this fault [5], [6].

Open circuit fault is an accidental disconnection in the PV array through cracking of a PV module, conductor wires in the bus, or junction box. This fault could be caused by periodic thermal stress, hail, and damage during processing and assembly[5], [7].

A ground fault is an accidental electrical short-circuit implying ground and one or more normally designed current-carrying conductors. For a grounded system where conductors are intentionally grounded, only one ground fault causes the fault current. However, for an ungrounded system, a double ground fault causes this fault. The ground fault could happen when a cable in a module junction box contacts a grounded conductor accidentally or unexpected insulation failure of cables. [5]–[8].

A short-circuit fault is a low-resistance connection unintentionally formed between PV modules or array cables with different potential. The main reasons for this fault consisting of incidentally short-circuiting current-carrying conductors as a coincidentally nail driven through unprotected wirings. Another reason is the insulation failure of cables caused by animals chewing. Finally, the fault could happen within the junction box through corrosion and mechanical damage[5], [8].

1.4 Faults on Battery side

Battery ground fault is an accidental ground common in the batteries due to the leakage of electrolyte to supporting structures. Similar to the PV module, if one ground is developed in a grounded battery, this fault is happening [4].

Battery short-circuit fault is a low-resistance connection at the battery terminal (external) or cell terminal (internal). The battery external short circuit is allowed when a fault at a charger or other external circuits, while the internal short circuit happens through the uncontrolled formation of crystalline marring the separator (sulfatation). Other reasons could be the shedding effect of lead, corrosion, and poor manufacturing [4], [9]. The magnitude of short-circuit fault current depends on a number of factors, more details can be found in chapter 3.

The battery's internal resistance is associated with the electrochemical reaction rate since the process of charge and discharge goes to the end as the battery ages or after a long cycle service (sulfatation and grid corrosion). The active sites on the battery plates decrease with time triggering an increase in electronic resistance which impacting the efficiency and lifetime of the battery [4], [10]. As shown in Figure 1.3, the internal resistance act as the gatekeeper of the battery, the lower

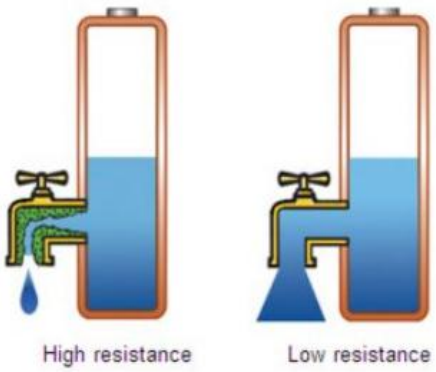


Figure 1.3 Effects of internal battery resistance [8].

the value, the less restriction the pack encounters. The elevated internal resistance causes the voltage to collapse and the battery to heat up, especially with heavy loads and high current pulses [11].

An open-circuit fault of the battery is a disconnection that removes it from the line, open circuit intercell connectors caused by mechanical damage or manufacturing defect lead to this fault. The battery terminals could also corrode which results in an open electrical connection[4], [9].

1.5 Visual inspection of PV modules

Visual inspection is used as the first step of the analysis, it allows to determine some defaults by sight. Yellowing, delaminations, bubbles, cracks in cells, misalignments, and burnt cells are the defects mostly detected using this method[8], [12], [13]. This first step decides whether a PV module requires further tests or not. The visual inspection should be performed under natural sunlight that emits a good quality intense light. Also, Reflections can result in defective images which leads to a false conclusion. To avoid such a problem, the inspection should be performed from different angles to check the layer where the defect could occur.

1.5.1 Yellowing and browning

This defect consists of the degradation of the EVA (ethylene vinyl acetate) or the adhesive material between the cells and the glass. The color of the material changes from white to yellow and in some cases from yellow to brown. It causes a change in the transmittance of the light reaching the solar cells and thus a decrease in the power generated. This change affects the transmittance of the light reaching the solar cells and thus a decrease in the power generated. The main cause of this defect is UV radiation and water exposure combined with temperatures above 50 C° that cause a change in the chemical structure of the polymer. Figure 1.4 shows an example of the browning effect on a cell.

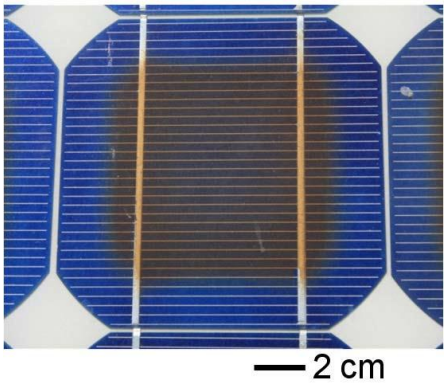


Figure 1.4 browning effect on a PV cell

1.5.2 Delaminations

Delamination consists of the loss of adherence and detachment between different layers of the PV module. This default appears between polymeric encapsulant and cells or between cells and the front glass. Two major effects can result from delamination: a light decoupling where reflection increases as well as water penetration inside the module structure. Delamination can be more critical if it occurs in the borders of the module causing electrical risks to the module and the installation. Figure 1.5 shows an example of delamination default appears on the PV module.



Figure 1.5 Delamination default of a PV module [12]

1.5.3 Bubbles

This default is similar to delamination in which the loss of adherence of the EVA affects only a small area and is combined with the blowing of areas. A bubble usually is due to a chemical reaction where some gasses are released. When it occurs in the back side of the PV module, a bulk appears in the polymeric encapsulant or the back cover, forming a bubble. Bubbles are not very common on the front side of the PV module. But it can also appear between the glass and the cells. In this case, the bubbles are caused by a detachment between the part of the cell and the glass. Bubble causes an overheating of the cell which reduces its life. Also, in the case of bubbles on the front side, the reflection is increased as there is a decoupling of the light which can reduce the light reaching the cell. Figure 1.6 shows an example of a bubble defect on the front and back side of a PV module.

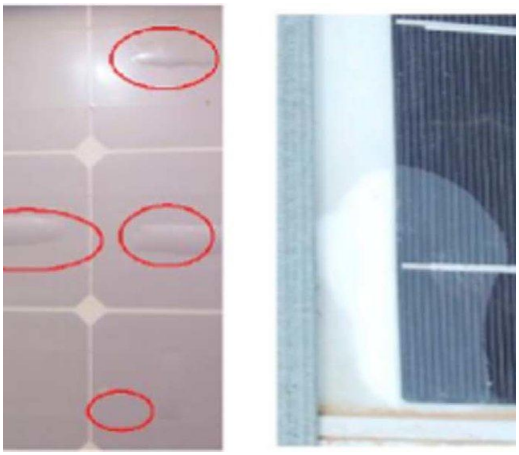


Figure 1.6 Bubbles on the front and the back side of PV module

1.5.4 Cracks in cells

This default consists of small cracks in the cells often not visible by sight that may affect both sides of the cell. The reduction of thickness and the increase in the area, make the cells more fragile and susceptible to fractures during their manipulation, module lamination, and storage. Apart from the risk of power loss, there is also the chance of hot spots being formed. This can happen when a cracked cell has a localized reverse current path in the still active cell part. Figure 1.7 shows a clear example of cell cracks.



Figure 1.7 Cracks in a PV cell [13]

1.5.5 Defect in anti-reflective coating (ARC)

To improve the performance of PV cells, an ARC (anti-reflective coating) is added to maximize the light that reaches the active area of the cell. The materials normally used are silicon dioxide and silicon nitride, and the thickness is chosen such that only a minimal part of the light escapes. A change in the ARC coloring can happen during the life service of the PV module, this color change should not cause a decrease in the wavelength radiation that the cell uses, but rather only affect a part of the visible radiation. This defect is related to the oxidation of the ARC which could cause loss of adherence between the cells and the glass. Figure 1.8 shows a color change of ARC in a PV module.



Figure 1.8 discoloring effect due to a change of ARC [12]

1.5.6 Hot spot

A hot spot is an area of a PV module featured by a very high temperature that could damage a cell or any other element of the module. Several cell failures may cause hot spot such as partial shadowing, cells mismatch, or failures in the interconnection between cells. A shadowed cell could operate in reverse mode in which the cell consumes energy and thus can overheat and hot spot cell, consequently, damage can occur in the cell or module. Bypass diodes are placed in connection boxes, which limits the reverse voltage that can reach a shaded cell. Figure 1.9 shows an example of how a hot spot affects a cell.

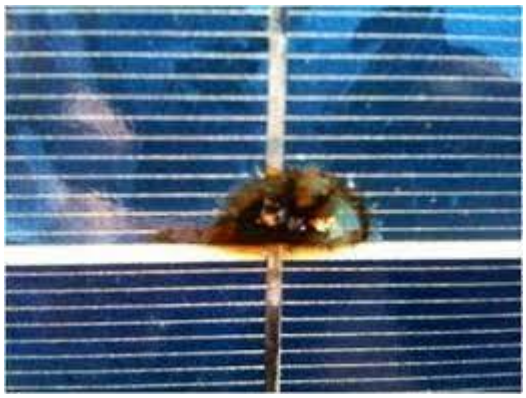


Figure 1.9 Hot spot damage on PV cell

1.6 Performance evaluation of SAPV system based on power loss parameters

Energy balance together with energy efficiency and indices of performance has been proposed in [14]–[16] to evaluate the overall performance of the SAPV system. The analysis method based on the normalized power loss parameters gives a good indication of the SAPV system performance. The main power loss parameters are : Yr, Ya, Yf, Lc, Ls and the system performance indices are: PR, PF, and MF [17]. Figure 1.10 illustrates how to obtain the parameters Yr, Ya, and Yf from a SAPV system.

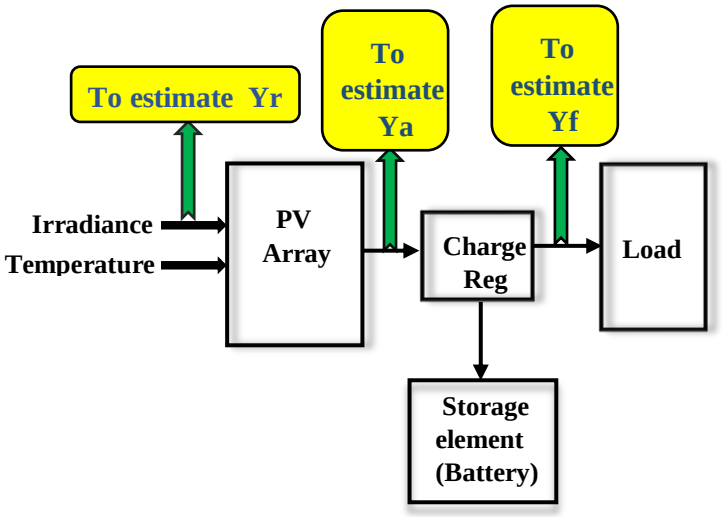


Figure 1.10 Scheme of getting energy parameters.

1.6.1 Reference yield

Yr is the number of hours per day that the sun's intensity has to shine with G0=1000W/m2 to irradiate the energy Ep onto the PV panels.

$$Y_r = \frac{E_p}{G_0} \qquad \text{[Wh/(d*Wp)] or [h/d]} \tag{1.1}$$

$$E_p = \int_0^{\Delta t} G\,dt \quad \text{[Wh/d*m}^2\text{]} \tag{1.2}$$

Where G is the irradiance, dt is a period of time (min).

1.6.2 Array yield

Y_a the number of hours per day in which the PV panels have to operate with nominal power P_0 to generate array energy E_a.

$$Y_a = \frac{E_a}{P_0} \qquad \text{[Wh/(d*W}_\text{p}\text{)] or [h/d]} \tag{1.3}$$

$$E_a = \int_0^{\Delta t} I_a V_a dt \quad \text{[Wh/d]} \tag{1.4}$$

Where I_a and V_a are the output current and voltage of PV arrays, P_0 is the peak power.

1.6.3 Final yield

Y_f the number of hours per day which the PV panels have to operate with nominal power P_0 to generate the useful output energy $E_{use,PV}$.

$$Y_f = \frac{E_{use,PV}}{P_0} \quad \text{[Wh/(d*W}_\text{p}\text{)] or [h/d]} \tag{1.5}$$

$$E_{use,PV} = \frac{E_L}{(1+\frac{E_{BU}}{E_a})} \text{[Wh/d]} \tag{1.6}$$

Where $E_{use,PV}$ is the useful PV contribution energy, which denotes the energy supplied by the PV modules. E_{BU} is the buck-up energy and E_L is the energy consumed by the load.

1.6.4 Capture losses

L_c is defined as the difference between the yields: Y_r and Y_a where many losses can be flagged like (wiring, maximum power point, failure, thermal losses, etc).

$$L_c = Y_r - Y_a \quad \text{[Wh/(d*W}_\text{p}\text{)] or [h/d]} \tag{1.7}$$

1.6.5 System losses

L_s is defined as the difference between the yields Y_a and Y_f, where this parameter indicates the storage losses in the battery.

$$L_s = Y_a - Y_f \quad [\text{Wh/(d*W}_\text{p})] \text{ or } [\text{h/d}] \tag{1.8}$$

1.6.6 Performance ratio

PR is the ratio between the useful energy and the energy that would be generated by a lossless.

$$PR = \frac{Y_f}{Y_r} \tag{1.9}$$

1.6.7 Limitations of power loss fault analysis

The above-mentioned parameters could be affected by all kinds of lossless into the system, this could add complexity to distinguish the loss due to the faults. For instance, a SAPV system without MPPT causes an augmented Lc due to the Maximum Power Point losses, where Lc could be augmented due to the faults [18]. The judgment of the system using the Lc parameter could be misleading, furthermore, the discrimination of fault losses is hard. Also, an oversized SAPV system proceeds a frequent disconnection of the PV system to protect the battery from overcharge, this last reduce certain parameters and leads to false information about the system [14].

An example showing the progress of power parameters in the presence of faults has been established. The simulated system has been used for this purpose and the parameters Yr, Lc, and Ls have been calculated and plotted on a bar graph. The results are shown in Figure 1.11, in which the

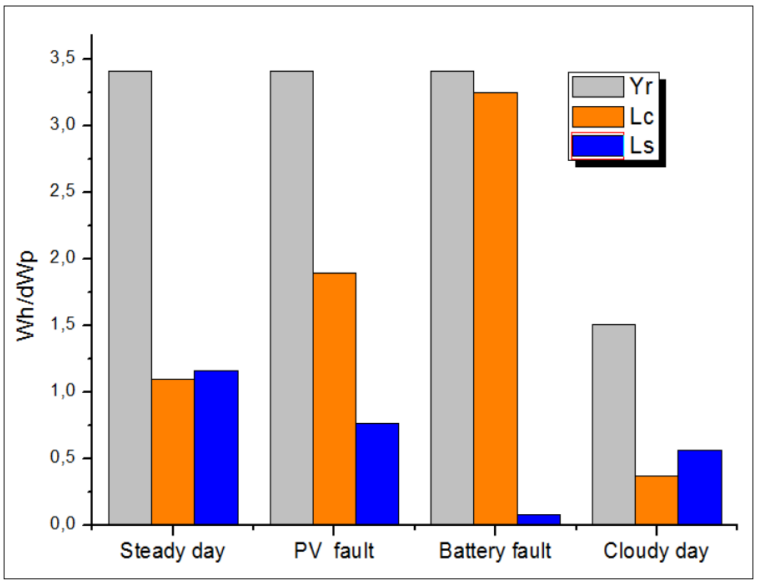


Figure 1.11 Diverse daily indices of performance.

Lc is increased in PV and battery fault case indicating a failure. However, this value is small on a cloudy day due to the low value of Yr. The value of Ls is significantly decreased in the battery fault case indicating a problem in the storage battery.

The above example shows the limitation of power loss parameters to determine the type of the fault and could confound with different losses.

1.7 A literature fault detection and diagnosis

1.7.1 Pv system case

1.7.1.1 I-V characteristics analysis

Current-voltage (I-V) curve offers most of the operating points of a PV module, string, or array. The analysis of PV characteristics makes possible the detection and location of faults such as mismatch fault, series losses, shunt losses, and reduced current or voltage due to a fault [7], [19]–[21] As shown in Figure 1.12.

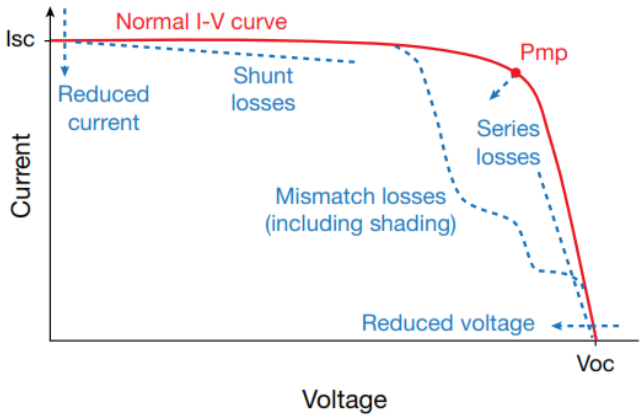


Figure 1.12 The IV characteristic affected by different classes [21].

1.7.1.2 Power comparison analysis

Several evaluation yields have been proposed for this method, the first one consists to compare the actual power yield (P_{actual}) with the expected one (P_{sim}) under real-time. A significant difference between the measured and simulated power yield may indicate a fault, where weather information such as solar irradiance and temperature are gathered and fed into the simulation model to expect the PV power output [7], [19], [21]–[23]. An example of a fault detection system is shown in Figure 1.13 where solar irradiance and ambient temperature are gathered from the satellite to predict the output power Psim and compare it with the monitored actual P_{actual} [23].

The second evaluation parameter is the performance ratio (*PR*) as a normalized power yield, this parameter considers the overall effects of system losses where faults take part. In normal operation, Its value ranges between 0.65 and 0.8, However, in the presence of fault this value is

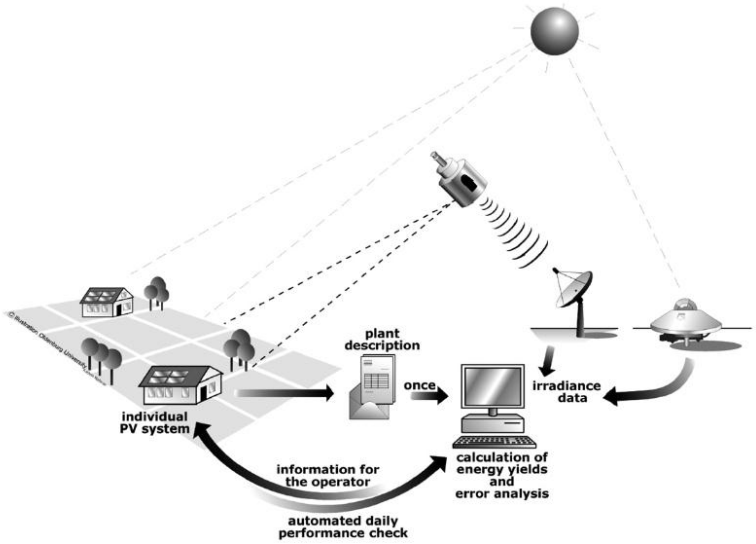


Figure 1.13 Overview system of PV fault detection using power comparison [18].

significantly reduced [16], [24].

The third performance index is capture losses (L_c) that represent the losses due to PV array operation. L_c can be divided into thermal capture losses (L_{ct}) and miscellaneous capture losses (L_{cm}). An automatic supervision of PV system based on the analysis of capture losses has been used to identify three groups of faults: faulty PV modules in the string, faulty string and a group of fault (partial shadow, aging, and MPPT error) [16], [24]–[26].

1.7.1.3 Time domain reflectometry

Time domain Reflectometry (TDR) is a diagnostic method that works by injecting waveform signals (steps or impulse signals) and observing the reflected waveform. The reflected waveform is compared to those generated from standard or, given impedance, therefore TDR can determine the faulty wires or cables as well as it is able to locate the fault. The TDR method has been used for PV diagnosis in [27]–[29], where some drawbacks are noted such as the system PV must be off-line to make the test. This property impacts the power yield and requires human experience to observe and learn the reflected waveforms, which impact its effectiveness as an automatic fault detection.

1.7.1.4 Infrared thermography

Infrared (IR) Thermography has been largely used as a thermal camera to identify Mismatch fault such as a hot spot on the PV module as shown in Figure 1.14. This method is based on the principle that all materials emit infrared radiation in a range of wavelengths that depend on the temperature of the material [30] [31]. The disadvantage of this method consists of needing a regular and repetitive inspection, which costs in terms of PV maintenance personal over the

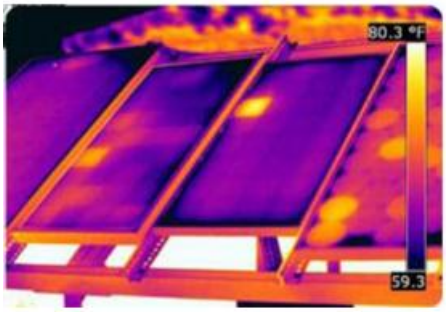


Figure 1.14 Infrared thermal image of short-circuited PV cell [26] .

lifespan of PV modules.

1.7.1.5 Residual current detector

Residual Current Detector (RCD) or Differential protection is the most method used in power systems like a transformer, motor, or generator. RCD works like a differential relay by monitoring the input and outputs current, where if the current difference is higher than a threshold, the fault alarm will be sent out. RCD has been proposed for fault detection in a PV system [17].

1.7.1.6 Internal series resistance

The equation current of one diode model for PV module is described in Chapter 2 eq.2, where the internal series resistance Rs could be used to detect the degradation inside a PV module. The actual Rs could be estimated using the I-V curve and then compared with Rs in Normal cases. Generally, the degraded PV module results in increased Rs which could be very useful for fault detection [32].

1.7.1.7 Machine learning

Machine learning algorithms aim to extract information (knowledge) from the historical data set of the system, in which prediction models are built. Many fault detection and diagnosis methods for PV systems have been proposed in the literature using these approaches such as ANN [33]–[35], BNN [36], decision tree [37], K-nearest neighbor, and SVM [38].

1.7.1.8 Statistical methods

A statistical method has been introduced for fault detection and real-time monitoring in a grid-connected PV system, where the energy output of inverters is utilized as input data [39]. The proposed approach has been validated using a real PV installation, where the test shows a successful in detecting a wiring mistake.

1.7.2 Battery case

The life span of PV modules is expected to be twenty years, however, the battery is less than ten years and tends to be shortened if it operates under poorly maintained conditions. For this reason, the battery represents 43% of the lifetime cost for the SAPV system [40], therefore monitoring the battery status to avoid overcharge and deep discharge is essential to extend the total system service life [41].

1.7.2.1 Internal resistance monitoring

Lead-acid battery internal resistance (IR) monitoring was proposed in [41] for a real system installed on a remote island in Korea, where IR could be a good indicator to monitor the battery aging. The method adopted to measure IR is a current interrupt technique that disconnects the battery during charge or discharge for 2 or 3 s every 30 min. The IR is calculated using ohm's law, $IR=\Delta V/\Delta I$, where ΔV and ΔI denote respectively the voltage and current differences between those of Normal operation and current interrupted period. The results show that the IR of the battery increases after a long cycle service, where continuous checking of IR is strongly recommended.

1.7.2.2 Short and Long term evaluation

A short and long-term evaluation of a PV-diesel hybrid system involving battery has been proposed in [42]. Short-term evaluation is carried out every day and it is based on the analysis of the battery voltage graph. This last indicates failures in the battery and possible errors as well as unfavorable operation of the system and degradation. Figure 1.15 shows the battery voltage graph, with different voltage levels that could be used to examine the battery operation. The white area is good, the grey area is acceptable for a shorter period, however, the black area is rare. Further

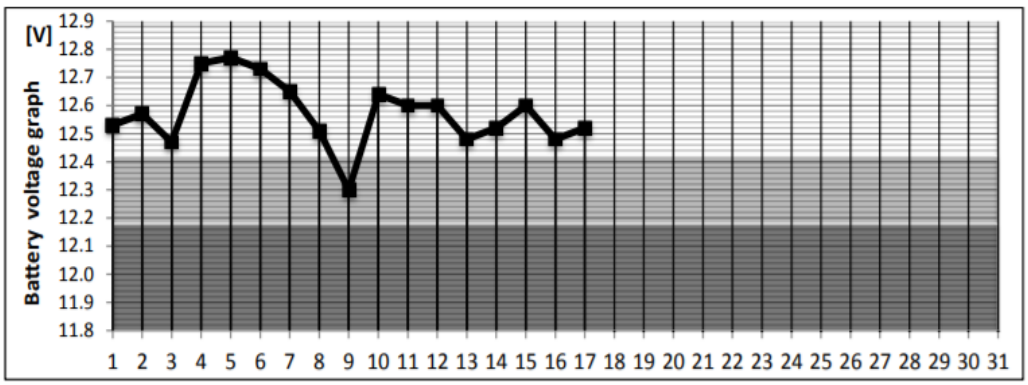


Figure 1.15 Battery voltage scenarios [37].

analysis with the load and generation curves could be done if necessary.

A long-term evaluation is performed every month, where many evaluated parameters have varied over the year. Yearly evaluation and comparison of the different years allow us to understand if there are changes in the power system over time or errors in the system that are difficult to detect by short-term evaluation. For the long-term evaluation, average values for each month are calculated and noted to put in the graphs. The parameters that will be evaluated are battery voltage, the load and generation, the share of PV, the normalized PV yield, the system losses, and the fuel consumption.

1.7.2.3 Method based on Estimation of Solar Radiation

Estimation of solar radiation to check the fault that occurs in a lead-acid battery for the PV system has been proposed in [43]. The GISTEL (Solar Radiation by Teledetection) model has been chosen as a satellite image to estimate the hourly global solar radiation. The data estimated are introduced into a PV array simulation to produce the output power. The battery in this case stores the energy to ensure the autonomy of the SAPV system, and on the other side, it allows to study its behavior under different situations. The work shows the effect of increasing internal resistance on the degradation of storage unit capacity as shown in Figure 1.16. The second effect is overcharging of the battery that reduces the level of water, which affects the whole system performance as illustrated in Figure 1.17 and Figure 1.18.

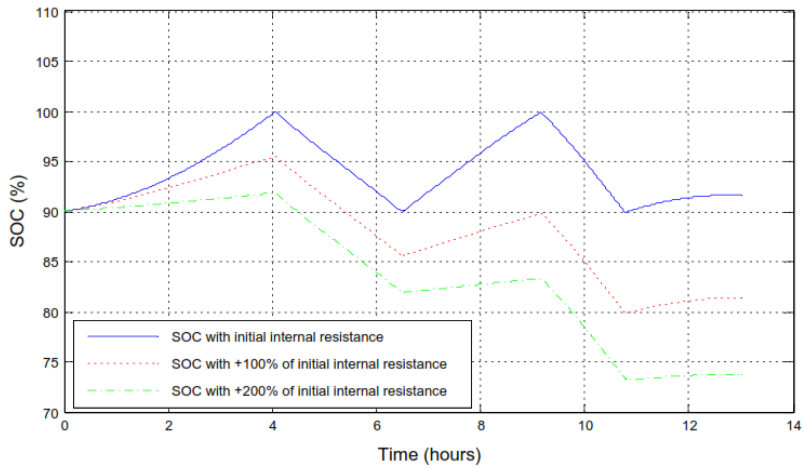


Figure 1.16 State of charge (SOC) with different internal resistance values [38].

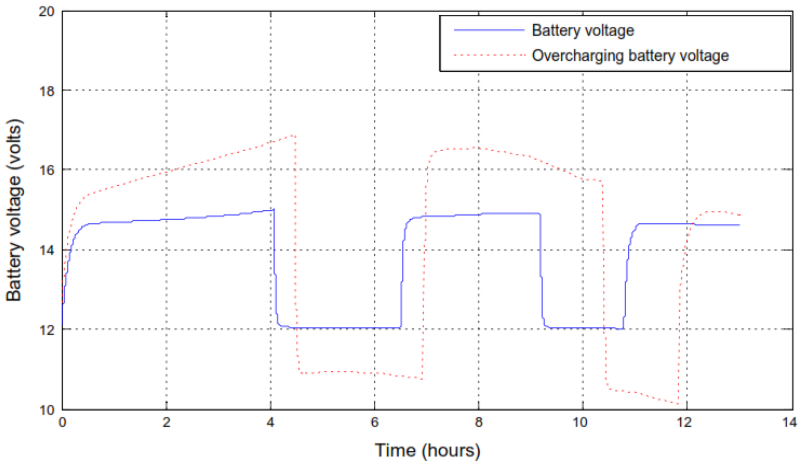


Figure 1.17 Battery voltage curves comparison of normal and overcharges effect [38]

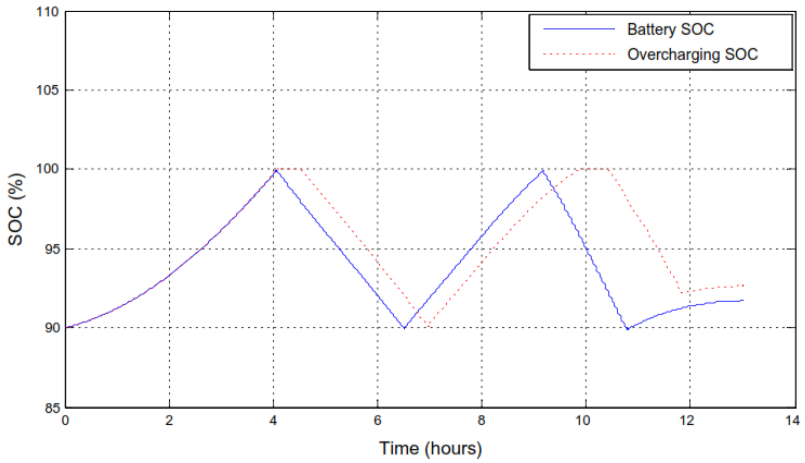


Figure 1.18 Battery state of charge comparison of normal and overcharges effect [38]

1.8 Manual troubleshooting of SAPV system

General guidance is given by Sandia Laboratory for finding problems in the SAPV system [44] is is illustrated by the flowchart in Figure 1.19 and summarized by:

1- Simple visual checking

The first thing is to look for blown fuses, tripped breakers, and bad connections. Repair as necessary and check the status lights, if any, on the charge regulator.

2- loads checking

The appliances, pumps, or other loads may have blown a fuse or failed. For this reason, check the load input voltage and current to verify their rightness. Another same load can be plugged into that circuit to see if it will work, if it does, the original appliance is suspect. If the correct voltage is not present, then we move to the next step.

3- Battery checking

Check the battery voltage, if a correct voltage is present at the output, then the circuit between the battery and the load must be inspected.
If the battery voltage is low, it must be recharged as well as the voltage and specific gravity for each cell is checked for looking the weak cell and repair it if necessary. If the battery voltage is still low, the problem may be with the charge regulator.

4-charge regulator checking

Check the input voltage at the charge regulator and ensure whether it is equal to the battery voltage or not. If yes, the charge regulator has the PV array connected to the battery that we should verify if the charging current is flowing from the PV array. If yes, the load must be disconnected to let the PV array charge the battery. If no current is flowing or the charge regulator input voltage is equal to the open circuit PV array, the charge regulator may have failed. If the charge regulator is okay, the problem could be with the PV array.

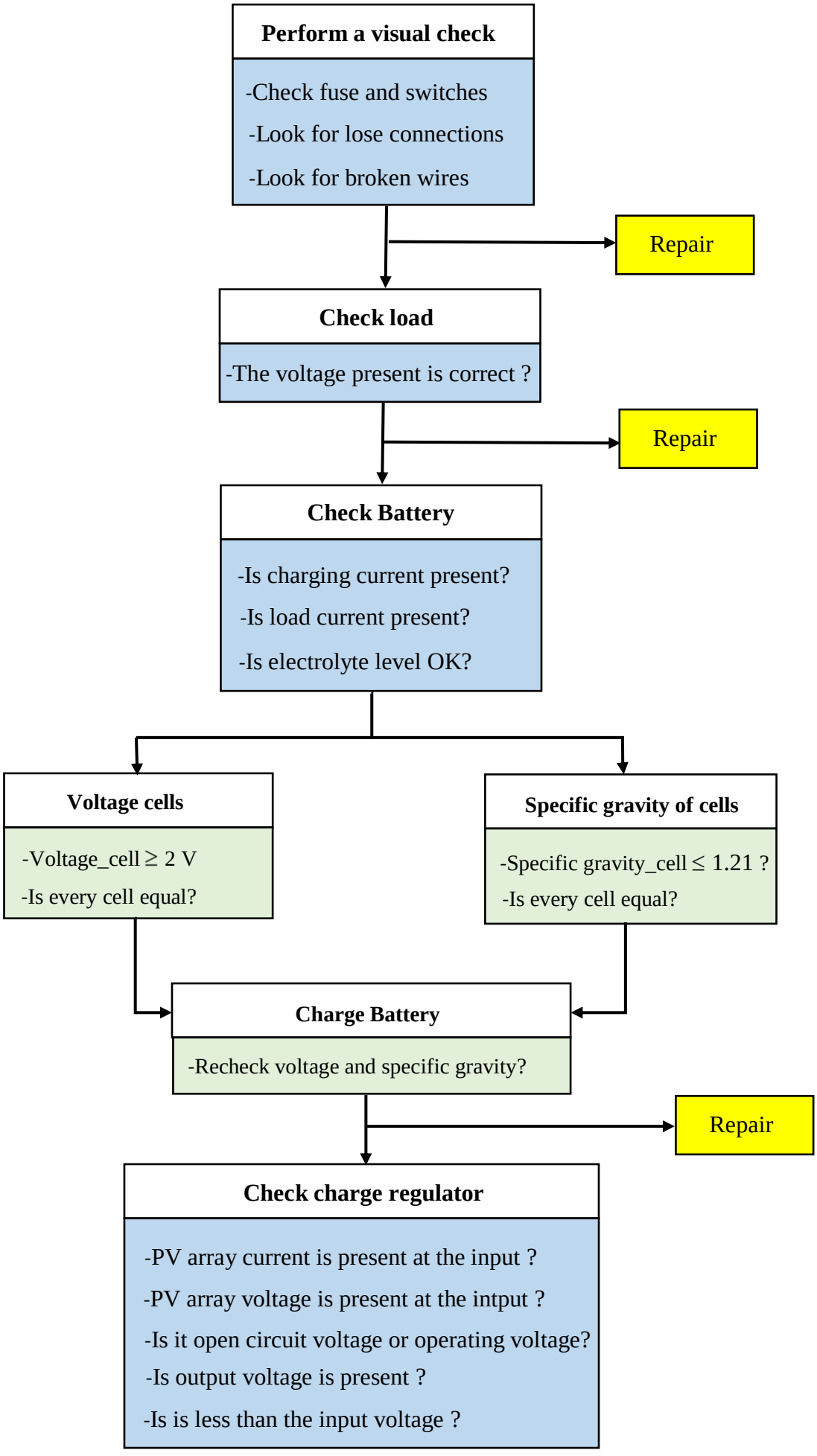
5-PV array checking

Check the PV array voltage at the output and check the PV array current by bypassing the charge regulator in which the PV array is directly connected to the battery. Shade each PV module and see if the current changes, repair if necessary, and make sure to return the system to its original configuration when you have finished troubleshooting.

1.9 Conclusion

This chapter explores the main typical faults in the SAPV system, where these faults could be divided into PV system faults and battery faults. Also, a literature review for fault detection, diagnosis, and performance evaluation is given for the PV system, battery, and whole SAPV systems. The benefits and drawbacks of each approach are discovered, in which the limitations of the proposed methods could make its application in real-world PV system weak.

The chapter concludes with troubleshooting guidelines given by Sandia Laboratory for manually finding and checking problems in the SAPV system. This method adds an extra cost to the PV installation and exposes human labor to the risk. Furthermore, the method could be inaccurate in finding the exact fault in the SAPV system.


Perform a visual check
-Check fuse and switches
-Look for lose connections
-Look for broken wires
Repair
Check load
-The voltage present is correct ?
Repair
Check Battery
-Is charging current present?
-Is load current present?
-Is electrolyte level OK?
Voltage cells
-Voltage_cell ≥ 2 V
-Is every cell equal?
Specific gravity of cells
-Specific gravity_cell ≤ 1.21 ?
-Is every cell equal?
Charge Battery
-Recheck voltage and specific gravity?
Repair
Check charge regulator
-PV array current is present at the input ?
-PV array voltage is present at the intput ?
-Is it open circuit voltage or operating voltage?
-Is output voltage is present ?
-Is is less than the input voltage ?

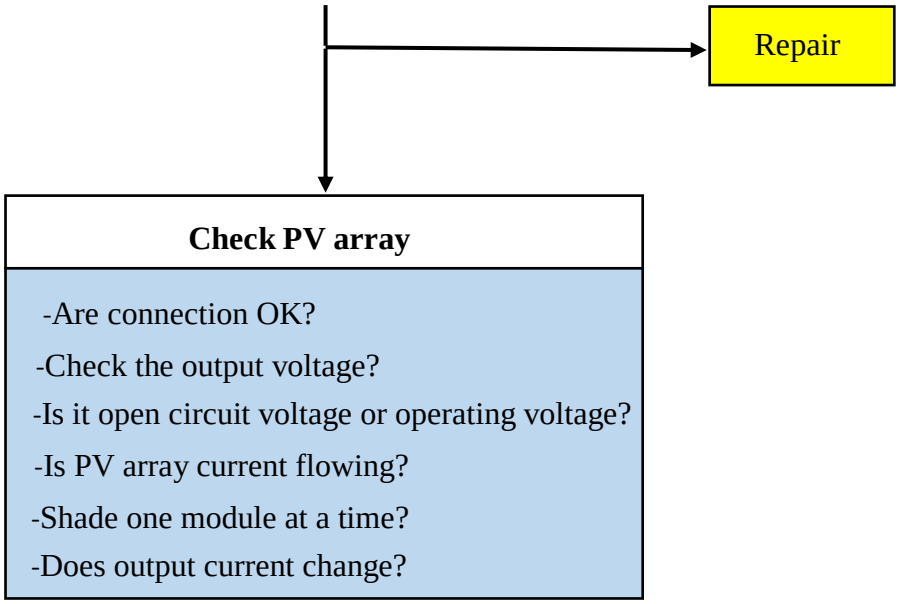


Figure 1.19 Troubleshooting guidance [39].

Chapter: 2 Stand-Alone Photovoltaic System: Generalities, Modelling and Simulation

2.1 Introduction

This chapter introduces a new simulation tool suitable for fault analysis in a stand-alone photovoltaic system using Matlab/SimPowerSystem environment. The simulation schemes use individual modules assembled in series-parallel to build the system, in addition, the simulation model takes as an input solar irradiance level and ambient temperature to predict the different system output. A small-scale experimental SAPV benchmark system has been established in simulation, in which the developed model shows an accurate output compared to the results of the experiments. Note that the first section of this chapter is dedicated to describing the main devices related to the stand-alone photovoltaic systems, explaining their operating mode, and show the impact of using such technologies on the system.

2.2 Stand-Alone photovoltaic system

Stand-alone Photovoltaic (SAPV) systems remain the most popular system worldwide, although the current interest is on the grid-connected system [1]. This system is designed to cover the electricity needs of the load with a continuous energy supply and store the electricity for the period of low generation. The off-grid system refers to the system not connected to the public grid, and it can be distinguished by the system containing batteries (SAPV system) or not (DCPV: Directly Coupled PV system). In the case of DCPV, the PV system is directly connected to a motor or pump which is used mainly for agricultural purposes [45].

The basic configuration of the SAPV system is shown in Figure 2.1, in which the PV modules are connected to the battery and load via the charge regulator as a protective element for the battery. Depending on the load profile, the supply can either in direct current (DC) load or

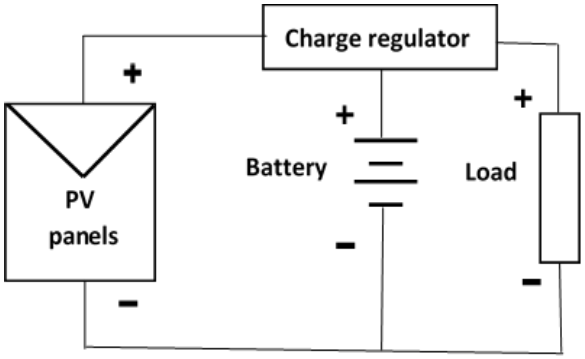


Figure 2.1 Typical SAPV system

alternating current (AC) load or both. In this case, some other elements such as DC-AC converters and AC-DC converters can be added.

2.3 Basic Elements for Stand-Alone photovoltaic system

2.3.1 PV system

The PV system converts directly the light or solar irradiance into electric energy, where silicon solar cells as a basic element are assembled and connected usually in series to form the PV module. The series and parallel connection of PV modules constitute a PV array (Figure 2.2), whereas a PV string consists of a series connection of PV modules according to the required output voltage. The number of PV string in parallel depends on the needed output power [46].

2.3.1.1 Fuse

An electrical protection device from overcurrent of PV modules and conductors. It is usually placed in series with PV string and has a rated current to 156 percent of rated short circuit current (Isc) at STC of PV module [3].

2.3.1.2 Blocking diode

Blocking diodes are used to prevent the reverse current coming from the battery or other sources. The battery delivers reverse current when PV modules are shading, low irradiance, or failure of PV modules [47]. It is recommended to place one blocking diode in each PV string to protect the weak string (due to failure or low irradiance) from the strong one [48].

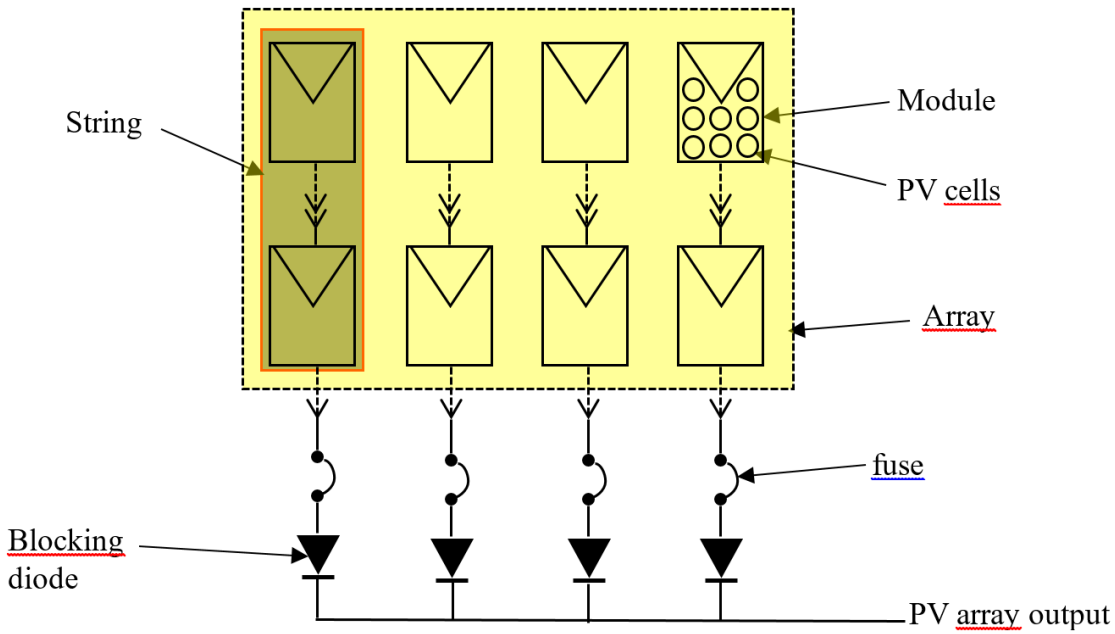
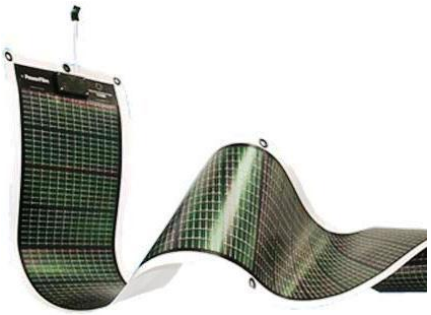


Figure 2.2 Basic structure of PV system

The PV cell is available with different types and technologies, Table 2-1 compares the most two familiar technologies: Crystalline-Silicon (C-Si) and Thin-film.

Tableau 2-1 Solar cell technologies comparison [7]–[11]

	Crystalline-Silicon (C-Si)	Thin film
		
Type and conversion efficiency	• Mono C-Si (25.3%) • Poly C-Si (21.3%)	• Cadmium Telluride (CdTe) (7-12%) • Copper Indium Gallium Selenide (CIGS) (10-15%) • Amorphous silicon (5-7%)
Advantages	• More conversion efficiency • Takes up less space	• Reduced cost • Less sensitive to temperature • Flexible support
Disavantage	• More expensive • Sensitive to temperature • Limited application	• Less conversion efficiency • More space is required
PV market availability	Around 85%	Arround 25%

2.3.2 Static characteristic of PV module

As shown in Figure 2.3, a PV module has a non-linear curve of current _voltage (I_V), along this graph contains all the possible operating points of the PV module. Three main parameters situated on the graph are: short-circuit current (I_{sc}), open-circuit voltage (V_{oc}), and maximum power point (MPP). The MPP represents the maximum provided current, voltage, and power respectively by the PV module.

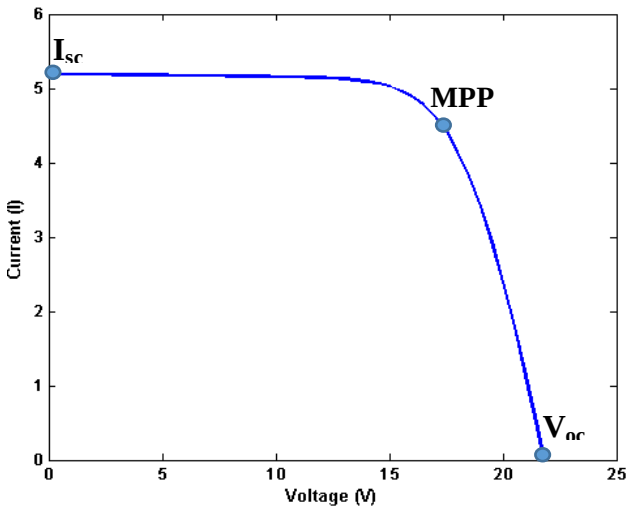


Figure 2.3 I-V curve of a PV module

2.3.2.1 Influence of irradiance and temperature on PV module

To illustrate the effect of irradiance on the PV module, Figure 2.4 shows the variation of I_V and P_V curves with different levels of irradiance ranging from 200 W/m^2 to 1000 W/m^2 and a fixed temperature (25 C°). It can be seen that the higher level of irradiance results in increased PV output current and power reflecting a direct correlation.

The influence of the temperature on the PV module is indicated in Figure 2.5, in which for a fixed level of irradiance (1000 W/m^2), a different temperature level ranged from -25 C° to 75 C°. It can be observed that the lower temperature level gives a rise in voltage and power.

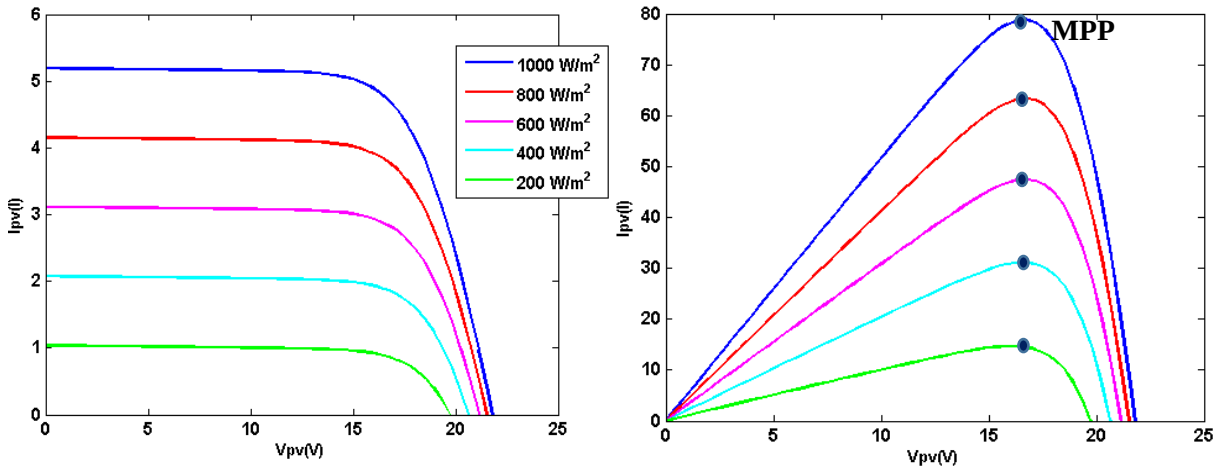


Figure 2.4 Irradiance effect on I_V and P_V characteristics

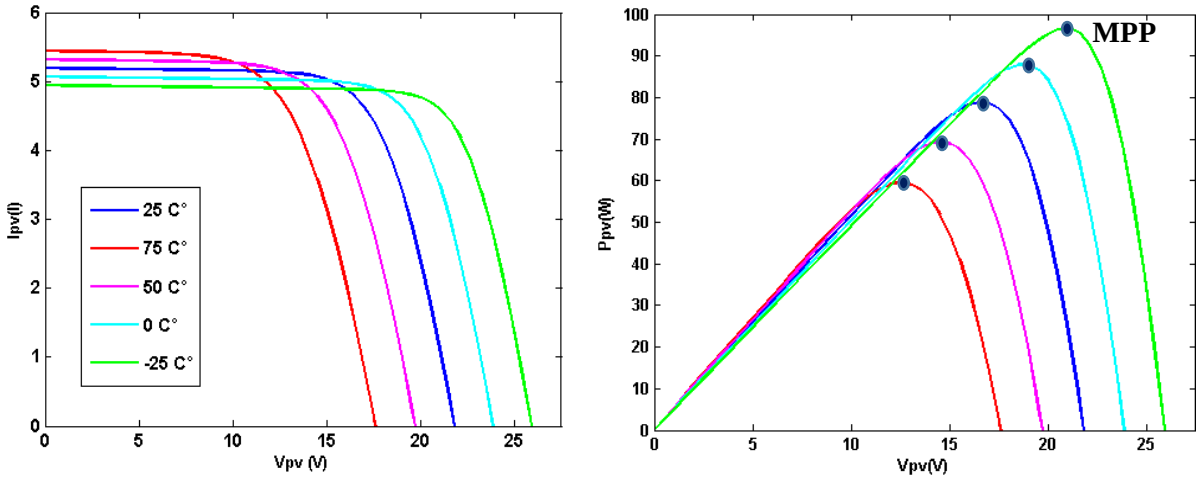


Figure 2.5 Temperature effect on I_V and P_V characteristics

2.3.3 The Battery

The storage battery element is placed between the PV modules and the load (Figure 2.1) and can be interpreted as capacitive load [49]. Figure 2.6 shows that the battery voltage Vbat is common to all the components, whereas the current flowing is given by: $I_{pv} = I_{bat} + I_{load}$.

The battery supplies the load at low PV modules generation or during the night, in this case the battery discharges and I_{bat} has a negative sign. In contrary, when the PV generation is availble during the day, the battery charges and the sign of I_{bat} is positive.

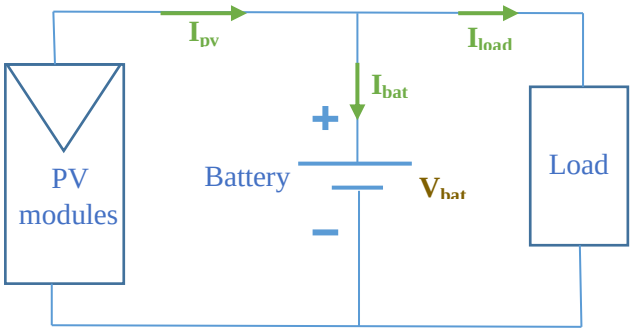


Figure 2.6 Basic SAPV system element

2.3.4 Battery type

The battery is formed of series-connected cell devices with a low voltage value ranging from 1.8 V to 3.8 V. The battery is constructed with different materials and structures. The main technologies used are Lead-acid, Nickel-cadmium (Ni-Cd), Nickel-metal hybrid (Ni-MH), and Lithium-ion (Li-ion). Other rechargeable battery technologies are under development and not yet commercially available, Table 2-2 compares the main used type of battery.

Tableau 2-2Main battery technologies comparaison [50], [51].

	Lead-acid	**Ni-Cd (Nickel cadmium)**	**Ni-MH (Nickel metal hybrid)**	**Li-ion (Lithium ion)**
Number of cycles	200-300	1500	300-500	500-1000
Weight energy density (Wh/kg)	30-50	48-80	60-120	110-160
Self discharge rate / month	5%	20%	30%	10%
Cost	Low	High	High	Verry High
Applications area	• stationary battery • start engine • PV system	• PV system	• small portable electronic devices • PV system	• Electric vehicles • portable electronic application

Main advantages	• adaptation with different use • Low cost	• resistance to extremely high & low temperature	• eleminating the cadmium • more compact than (Ni-Cd)	• High weight energy density rate • deepest discharge current
Main disadvantages	• lifetime is reduced by overcharge and deep-discharge. • require more space and heavy.	• Cadmium is toxic for the environment • Capacity decreased by memory effect	• Suffer from a high self discharge rate and memory effect.	• High price • Require protection element for PV system application

A lead-acid battery among other types is the most common accumulator since it covers a wide range of application areas involving the PV system. This technology has many advantages such as robustness, simplicity, and relatively low cost compared to the Ni-Cd type. The battery cell is formed of two plates, positive and negative immersed in a dilute sulphuric acid solution. The anode (or positive plate) is made of lead dioxide (PbO_2) while the cathode (or negative plate) is made of lead (Pb).

The chemical reaction in charge and discharge is given below:

$$PbO_2 + Pb + 2H_2SO_4 \underset{\text{charge}}{\overset{\text{discharge}}{\rightleftharpoons}} 2PbSO_4 + 2H_2O$$

The lead-acid battery is available with different types such as liquid electrolyte, gelled electrolyte, sealed, or flooded. Battery with liquid electrolyte can be sealed or open with caps allowing distilled water to be added to the electrolyte. A sealed battery or valve-regulated battery permits the release of hydrogen gas and doesn't allow the electrolyte to be added, it can be either AGM (Absorbent Glass Mat) or Gel [48][52].

The application of a Lead-acid battery as energy storage for PV system benefits from its best rate quality/price as well as its low self-discharge rate and has no memory effect. However, the overcharge and deep discharge may affect the battery and could cause its failure. To protect the battery from excessive charge and deep discharge, a charge regulator is used to maintain the battery voltage operation between two voltage limits.

2.3.5 Charge and discharge Curve

The two main operating modes of storage Lead-acid battery is charge and discharge mode. In the following, the difference of potential at its terminal is graphically shown with time where the battery used is 12 V / C= 50 Ah.

2.3.5.1 Charge curve

In charge mode, the accumulator receives a current from the PV module where its voltage is shown in Figure 2.7. The voltage increases slightly during charge up to 14.5 then increased rapidly to reach the overcharge mode.

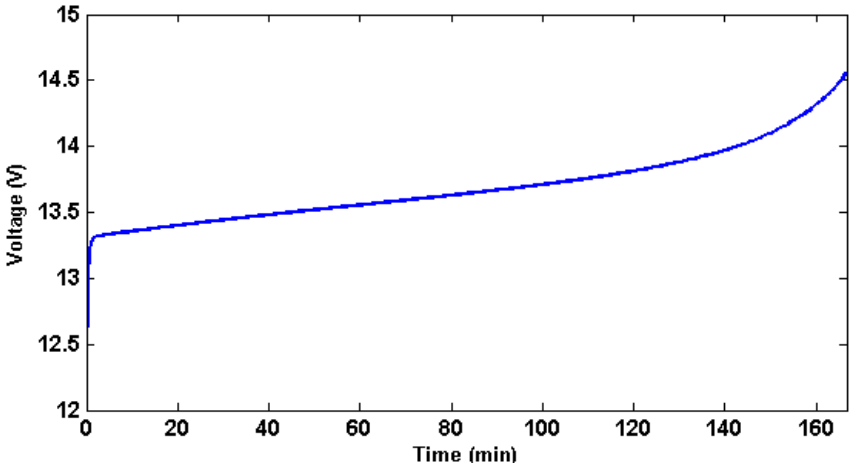


Figure 2.7 Charge curve

2.3.5.2 Discharge curve

In discharge mode, the accumulator gives a current to the load as shown in Figure 2.8. The voltage drops from its nominal voltage up to 10.5 V, from that value it will rapidly drop in

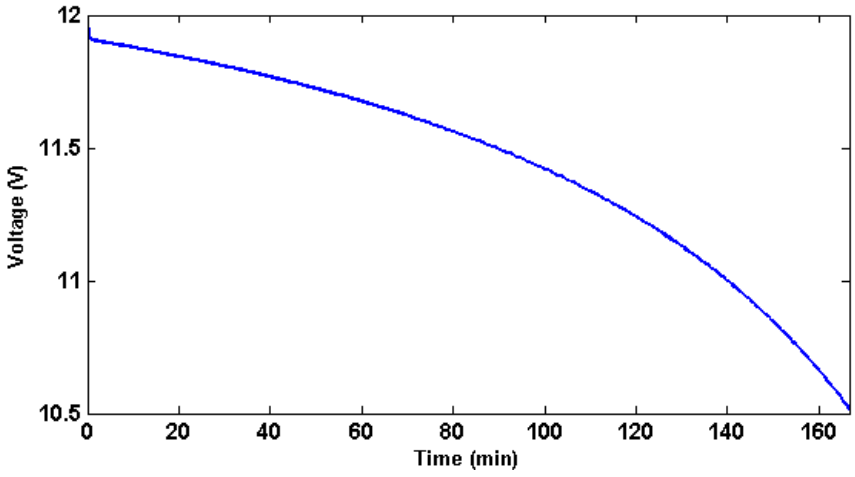


Figure 2.8 Discharge curve

undercharge mode.

2.4 The charge regulator

Two common types of charge regulators firstly used for PV system application: series and shunt regulator. Both types use the measured voltage level to estimate the battery state of charge and therefore control the charge and discharge. The development of microprocessors has led to the emergence of new technics called MPPT that better manage the battery energy flow. The MPPT technic allows getting the best performance from PV module, in which Pulse Width Modulation (PWM) charge regulator constitutes a fast and effective solution for reach a battery fully charge [53].

2.4.1 Series regulation

The series charge regulator as shown in Figure 2.9 includes two or more switches (or relay) placed in series with the battery [54]. This configuration prevents the battery from working outside the recommended low (V_{min}) and high (V_{max}) voltage. The charge regulator work by disconnecting the load when the battery reaches V_{min}, whereas the reconnection is done when the battery is sufficiently charged. On the other side, the charge regulator disconnects the PV modules from the battery when achieving V_{max} and reconnects it when the battery is enough discharged.

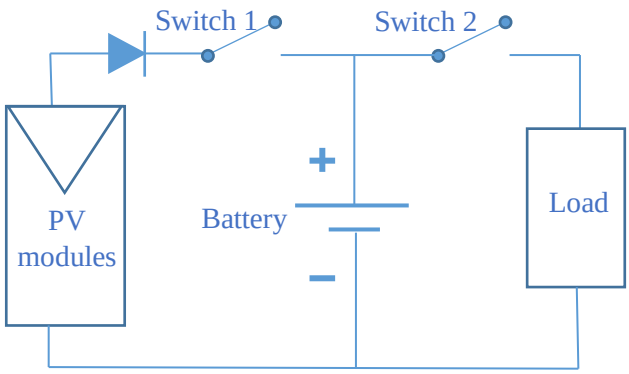


Figure 2.9 Series type charge regulator

2.4.2 Shunt regulation

The shunt charge regulator as shown in Figure 2.10 is made with one switch in parallel with the battery and another switch in series with the load. When the battery reaches the onset of the overcharge mode, switch 1 is closed and a shunt path for the current of PV modules is activated. In discharge mode, the load is supplied with current therefore the switch 2 is closed, once the battery is enough discharged the switch 2 is opened [53].

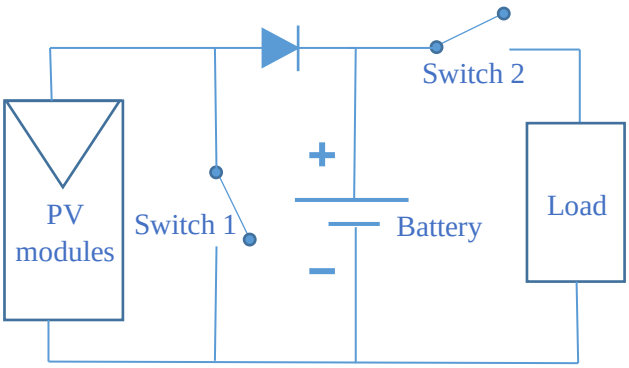


Figure 2.10 Shunt type charge regulator

2.4.3 PWM regulation

The PWM charge regulator uses an interrupt modulated by a pulse of variable width to control the battery voltage. MOSFET or power transistor is used for this regulator regarded the high frequencies operating required to maintain a constant voltage of the battery. The configuration of the PWM charge regulator is shown in Figure 2.11, in which a DC/DC converter is used. This last incorporates the MPPT to (harvest) pull out the maximum energy of PV modules and consequently achieving rapid and effective battery fully charge[53].

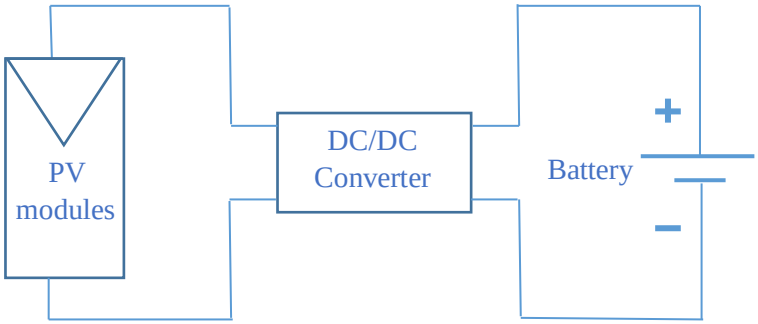


Figure 2.11 PWM type charge regulator

2.5 Modeling of Stand-alone photovoltaic system

2.5.1 Model for PV cells

Due to the non-linearity of the I_V characteristic of PV cells, this last couldn't be modeled with a constant current source. The addition of a parallel diode describes an ideal behavior of PV solar cells originally derived from that of the P-N junction. The real behavior of PV cells includes a series and parallel resistance as known as the one-diode model that is shown in Figure 2.12.

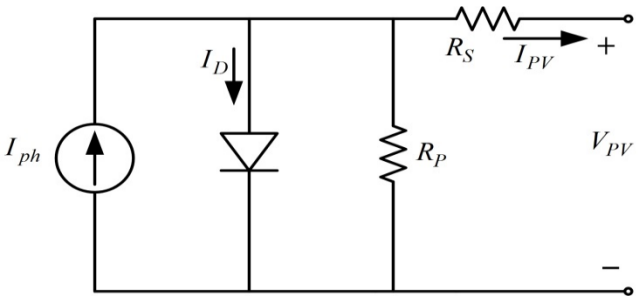


Figure 2.12 Equivalent circuit for one diode model

The solar cell current equation for the one diode model is given by [55]:

$$I_{PV} = I_L - \underbrace{I_0\left[\exp\left(\frac{V_{PV}+R_S I_{PV}}{AKT}\cdot q\right)-1\right]}_{I_D} - \underbrace{\frac{V_{PV}+R_S I_{PV}}{R_p}}_{I_P} \tag{2.1}$$

Where

I_{PV} = solar cell output current (A)

V_{PV} = solar cell output voltage (V)

I_L = light generated current (A)

I_D = diode current (A)

I_P = parallel resistance current (A)

I_0 = diode saturation current (A)

R_S = series resistance of PV cell (ohm)

R_P = parallel resistance of PV cell (ohm)

T = ambient temperature (Kelvin)

A = diode ideality factor ($1 \leq A \leq 2$)

q = electron charge (1.602×10^{-19} C)

K = Boltzmann's constant (1.38×10^{-23} J/K)

The equation model describing the behavior of the PV module that consists of N_s series PV cells is given by [56], [57]:

$$I_{PV} = I_L - I_0 \left[\exp\left(\frac{V_{PV} + R_S I_{PV}}{AKT.N_S} \cdot q \right) - 1 \right] - \frac{V_{PV} + R_S I_{PV}}{R_p} \tag{2.2}$$

The light generated current I_L is described as:

$$I_L = \frac{G}{G_{STC}} \cdot \left[I_{L,STC} + B(T - T_{STC}) \right] \tag{2.3}$$

Where

G = solar irradiance (W/m^2)

G_{STC} = reference solar irradiance (1000 W/m^2)

B = temperature coefficient of the light generated current (A/K)

$I_{L,STC}$ = reference light generated current (A)

T_{STC} = reference temperature (K)

The diode saturation current I_0 is expressed by [58]:

$$I_0 = I_{0,REF} \cdot \left(\frac{T}{T_{STC}}\right)^3 \exp\left[\frac{q.E_g}{AK}\left(\frac{1}{T_{STC}} - \frac{1}{T}\right)\right] \quad (2.4)$$

Where $I_{0,REF}$ is the reference diode saturation current and Eg is the bandgap energy that depends on the material semiconductor, for crystalline silicon, it is approximately 1.12 eV.

2.5.2 Lead-acid battery modeling

The modeling of lead-acid batteries, as well as the estimation of battery state of charge, is one of the most complicated tasks [59]. In this section, the implemented Matlab/SimPowerSystem battery dynamic model for lead-acid type is adopted and described. The battery electrical circuit model as shown in Figure 2.13 represents the battery as a variable voltage source V in series with a resistor R to represent the internal losses during charge and discharge mode. In each operation

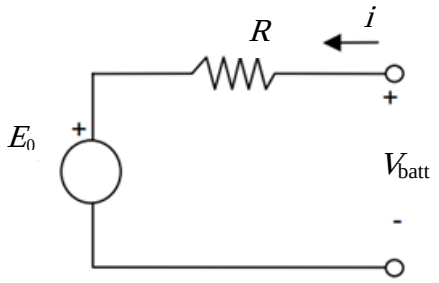


Figure 2.13 Equivalent circuit for battery model

mode, a different expression is assigned to the values of V and R.

The voltage equation model used for charge and discharge of the implemented dynamic lead-acid battery is given as follows [60]:

- For charge :

$$V_{batt} = E_0 - R \cdot i - k\frac{Q}{it - 0.1 \cdot Q} \cdot i^* - k\frac{Q}{Q - it} \cdot it + \exp(t) \quad (2.5)$$

- For discharge :

$$V_{batt} = E_0 - R \cdot i - k\frac{Q}{Q - it} \cdot \left(it + i^*\right) + \exp(t) \quad (2.6)$$

Where

V_{batt} = the battery voltage (V)

E_0 = the battery constant voltage (V)

k = polarization resistance (ohm)

Q = the maximum battery capacity (Ah)

it = the extracted battery capacity (Ah)

i = the battery current (A)

i^* = the battery filtered current (A)

$\exp(t)$ = the exponential zone voltage (V)

2.5.3 Load representation

To simulate the load characteristic, a controlled current source is used for this purpose. The controlled signal current is set to (P_{load} / V_{bat}), where P_{load} is the constant load power and V_{bat} is the variable measured battery voltage. Otherwise, a resistive load is simply represented by resistance in parallel with the battery.

2.6 Simulation in Matlab/Simulink

A whole SAPV system model is built using a toolbox Matlab/SimPowerSystem as illustrated in Figure 2.14. The simulation scheme consists of typical components such as PV modules, storage battery, DC load, series switch controller, blocking diode, grounding system, and connection wires.

To simulate the behavior of the SAPV system under real working conditions, the simulation takes as input a real daily profile of solar irradiance and ambient temperature captured from CDER to predict the system output. Note that the SimPowerSystem toolbox integrated with Matlab/Simulink environment has also the following advantages:

- The modeling tool consists of physical components and blocks such as battery block, diode block, resistance, etc.
- The environment offers also a simple and flexible interface, including numerical and control system tools.
- The modularity and scalability of each component (PV modules, battery, and load) allow creating the different configurations of the SAPV system.

Regarded the advantages and flexibility offered by this environment, the interconnection studies of PV modules, batteries under normal and fault condition is possible.

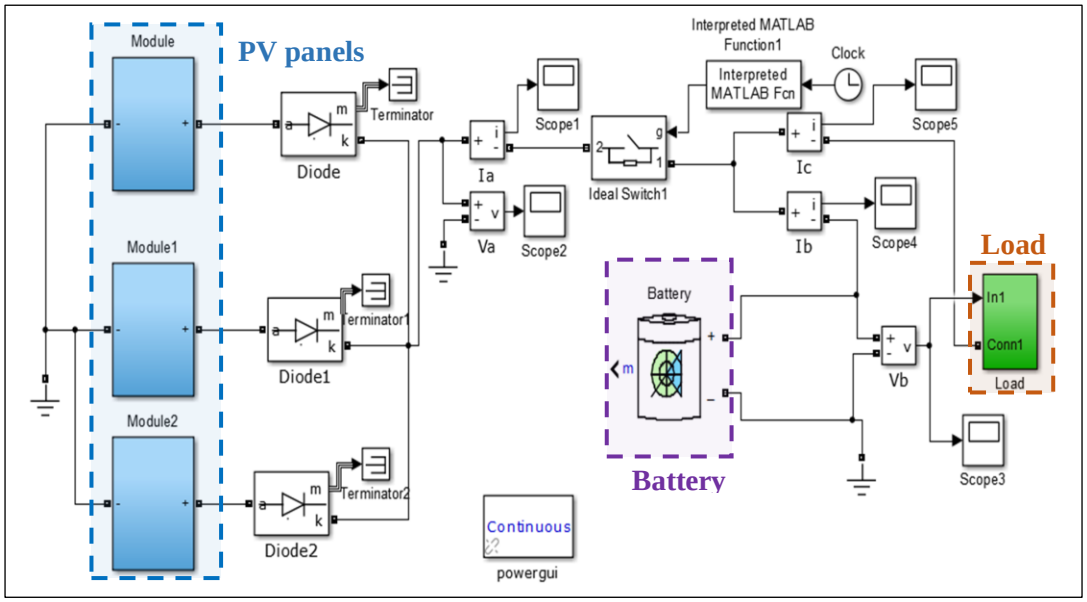


Figure 2.14 SimPowerSystem based model of SAPV system

2.6.1 SAPV benchmark system

A small-scale SAPV system installed at CDER has been established for verification purposes with our previous simulation model. Figure 2.15 illustrates the experimental SAPV system used, as well as the acquisition system. Note that the real SAPV system has the same schematic diagram as the simulation model in Figure 2.15. The detailed electrical parameters for PV modules, battery, load, and the acquisition data system are given in Table 2-3. The PV system parameters such as (Rs, Rp, etc.) can be tuned by the test-error method, whereas the battery parameters are extracted using the actual battery discharge curve.

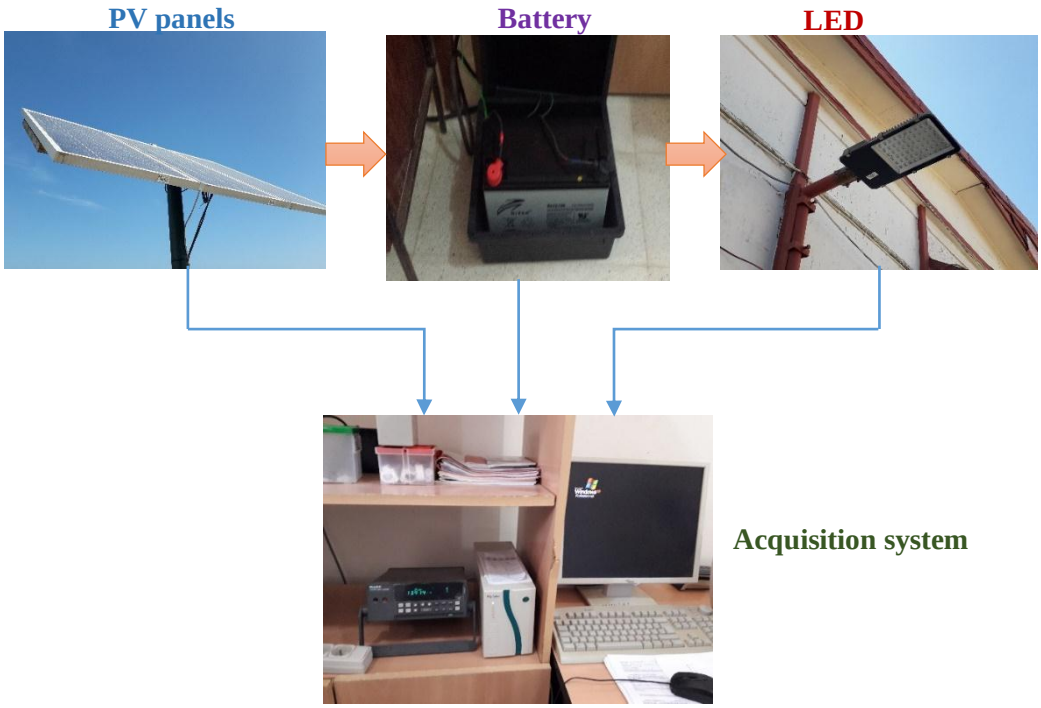


Figure 2.15 SAPV system experimental set-up at CDER, Bouzareah, Algeria

Tableau 2-3 Electrical parameters of main component SAPV system and acquisition system

Individual component	**Electrical parameters**
PV modules (Poly C-Si)	AT STC: P_{max}=255 Wc (3 × 85 Wc) V_{mpp}=17.9 V I_{mpp}=14.31 A V_{oc}=22.0 V I_{sc}=15.6 A
Battery (Lead-acid)	C=70 Ah AGM valve regulated lead-acid Battery V=12 V
Load (Lighting system)	75 W/ 12 V muli-LED lamp
Data acquisition (Fluke NetDAQ 2645A)	#. Analog input: 20 Max. voltage Input: 50V Accuracy on DC volts : 0.02%

2.6.2 SAPV system validation model

The SAPV system developed model is compared with the experiments. For this reason, the simulation input takes a real solar irradiance level and ambient temperature captured from the site of CDER\Bouzareah. The meteorological profile is illustrated in Figure 2.16, where four days are taken in December 2017. The simulation approach assumes that all the PV modules work under the

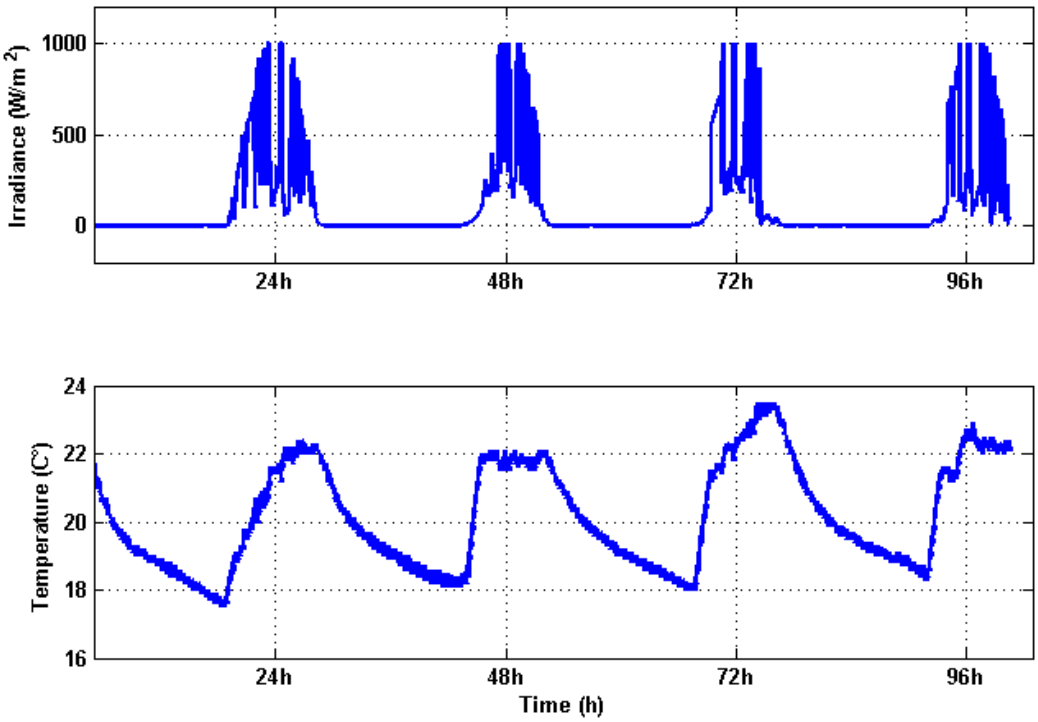


Figure 2.16 Captured profile of solar irradiance and ambient temperature

same solar irradiance and temperature, and have identical electrical characteristics.

The comparison between the simulation results and the experimental measurements is summarized in the graphs of Figure 2.17. Figure 2.17(a) shows the expected Ipv (in blue) and real (in red) PV current respectively, in which the results indicate a good agreement between these two. Figure 2.17(b) shows the simulated and measured battery current (IBat), in which a good matching is noted for both charge and discharge mode. Figure 2.17(c) shows the estimated and experimental battery voltage (VBat), where a slight difference is observed in battery voltage for charge and discharge mode due to the aging phenomenon of a real battery.

Figure 2.18 shows the simulated and experimental load power (Pload), it can be seen that the load power is maintained at 75 W by both simulation and measurement which validate the simulation approach.

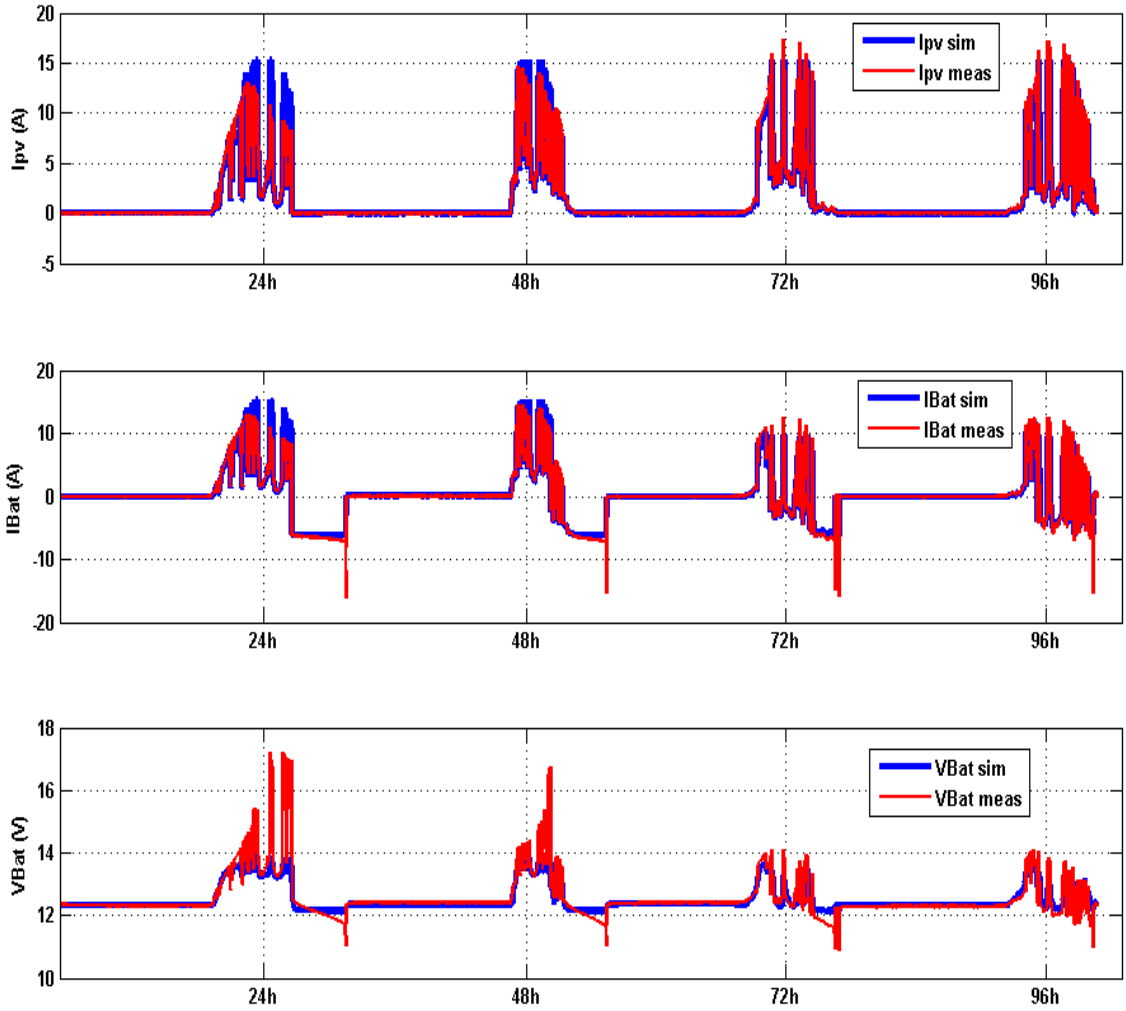


Figure 2.17 (a),(b) Simulated with measured PV and battery current, (c) battery voltage

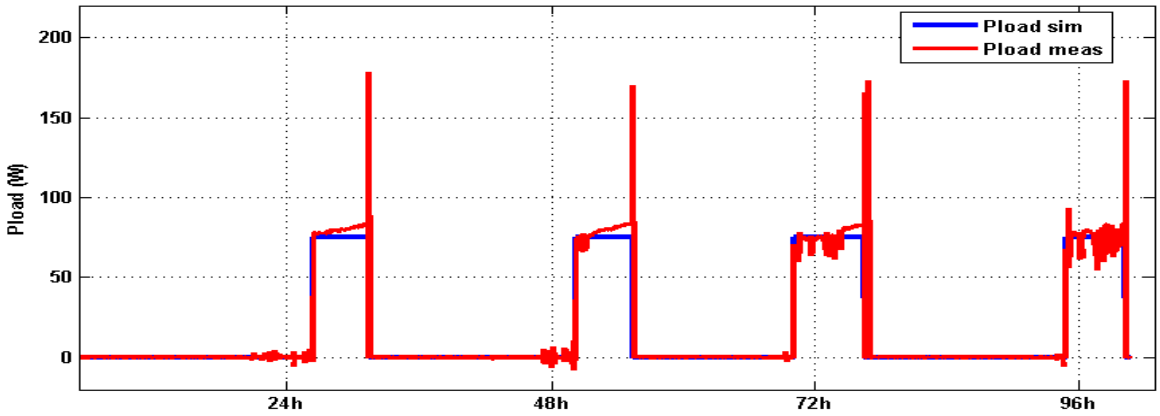


Figure 2.18 Simulated versus experiment of load power

2.7 Conclusion

In this chapter, the most common technology for SAPV system constituted elements is presented. Regarding the cost and performance, C-Si is the most used technology for PV modules, whereas the lead-acid battery technology occupies this place together with the PWM type charge regulator.

Mathematical modeling of PV module and battery has been given, where a SAPV benchmark system has been built under Matlab/SimPowerSystem. The simulation uses the developed one diode PV model, battery SimPwerSystem based model, and a controlled current source for the DC load. The created simulation model uses the daily captured solar irradiance and ambient temperature as input to estimate the output of the SAPV system in real environmental conditions.

The simulation is experimentally verified using the benchmark system installed at CDER/ Bouzareah, in which the real measured output voltage/current of PV modules, battery, and load is compared to the simulated one. The results show a similarity of results revealing the ability of the created simulation to predict the real output. Based on the developed simulation model, some fault scenarios will be created on a PV module or battery in order to simulate and study the system under these typical fault conditions.

Chapter: 3 Battery Internal Fault Monitoring

3.1 Introduction

Nowadays, the battery is regarded as a black box or maintenance-free element since it powers the load for a number of cycles until showing the sign of inability before replacing them. As a result, the system cost will increase and the battery becomes a potential safety concern. Therefore, battery problems should be found and corrected before affecting the system operation. The battery internal short is known as the most important failure influencing reliability, efficiency, and lifetime. This fault is unnoticeable, hardly detectable by conventional protection devices such as fuse and causes premature aging and damage of the battery. To solve this issue, this chapter introduces two machine learning techniques, namely Anomaly detection, and Support Vector Machine as battery internal fault detection and classification respectively. The advantages of adopting such methods consist basically of using unlabeled data for the training rather than the hardly labeled data in a real battery. Anomaly detection algorithm use completely unlabeled data or healthy data for developing battery fault detection. Support vector machine requires a few numbers of labeled data in order to build the battery fault classification. Simulation data have been used to

develop and validate both algorithms using the implemented simulation in Chapter 2. The simulation environment considers the battery unit as series-connected battery cells that form the battery, this allows simulating different internal faults in the battery. The effectiveness of the proposed methods is verified in test real-time with data that have not been used in the training phase. The results show the capability of both methods to detect and classify the fault occurrence in the battery.

3.2 Lead-acid battery constitution

The lead-acid battery constituted of several cells connected in a series configuration to obtain the anticipated voltage of 12 V, in which the cell nominal voltage is 2 V. The battery cell as shown in Figure 3.1 is composed of an alternately assembled group of positive plates (PbO_2) and negative plates (Pb), in which the number of plates and their dimensions characterize the cell capacity. An insulating separator is used between different polarity plates to avoid possible short-circuit. Positive plates are placed together in a pack as well as negative plates, then these packs are gathered together and put in a container with electrolyte to form a cell [61]. The electrolyte is a

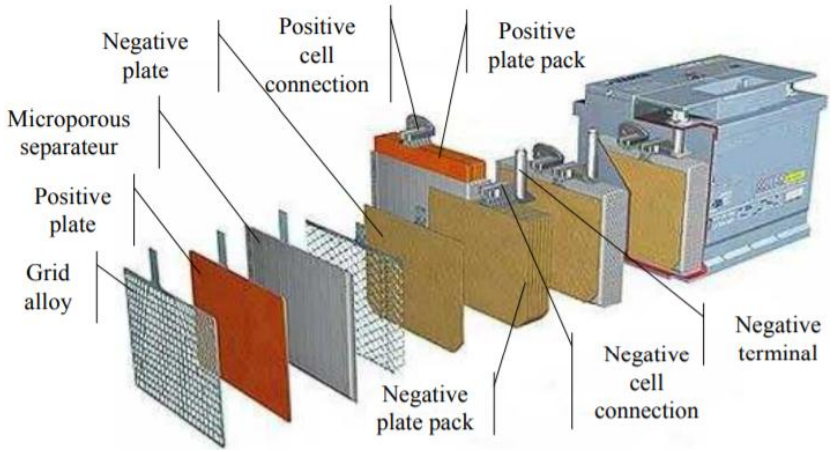


Figure 3.1 The internal structure of a flooded lead-acid battery [1]

mixture of sulfuric acid (H_2SO_4) and distilled water.

3.3 Causes of internal short-circuit

3.3.1 Corrosion

The phenomenon of corrosion or known as ‘‘shedding or softening’’ appears on the grids, in which chunks of lead fall off and reduce the performance. Figure 3.2 illustrates an innard corroded battery. When the battery sheds its lead to the bottom of the container, a conductive layer forms that gradually fill the allotted space where with time, it reaches the plates creating a shorting

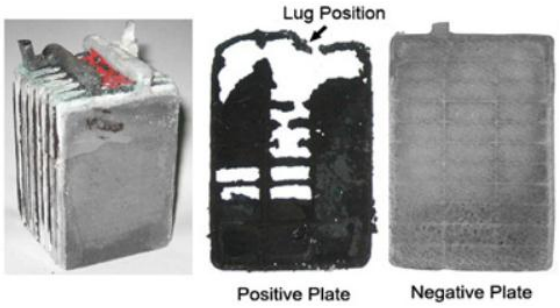


Figure 3.2 Corroded plate of lead-acid battery

effect. The term ‘‘elevated self-discharge’’ or ‘‘soft short’’ describe better this fault condition [9].

3.3.2 Mossing

This happens when the separator and plates are slightly misaligned as a consequence of poor manufacturing and this causes a part of the plates to become naked. The exposed part of plates promotes the formation of conductive crystal moss around the edges, which leads to elevated self-discharge.

3.3.3 Lead drop

Another cause of the short may occur, in which pieces of lead are detached from the soldered bars connecting the plates. Differently, from previous soft short that develops through corrosion, this fault could occur earlier in the battery life due to a manufacturing default causing a persistent voltage drop.

3.3.4 Mechanical failure

The most potent form of short consists of mechanical failure, where the suspended plates becoming detached accidentally and touch each other. As a result, a sudden high discharge current happens that leads to excessive heat accumulated. Generally, poor manufacturing, as well as brutal shock and vibration, are the main reason for this fault.

3.4 Key Factors

The complex behavior of an electrochemical battery due to a number of phenomena inside it makes the fault analysis more complicated and harder than any other energy source. The electrical

short-circuit cells developed may not cause significant overcurrent because of the following factors [4]:

- The battery terminal voltage at the time of the fault, as well as the external circuitry, can influence the fault currents.

- The positive and negative plates are designed to be immersed in the electrolyte, where the loss of electrolyte leads to reduced battery capacity, and therefore the intern short-circuits current may be lower.

-The State of Charge (SOC) is expressed in fraction or percentage to denote the capacity still available in the battery. Depending on the SOC value, the current of short-circuit cells may be higher or lower.

3.5 Limitations of the electrical protection device

The battery protection against internal short-circuit using conventional electrical protective devices such as a fuse or circuit breaker is a pretty complicated task due to the lack of a clear rule to rate a fuse [4]. Moreover, assuming that the right sizing fuse is available, the location of this fuse involves additional complexity in the circuit. Figure 3.3 shows two common placements of fuses in the battery circuit, terminal protection line (Figure 3.3(a)) and midpoint fuse (Figure 3.3(b)). As the short-circuit could occur between the upper and lower cells as shown in Figure 3.3(a), this will not be sensed by the main terminal protection. However, the midpoint fuse circuit will prevent (interrupt) such fault. Many battery installations employ midpoint fuse to bring more protection from battery failures, however, the location of fuse in this way is not the answer in all situations. As an example of serious damage results from a battery fire, the reason was a charger fault that led to short-circuit the main battery terminals and therefore the midpoint fuse failed to interrupt this fault. Many midpoint fuses could exist rather than a single fuse (Figure 3.3(b)), however, the increase of fuse within a line circuit is accompanied by an increase of series resistance and a greater probability of defected fuse that would remove an unfaulty battery from the operation.

The study in [4] concludes that the fuse, wherever located, is of limited value in ensuring battery protection against internal short-circuit.

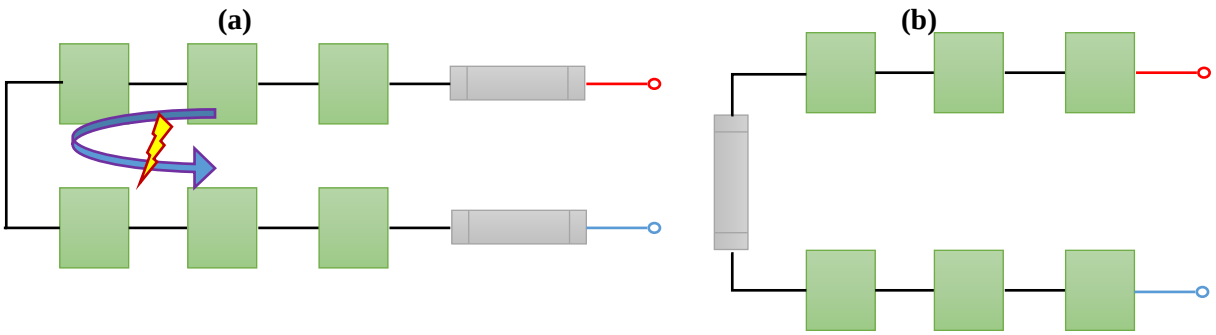


Figure 3.3 Battery protection using : (a) terminal protection fuse, (b) midpiont fuse

3.6 Battery model considerations

Based on the simulation model developed in chapter 2, a small SAPV system composed of 2 PV modules (212 Wp) connected with a battery of 200 Ah and a resistive load of 50 W is considered. To simulate the battery cell interconnection under normal and fault scenarios, the battery unit is viewed as basic cells connected in series. The cells consist of identical batteries of 2V/200 Ah to represent the battery cells as shown in Figure 3.4. In this way, the modeling and simulation of the battery become a key step for fault analysis.

The PV panel used is Isofoton 106W-12V, where the extracted parameters are obtained from [26] and the general electrical characteristics of the adopted SAPV system are summarized in Table 3-1. The configuration of the battery used in the simulation model allows creating different short-circuit cells (from 1 to 6 cells) as shown in Figure 3.5 with 1 cell in short-circuit. Table 3-2 shows the established faults as well as the symbol to denote these faults.

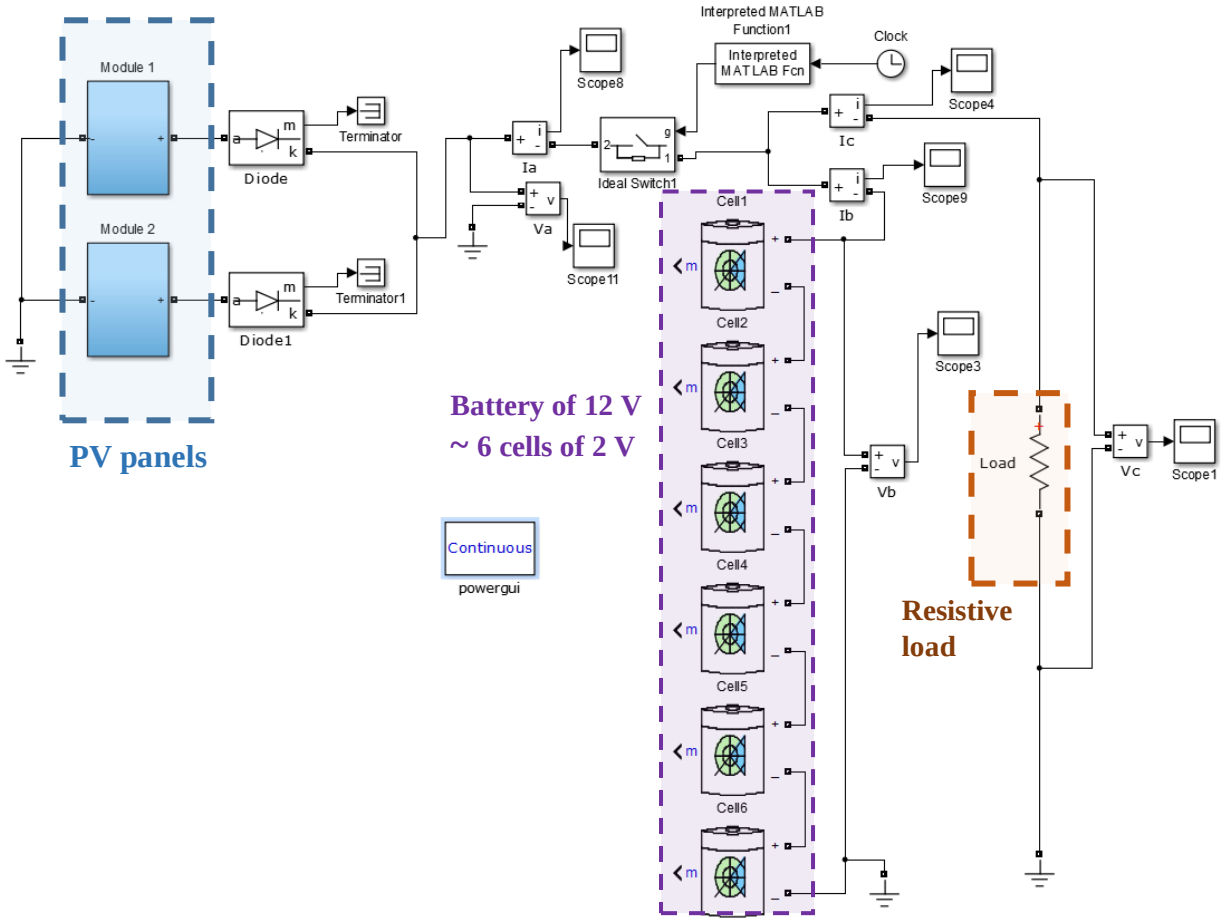


Figure 3.4 Battery cells configuration for fault analysis

Tableau 3-1 Electrical characteristics of SAPV system component

PV panels	Battery	Load
At STC: Pmpp =212 Wp (106×2) Vmpp=17.40 V, Impp=12.20 A Isc=13.08 A, Pvoc=21.60 V	200 Ah (200 Ah for cell) Vs=12 V (2V for cell) SOC0=90% (90% for cell)	P=50 W V=12 V

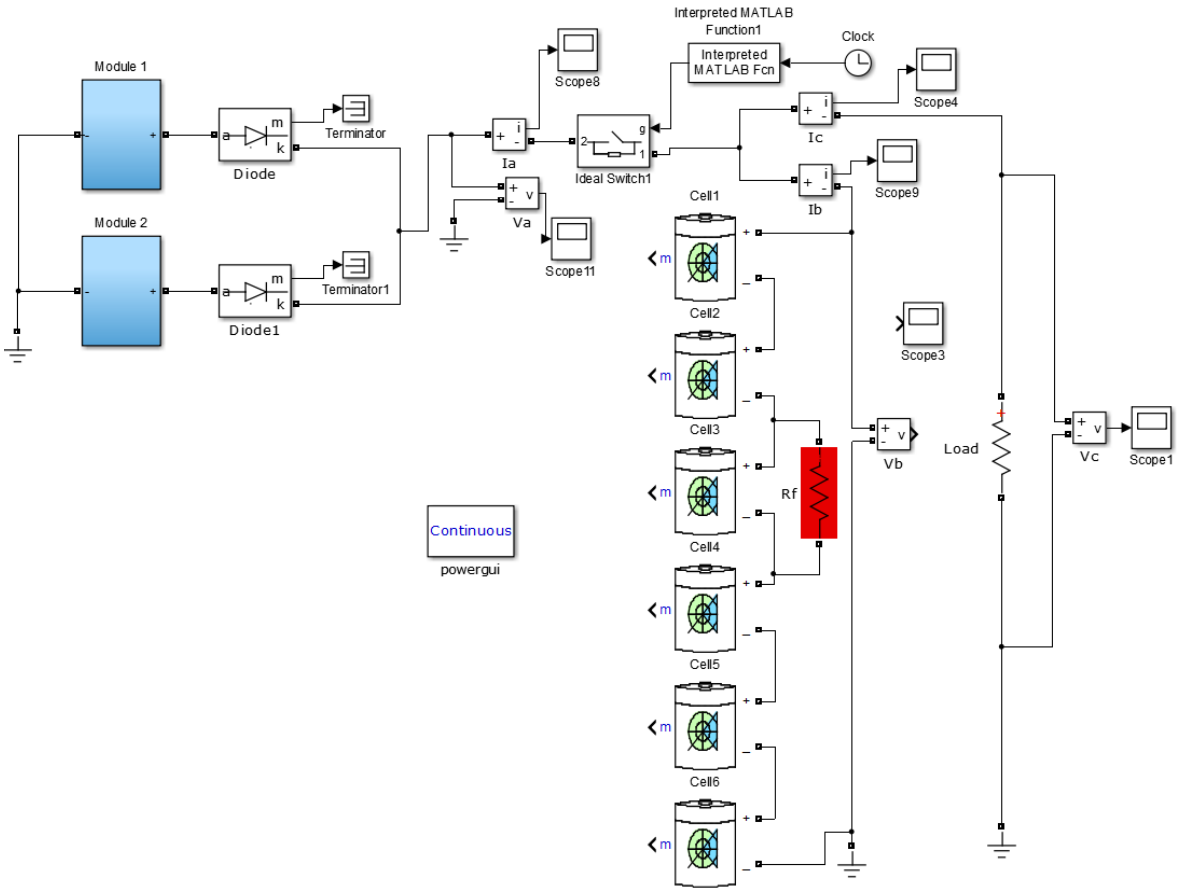


Figure 3.5 Simulation of the battery under short-circuit cell condition

Tableau 3-2 Faults notation in battery

State of battery	**Symbol**
Normal operation	N
Short-circuit one cell	F1
Short-circuit two cells	F2
Short-circuit three cells	F3
Short-circuit four cells	F4
Short-circuit five cells	F5
Short-circuit six cells	F6

3.7 Proposed battery fault detection

This chapter attempts to effectively detect the battery's internal short-circuit that leads to taking immediate and adequate action concerning the defective cells. Regarding the previously discussed battery issues as well as the difficulty of obtaining battery fault data, unsupervised machine learning methods handling unlabeled data address better the faults in the battery. Anomaly detection algorithm is proposed as battery internal short-circuit fault detection. The method has been largely used for fault detection [62], specifically for PV systems [63], [64]. The method benefits from using only unlabeled data during its development. The unlabeled data consist of healthy data or Normal data, this would bring more simplicity, safety, and easy application for a real battery. In addition, the proposed approach basically using only the readily available battery voltage and current to build the anomaly detection model, which will limit using extra sensor circuits. The validation of the method has been done using the simulation data of the previously described battery model included in the simulation.

3.7.1 Anomaly detection

Anomaly detection or known as novelty or outlier detection is one of the most machine learning techniques used in fault detection [65] [66]. Anomaly detection aims to detect abnormal or unusual or wrong data. Anomaly detection assumes that the data are distributed under Gaussian (or Normal) distribution and this last can be modeled using two parameters: the mean μ and the variance σ^2. As a result, the normal data are situated near the mean μ and the outlier data are far away from them as illustrated in Figure 3.6, in which the green dots represent the normal data and the red dots represent the outlier one. Also, it can be seen from this figure that the normal data have a higher Gaussian probability density compared to the outlier data.

Three main steps are required to build the anomaly detection model, the first is the training step, in which the Gaussian distribution is estimated by the parameters μ and σ^2. The second is the validation step, in which some threshold ε is selected as a limit of being an anomaly (outlier) compared to the Gaussian probability function. The third is the testing step, in which a test is performed to check the performance of the model.

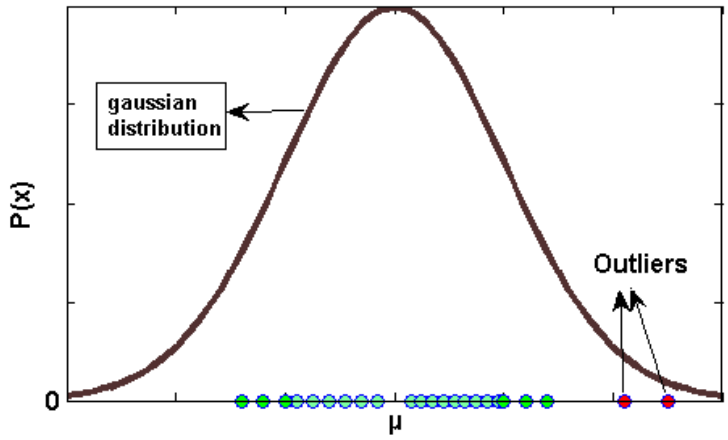


Figure 3.6 Illustration of Gaussian distribution with data

3.7.1.1 Gaussian distribution

Fit a Gaussian model from data relies on the assumption that a huge number of data used is normal. For each feature x_j (j=1,…,n), an estimated Gaussian distribution parameters μ_j and σ_j^2, the Gaussian probability density is defined as:

$$P(x) = \frac{1}{\sqrt{2\pi}\sigma} \exp\left(-\frac{1}{2\sigma^2}(x-\mu)^2 \right) \tag{3.1}$$

3.7.1.2 Estimation parameters for Gaussian distribution

The parameters of Gaussian distribution μ_j and σ_j^2 for the jth feature are respectively estimated as follow:

$$\mu_j = \frac{1}{m}\sum_{i=1}^{m} x_j^{(i)} \tag{3.2}$$

$$\sigma_j^2 = \frac{1}{m}\sum_{i=1}^{m}\left(x_j^{(j)} - \mu_j \right)^2 \tag{3.3}$$

a. Choosing the value of threshold ε

To determine if a sample is an anomaly or not, the procedure consists to compare its Gaussian probability density value to a threshold or a limit. If the probability is lower than a certain threshold ε, then this sample is an anomaly. Hence, the selection of the threshold ε could be done by a trial-

error method using the criteria $F1$ score metric given in equation 3.4. The trial-error method as illustrated in Figure 3.7 proceeds to try several values of ε, in which the selected ε value corresponds to the maximum $F1$ score [62].

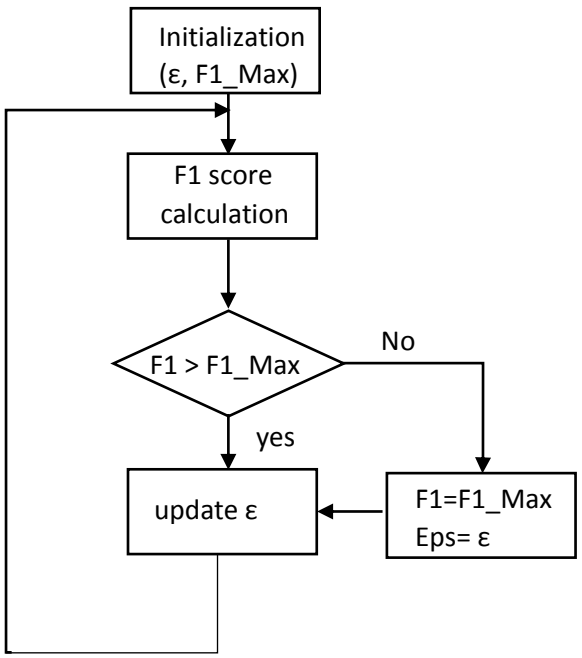
$$F1 = \frac{2 \cdot prec \cdot rec}{prec + rec} \tag{3.4}$$

Where *prec* and *rec* defined below is the precision and the recall respectively:

$$prec = \frac{tp}{tp + fp} \tag{3.5}$$

$$rec = \frac{tp}{tp + fn} \tag{3.6}$$

Where *tp* is the true positive which means that the algorithm successfully classifies it as positive or anomaly. *Fp* is the false positive which means that the algorithm incorrectly classifies it as positive or anomaly. Finally, *fn* is the false negative which means that the algorithm wrongly classifies it as not an anomaly.



3.7.1.3 Results and discussion

A real profile of irradiance and temperature is captured from CDER, Bouzareah, Algeria as shown in Figure 3.8. The profile corresponds to nine clear days and used as simulation input to

Figure 3.7 Flowchart of the procedure to select the threshold ε

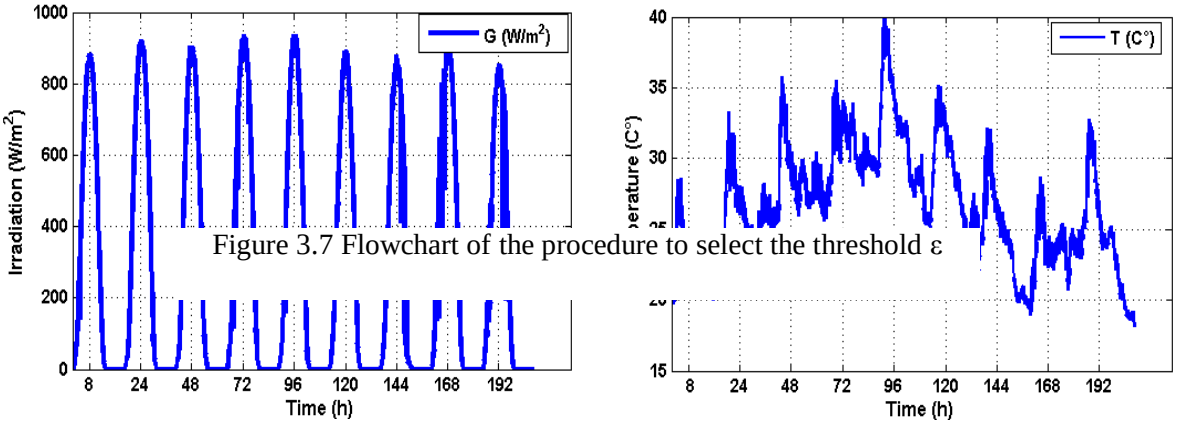


Figure 3.8 Captured irradiance and temperature profile

generate faults and normal data.

To show graphically the ability of the Anomaly detection algorithm to detect the faults in real-time, some faults have been tested. For this purpose, the time evolution of the probability density function is plotted along with the threshold ε before and after the fault occurrence.

The first test performed consists to check the normal operation of the battery as shown in Figure 3.9. The figure shows that the Gaussian probability doesn't drop below the threshold ε which confirms the not presence of a fault. Note that, a small decrease under the threshold into three different regions is marked which can be interpreted as false alarms.

The fault F3 is tested and the result is illustrated in Figure 3.10, in which the graph of the Gaussian probability decreases under the threshold ε after a certain time of the fault occurrence.

A test is performed for the fault F2 as shown in Figure 3.11, in which the graph of the probability density decreases under the threshold ε with a much spent time than F3.

The test of fault F2 is repeated with Rf≈0 as illustrated in Figure 3.12, in which the graph of the probability density instantly drops below the threshold ε and the battery has a high current flow.

The fault F4 is tested and the result is displayed by the graph of the probability density in Figure 3.13, in which the detection of fault is done after a specific time of occurring the fault.

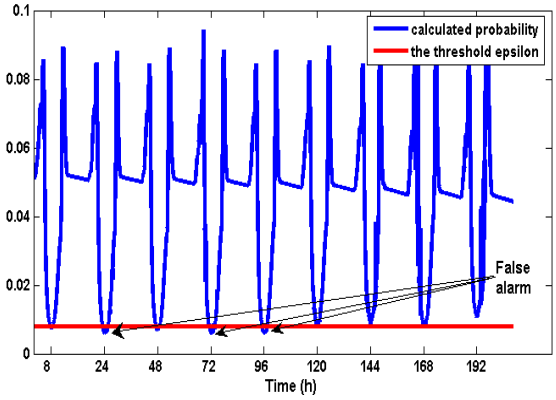


Figure 3.9 Test result : N

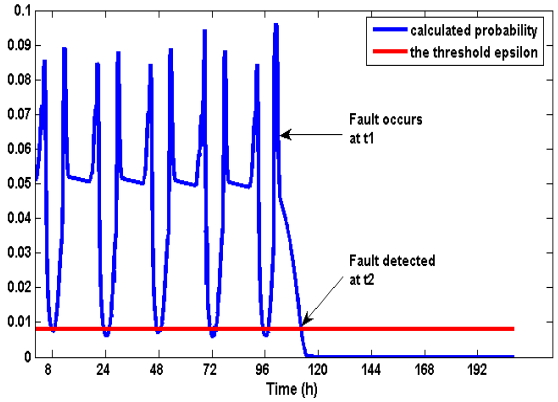


Figure 3.10 Test result : F3

The last test is dedicated to the fault F5 as shown in Figure 3.14, in which the graph of the probability density drops below the threshold after the fault occurrence at a faster time compared to F4, F3, and F2.

The above results demonstrate the capability of the Anomaly detection algorithm to detect all the internal short-circuit fault types. The time of detection of the faults is noted to differ from a

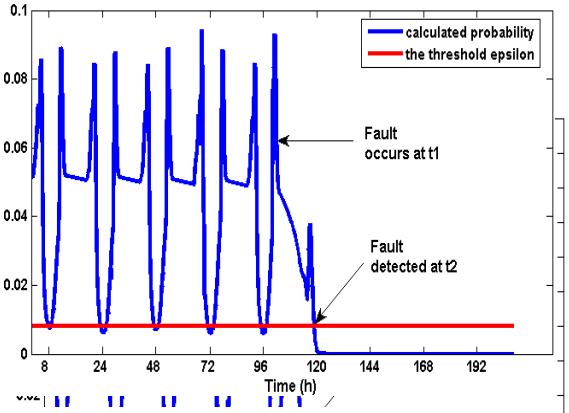


Figure 3.11 Test result: F2

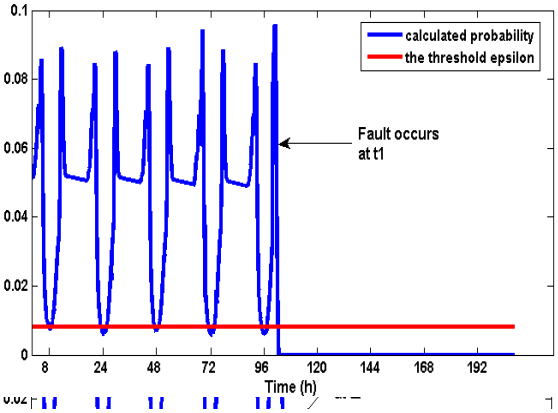


Figure 3.12 Test result: F2 with (R≈0)

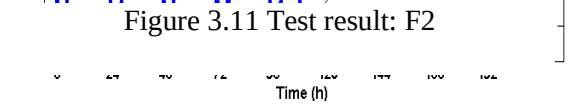


Figure 3.13 Test result: F4

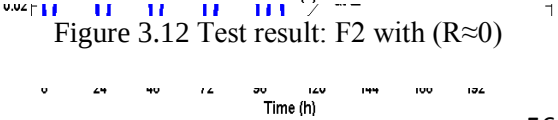


Figure 3.14 Test result: F5

fault to another according to the number of the infected cells and the resistance of the fault circuit.

3.7.2 Proposed battery fault classification

The battery fault classification is an important task that aims to determine the fault types in the battery. Similar to fault detection, fault classification faces the problem of obtaining labeled data of battery faults. To resolve this issue, a supervised Machine learning algorithm based on Support Vector Machine (SVM) is proposed. The method has the advantage of requiring a few numbers of labeled data for training [67] . Another benefit of the method is their higher ability of generalization beyond that of the ANN and HMM algorithm [67]. SVM algorithm has been used in many research areas involving fault diagnosis [68]–[71]. The few numbers of training data required by the SVM are obtained from the battery simulation model described above. In addition, the performance evaluation of the SVM method has been performed using simulation data.

3.7.3 SVM algorithm

As shown in Figure 3.15, SVM aims to find the optimal hyperplane that maximizes the margin distance separating the two classes. The data lies on the margin are the support vectors and those that create a limit boundary. SVM is intended for binary classification, however, it can be extended to multi-class using several ways, such as “one vs one”, “one vs all”, etc. In this work, the’’one vs one’’ is used to construct a C (C-1) /2 binary SVM, where C is the number of classes. Note that each class C represents one type of fault or the healthy state when considering the fault classification problem.

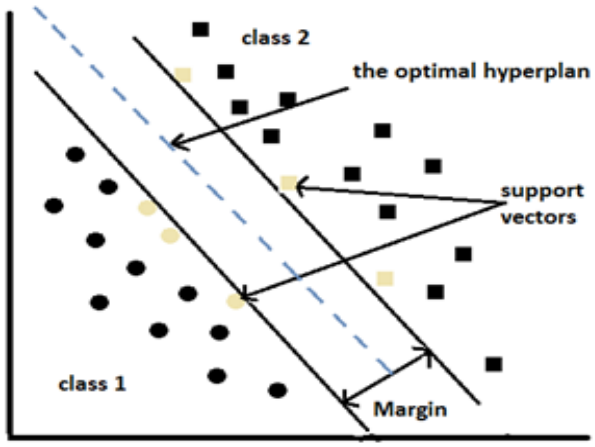


Figure 3.15 Schematic of separating binary class by svm

3.7.3.1 Mathematical formulation

Let the input data x_n (n=1,…,N) , in which N is the number of sample data and y_n is the corresponding output belong to {1,-1} indicating the first and second class. To find the optimal hyperplane separating data, the following minimization problem must be solved [72].

$$\min J(\theta) = \frac{1}{2}\sum_{n,m=1}^{N} \theta_n \theta_m y_n y_m k(x_n, x_m) - \sum_{n=1}^{N} \theta_n \tag{3.7}$$

$$\text{Subject to} \quad \sum_{n=1}^{N} \theta_n y_n = 0 \quad 0 \le \theta_n \le D \quad \text{for} \quad n = 1, ..., N$$

Where the Gaussian kernel function is defined as:

$$k(x_n, x_m) = \exp\left(-\frac{\|x_n - x_m\|^2}{2\sigma^2}\right) \quad \text{and} \quad \theta = \begin{bmatrix} \theta_1 \\ \vdots \\ \theta_N \end{bmatrix} \text{ are the Lagrange multipliers.}$$

The optimization problem in equation (3.7) that would be solved, in which the support vectors $x_1, x_2, \ldots, x_s$ and the corresponding y_n ,θ_n are saved, where s is the number of support vectors.

For a new example given x:

$$h(x) = \begin{cases} 1 & \text{if } sign\left(\sum_{n=1}^{S} \theta_n y_n k(x_n, x) + b\right) \ge 0 \\ -1 & \text{otherwise} \end{cases} \tag{3.8}$$

Where b is the bias value.

3.7.3.2 Results and discussion

A real meteorological profile (irradiance and temperature) captured from the site of CDER as illustrated in Figure 3.16, has been used as simulation input. Note that the simulation of battery faults is carried with R_{fault}=0.1ohm.

The battery fault classification approach is described in the flowchart in Figure 3.17, in which the fault detection using the previous Anomaly detection is running before the adopted SVM algorithm. The data collected from the simulation are 12947 samples which would be used for

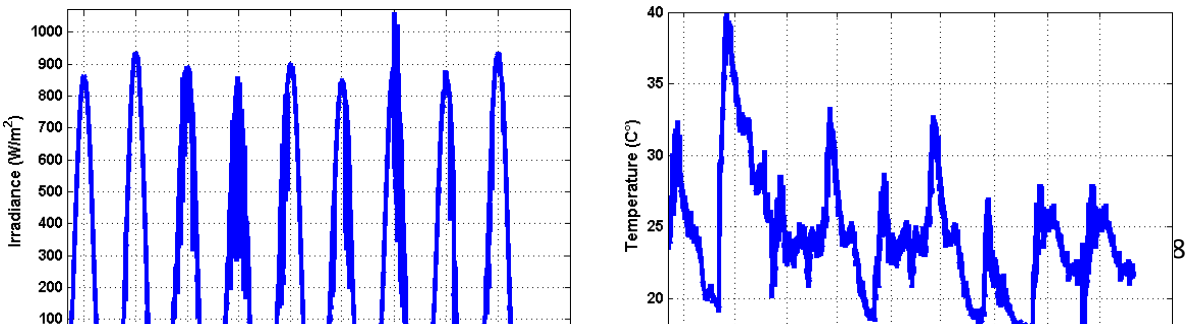


Figure 3.16 Irradiance and Temperature profile

training, validation, and test the Anomaly detection and SVM algorithm.

Table 3-3 shows the fitted parameters and the accuracy obtained from both algorithms. As shown in the table, the number of training data for SVM is less than for Anomaly detection, which is a property of the SVM algorithm. In addition, the high accuracy obtained reveals the effectiveness of both methods as well as the well-fit parameters.

Tableau 3-3 Main training parameters for AD and SVM

	# of training and validation data	Fitted parameters	Accuracy (%)
AD	7193	Th=0.0051	98.22
SVM	1439	$D = 1$ $\sigma = 10$	97.96

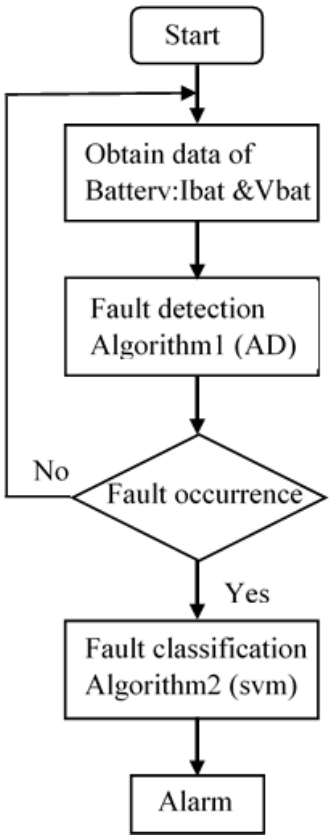


Figure 3.17 Flowchart of the proposed fault diagnosis process

b. Real-time test

A graphical faults monitoring is proposed by showing the progress of faults diagnosis in real-time. For this purpose, the time-variant of the probability density function and the SVM output are plotted separately before and after the faults' occurrence. The predicted classes by SVM are represented by a scatter plot together with the actual classes as a reference to clearly show the difference. Note that in all the tests the SVM algorithm is intentionally running before and after the faults to provide more precision about the faults diagnosis.

The first test is dedicated to the Normal operation, in which the graph of the probability density in Figure 3.18 shows no decrease under the threshold except in two positions which indicate two false alarms. The plot of SVM output is shown in Figure 3.19, in which the Class N is indicated along the test with some misclassified data.

The first tested fault is F1 as illustrated in the fault detection and classification in Figure 3.20 and Figure 3.21 respectively. The graph of the probability density in Figure 3.20 shows a decrease under the threshold after a certain time of fault occurrence. In the meantime, the plot of SVM output in Figure 3.21 spots the fault F1 that mark some delay and misclassified data.

The second tested fault is F3, in which the results of fault detection and classification are shown in Figure 3.22 and Figure 3.23 respectively. The graph of the probability density decreases below the threshold more quickly after the fault occurrence. As well, the plot of SVM output denotes the fault F3 with some delay and misclassified data.

The third tested fault is F6, in which the results of Anomaly detection and SVM algorithm are shown in Figure 3.24 and Figure 3.25 respectively. The graph of the probability density in Figure 3.24 descends immediately after the fault occurrence. The plot of SVM output indicates the fault F6 with some classification errors.

The above faults monitoring graphs show clearly the ability of Anomaly detection and the SVM algorithm to detect and classify the faults in real-time. Considering that some errors in classification and delay in detection are noted, Table 3-4 gives the accuracy value for each fault test to quantify the marked errors. The table shows that the accuracy of Anomaly detection and SVM algorithm to identify the Normal operation is high and is about 98%. Whereas, the accuracy to

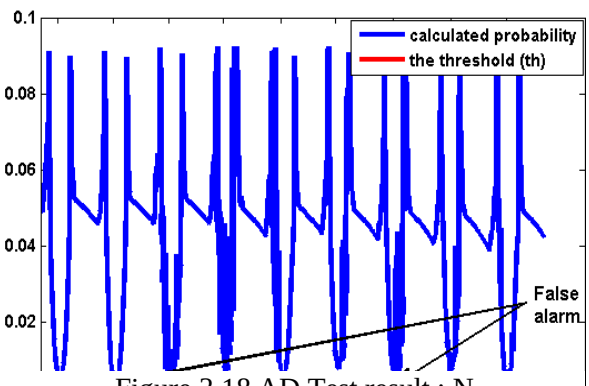


Figure 3.18 AD Test result : N

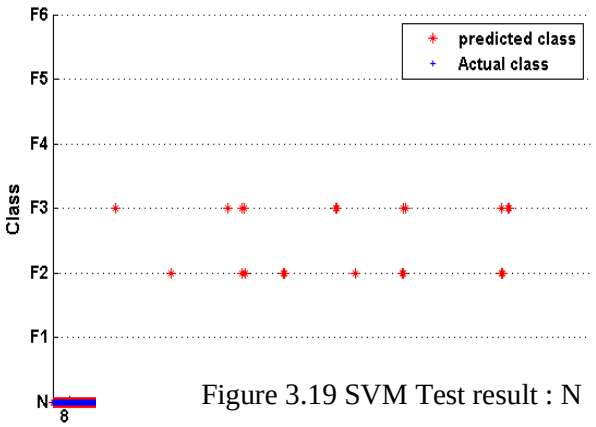
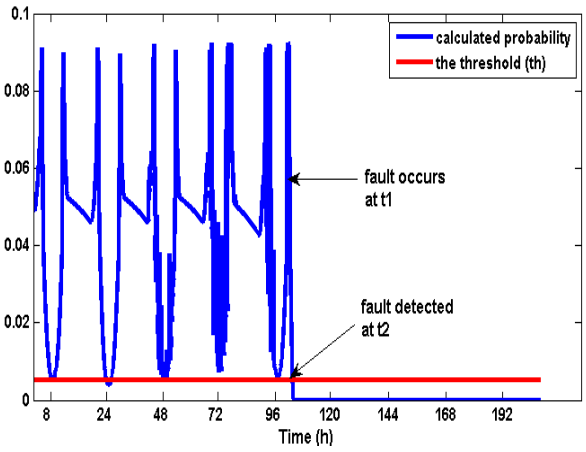


Figure 3.19 SVM Test result : N

assess the faults F1 to F6 ranges from 95% to 98%, in which an elevated battery self-discharge increases the accuracy.



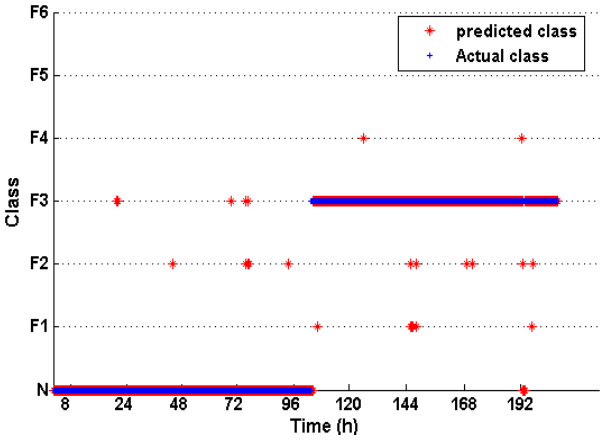


Figure 3.22 AD Test result : F3

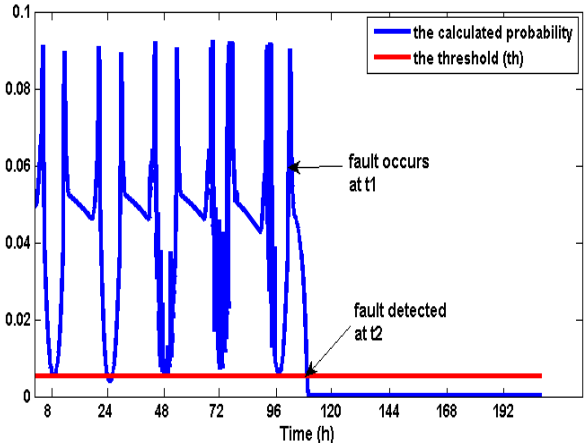


Figure 3.20 AD Test result : F1

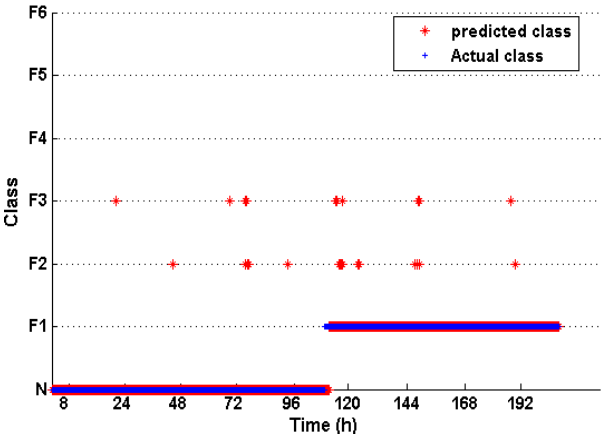


Figure 3.21 SVM Test result : F1

Figure 3.23 SVM Test result : F3

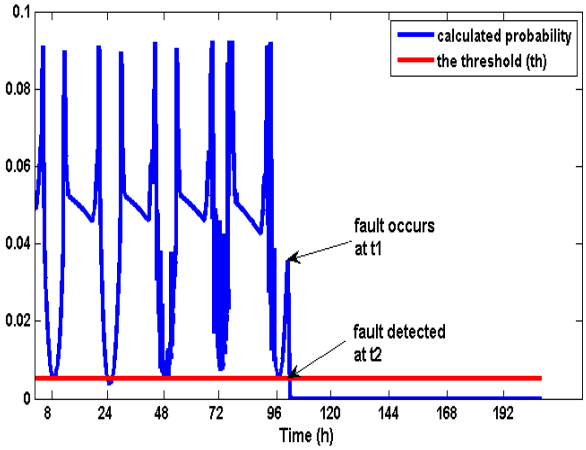


Figure 3.24 AD Test result: F6

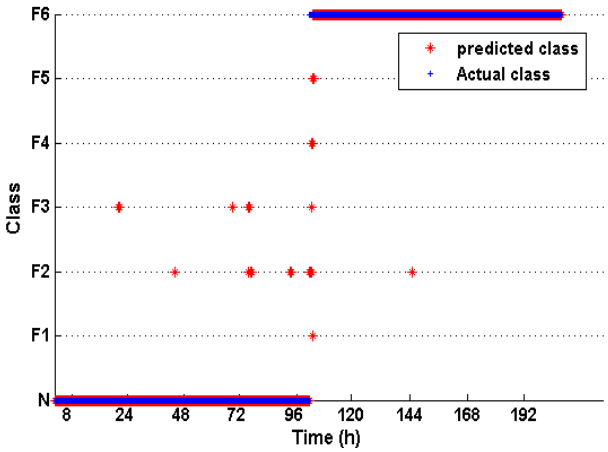


Figure 3.25 SVM Test result: F6

Tableau 3-4 Individual class accuracy with AD and SVM algorithm.

Battery State	AD		SVM	
	# of good classification	Accuracy (%)	# of good classification	Accuracy (%)
N	12813	98.97	12714	98.20
F1	12332	95.25	12411	95.86
F2	12585	97.21	12507	96.60
F3	12678	97.93	12592	97.26
F4	12725	98.29	12583	97.19
F5	12752	98.50	12667	97.84
F6	12777	98.69	12799	98.86

3.8 Conclusion

The battery in the PV system can fail or degrade in a number of ways, which makes fault detection and isolation a very complicated task. This chapter proposes battery short-circuit cell faults monitoring using anomaly detection and SVM algorithm. The proposed methods present several advantages over other training algorithms. The anomaly detection is developed through

Normal data that can be easily obtained, furthermore, the data consists simply of battery voltage and current taken for a period of time. The SVM classification algorithm requires a few numbers of training data for its development and has a high generalization ability. Both methods are very consistent with the battery faults cases.

The proposed methods have been developed and validated using simulation data of the battery, in which an adequate battery simulated model has been adopted. Real-time monitoring is carried out to demonstrate the feasibility of both methods to recognize the faults, in which the anomaly detection and SVM output are plotted in real-time before and after the fault. The results show the ability to detect the faults with fewer errors that are quantified by the accuracy metric for each fault class.

Chapter: 4 Fault diagnosis in stand-alone photovoltaic system using Artificial Neural Network

4.1 Introduction

The fault that occurs in a stand-alone photovoltaic system can affect the entire system's performance, leading to a possible fire hazard, battery explosion, and DC arc. A fault classification approach using supervised machine learning Artificial Neural Network (ANN) is proposed to properly detect and identify the fault in the system. The method has been validated using experimental data of the set up small-scale SAPV system at the university of Médea. The established faults experiment consists of a short circuit of PV module, an open circuit of PV module, and an external battery short-circuit. The effectiveness of the proposed fault detection and classification (FDD) has been verified, in addition, Graphical User Interface (GUI) Matlab has been created to achieve an automatic fault diagnosis.

Section two attempts to enhance the previous FDD based on ANN by using power loss parameters as input networks. Furthermore, because of the difficulties in obtaining data of fault from a real SAPV system, an improvement in obtaining data has been made. Data of normal operation is obtained from a real measurement, when simplicity and safety are concerned, whereas, fault data are obtained from the simulation using the developed model environment in chapter 2. Three common types of ANN were trained, tested, and compared to choose the most efficient network to predict the faults in the system. The results indicate that Multi-Layer-Perceptron (MLP) network type is the most accurate network to recognize the faults with 95%. In addition, some test has been carried out in real-time to show its effectiveness.

4.2 ANN and the brain (motivation)

Artificial Neural Network (ANN) is originally inspired by a biological neural cell, where this last as shown in Figure 4.1 is constituted of three main elements: dendrite, nucleus, and axon. The role of the dendrite is to carry the information to the neuron, whereas the axon transfers the information to the other neurons, and finally the cell body that contains the nucleus connects the dendrite and axon. The concept of ANN returns to mimic the human brain as this one can learn to process all our senses, like sight, hearing, touching, etc. Also, the brain can learn to do many other things such as calculus and language.

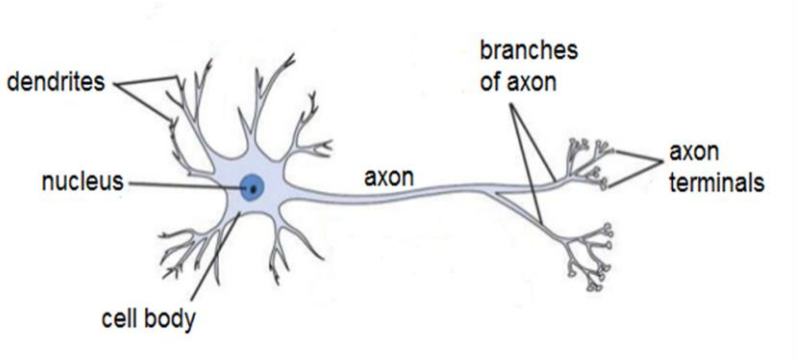


Figure 4.1 Schematic of a biological neuron

A famous experiment has been done by neuroscientists called ‘‘Neuro-rewiring experiments’’, in which they cut in animal brain the wire from the ears to the auditory cortex (a part of the brain responsible for hearing). This wire takes the sound signal from the ears and processes to hear, then they rewire the auditory cortex part with the eye wire that was previously connected to the optic nerve (the part of the brain responsible for seeing). Therefore, the signal from the eyes is getting routed to the auditory cortex.

The results of this experience reveal that the animal performs really a visualization task which explains that the auditory cortex truly learns to see. A similar result can be obtained if we rewire with another part of the brain, such as the somatosensory cortex that processes the sense of touch. In this case, the somatosensory cortex will learn to see. From these examples, it can be concluded that if the same physical part of the brain can process sound or touch, or sight, then it might be one learning mechanism that can perform all these senses and that which makes the brain learn by itself.

ANN is an approximation to the brain learning mechanism interpreted by a computer implementation of a learning algorithm that deals with the different types of data and learns from it. Nowadays ANN is becoming the state of art for many applications, in which ANN strongly benefits from the progress of computer tools in terms of speed to run a large scale ANN.

4.3 The basic concept of ANN

4.3.1 Single neuron Perceptron

The first artificial neuron was introduced by McCulloch and Pitts [73] to compute any arithmetic or logical function. Then Rosenblatt developed the perceptron class to solve pattern recognition problems [74]. The perceptron constitutes a building block for the Neural network, in which, it consists mainly of weights (w), bias (b), and activation function ($f\ (a)$) as shown the Figure 4.2. The input x_i are multiplied by the weights w_i and then pass to the summing unit as well

as the bias *b*. Then an activation function *f (a)* is applied to the resulting sum in order to calculate the neuron output as given below:

$$f(a) = f\left(\sum_{i=1}^{n} w_i x_i + b\right) \tag{4.1}$$

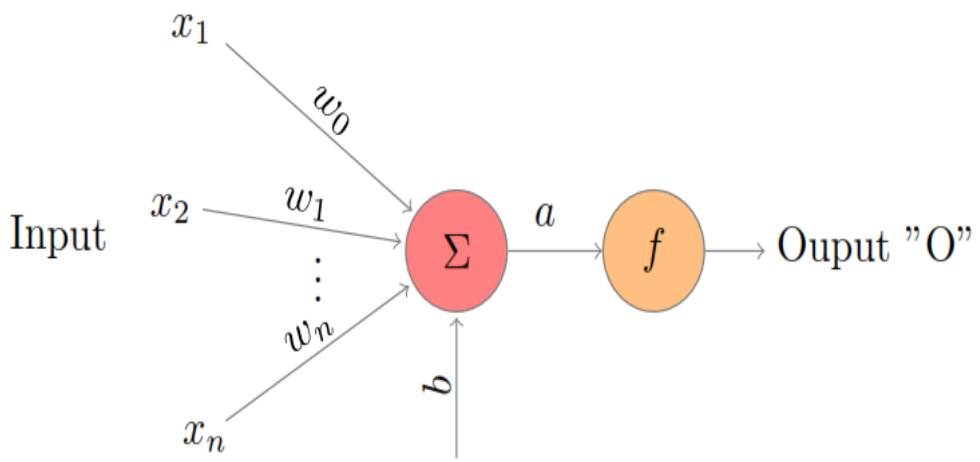


Figure 4.2 Neuron perceptron model

If the activation function takes the form of a step function, then the output of a neuron can be either 0 or 1. In this case, the perceptron performs a classification task of input data x_i that divides it into two regions as shown in Figure 4.3. The linear boundary (hyperplane) that separate the two regions is defined by:

$$\sum_{i=1}^{n} w_i x_i + b = 0 \tag{4.2}$$

The key contribution ported by Rosenblatt was the introduction of learning rule, that adjust the weights and biases of the network in order to correctly classify all the input data into two categories as shown in Figure 4.3.

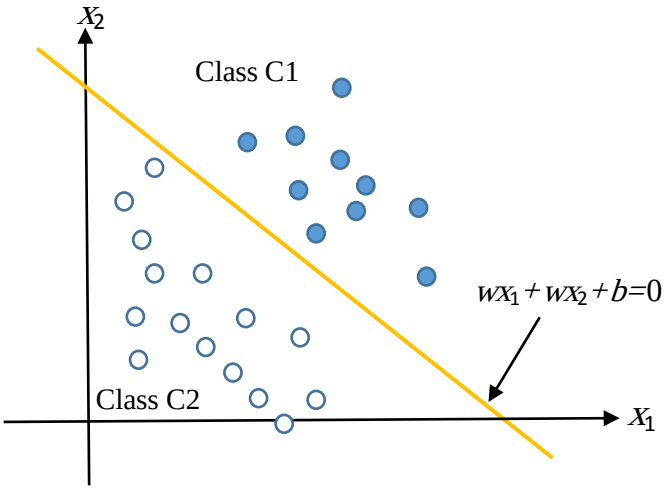


Figure 4.3 Decision boundary for two input

4.3.2 Multi layer perceptron

The single layer perceptron showed some limitations when generating a linear boundary, since many classification problems are not linearly separable. To overcome this limitation Rosenblatt proposed a more complex network called Multilayer Perceptron (MLP), in which this network consists of one input layer, one or more hidden layer, and one output layer [75]. Note that the output of each layer is the input to the next layer as shown in the example of MLP with a three-layer in Figure 4.4. Rosenblatt has failed to extend their learning rule to the MLP network, which caused the suspension of ANN for a decade until the discovering of the backpropagation training

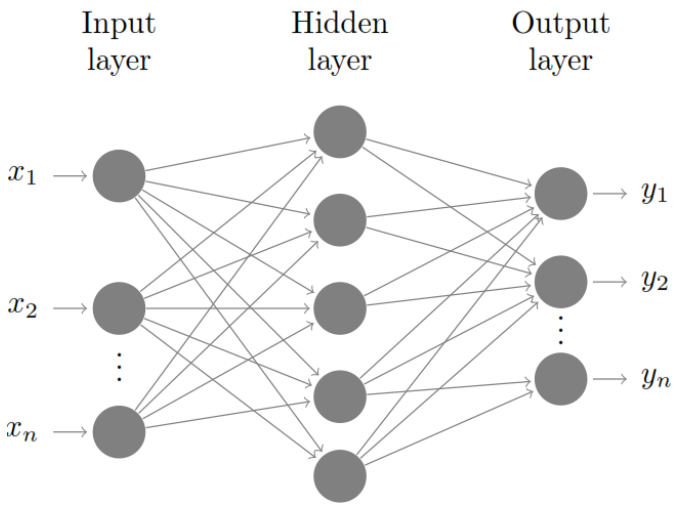


Figure 4.4 Three layer Network

algorithm for the MLP network in 1980 to solve many non-linear problems [76].

4.3.3 Backpropagation Training algorithm

The backpropagation (BP) algorithm for training MLP networks has played an important role in the resurgence of neural network interest. To date, the BP training algorithm remains the most widely used [77], [78]. The algorithm will adjust the weights and biases of the network by minimizing a cost function (quadratic error) using essentially a numerical optimization gradient descent.

The errors between the targets and computed output network can be expressed in terms of mean square error (*MSE*) or sum square error (*SSE*). The most widely used is *MSE* that is defined for *Q* training data as follows:

$$E = MSE = \frac{SSE}{Q} = \frac{1}{Q}\sum_{q=1}^{Q}(T_q - O_q)^2 \tag{4.3}$$

The summarized feedforward BP algorithm [79] for the input data set $P = [P_1, P_2, \ldots, P_Q]$ with the targets $T = [T_1, T_2, \ldots, T_Q]$ and computed outputs $O = [O_1, O_2, \ldots, O_Q]$ is given below:

1. Propagate the input forward the network, by computing all the activation:

$$a^0 = P \tag{4.4}$$

$$a^{m+1} = G^{m+1}(w^{m+1}\, a^m + b^{m+1}) \tag{4.5}$$

for $m = 0,1,..., M-1$. and $z^{m+1} = w^{m+1}a^m + b^{m+1}$

$$a = a^M \tag{4.6}$$

Propagate the sensitivities backward the network:

$$s^M = -2G'^M(z^M)(T-a) \tag{4.7}$$

$$s^m = G'^m(z^m)\,(w^{m+1})^T\, s^{m+1} \tag{4.8}$$

2. Update the weights and biases by the following gradient descent:

$$w^m(k+1) = w^m(k) - \alpha s^m (a^{m-1})^T \tag{4.9}$$

$$b^m(k+1) = b^m(k) - \alpha s^m \tag{4.10}$$

where α is the learning rate.

The basic BP with gradient descent suffers from its long time of convergence resulting in choosing a small value of learning rate α. To improve the convergence speed of the algorithm, the researcher looks for fast training algorithm by developing heuristic techniques such as varying the learning rate using momentum and rescaling variables [79]. Other research has focused on standard numerical optimization algorithms since the training of MLP refers to a numerical minimization problem. These methods have been successfully applied in this context [79], in which Levenberg-Marquardt and conjugate gradient algorithm provide fast convergence of BP.

4.3.4 Levenberg-Marquardt algorithm

Levenberg-Marquard (LM) algorithm is a well-suited training algorithm for neural networks. This technique uses a modification to the Gauss-Newton's method [75], [79]–[81], in which the mean square error defined below is used as a performance metric.

$$E = \sum_{q=1}^{Q} (T_q - O_q)^T (T_q - O_q) = \sum_{q=1}^{Q} e_q{}^T e_q = \sum_{q=1}^{Q} \sum_{j=1}^{C^M} (e_{j,q})^2 \tag{4.11}$$

For Q training data and C neurons at layer M, where $e_{j,q}$ is the j^{th} element of the error in the q^{th} input/target.

The modification to the Gauss-Newton method is given as:

$$\Delta x = \left[J^T(x)\ J(x) + \mu\, I \right]^{-1} J^T(x)\, v(x) \tag{4.12}$$

where $J(x)$ is the Jacobian matrix expressed as follows:

$$J(x) = \begin{bmatrix} \frac{\partial v_1(x)}{\partial x_1} & \frac{\partial v_1(x)}{\partial x_2} & \cdots & \frac{\partial v_1(x)}{\partial x_n} \\ \frac{\partial v_2(x)}{\partial x_1} & \frac{\partial v_2(x)}{\partial x_2} & \cdots & \frac{\partial v_2(x)}{\partial x_n} \\ \vdots & \vdots & \ddots & \vdots \\ \frac{\partial v_N(x)}{\partial x_1} & \frac{\partial v_N(x)}{\partial x_2} & \cdots & \frac{\partial v_N(x)}{\partial x_n} \end{bmatrix} \tag{4.13}$$

The key step in the LM algorithm is the computation of the Jacobian matrix that returns to compute the derivatives of the errors, for this last, we put:

$$v^T = [v_1\, v_2 \ldots v_N] = [e_{1,1}\, e_{2,1} \ldots e_{c^M,1}\, e_{1,2} \ldots e_{c^M,Q}] \tag{4.14}$$

$$x^T = [x_1\, x_2 \ldots x_n] = [w^1_{1,1}\, w^1_{1,2} \ldots w^1_{c^1,R}\, b^1_1 \ldots b^1_{c^1}\, w^2_{1,1} \ldots b^M_{c^M}] \tag{4.15}$$

In the following , a summarized BP training method with the LM algorithm is given [79]:

1. Propagate all the input to the network in order to compute the corresponding output using (Eq.4) and (Eq.5).
2. Calculate the errors $e_q = T_q - O_q$ and the error E in (Eq.11).
3. Compute the sensitivity vector as:

$$s_q^M = -G'^M(z_q^M) \tag{4.16}$$

$$s_q^m = G'^m(z_q^m)\, w^{m+1}\, s_q^{m+1} \tag{4.17}$$

4. Compute each element of the Jacobian matrix for weight and bias respectively as follows:

$$[J]_{h,l} = \frac{\partial v_h}{\partial x_l} = \frac{\partial e_{k,q}}{\partial w_{i,j}^m} = s_i^m\, a_{j,q}^{m-1} \tag{4.18}$$

$$[J]_{h,l} = \frac{\partial v_h}{\partial x_l} = \frac{\partial e_{k,q}}{\partial b_i^m} = s_i^m \tag{4.19}$$

5. Solve the (Eq.12) to obtain Δx.
6. Update the new value $x+\Delta x$ and recompute E of (Eq.11), if the error E is smaller than computed in step 1, then reduce μ by factor β, let $x= x+\Delta x$ and go back to step 1, if the error E is not reduced, then increase μ by factor β and go back to step 3.

4.4 Application of ANN for FDD in SAPV system

ANN has been widely utilized for fault detection and classification [82] due to its high ability to approximate any non-linear function and its strong resistance to noise data [83]. The ANN provides an excellent discriminative tool for data using the historical data and the learning property. Over the past decade, most research on FDD using ANN in the field of PV systems has conducted for the grid-connected and DCPV system [35], [84]–[88]. Hence, this chapter proposes FDD in the SAPV system using ANN. The ANN detection model classifies the data into ‘’Faulty’’ and ‘’Normal’’, whereas the ANN diagnosis model classifies the data in one of the following fault types: ‘‘short circuit of PV module’’, ‘‘Open circuit of PV module’’, ‘‘external battery short-circuit’’. The proposed ANN method has been validated using experimental data issued from the benchmark SAPV system installed at LREA, University of Médéa, Algeria. The data collected from the system are pre-processed and randomly divided into training-set and test-set. Figure 4.5 shows the main steps to build both ANN fault detection and diagnosis from the top to the down.

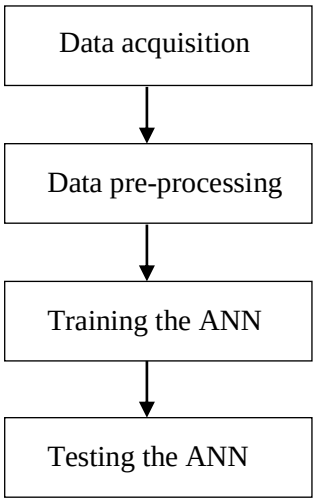


Figure 4.5 Steps to develop ANN prediction model

4.4.1 Data acquisition

4.4.1.1 Experimental SAPV system

The mounted benchmark SAPV system at the university of Médea is composed of 2 PV modules connected with a battery and a load by means of a charge regulator as described in Figure 4.6. The PV module is a monocrystalline type with a nominal power of 90 Wp, whereas the battery is a lead-acid type of 12 V in which the charge regulator does not integrate the MPPT. A Halogen lamp is used as an appliance, which is considered as DC load. The intentionally created faults on the system as illustrated in Figure 4.7 consist of the short-circuit of PV module (F1), open-circuit of PV module (F2), external battery short-circuit (F3). The electrical characteristics of each component are given in Table 4-1.

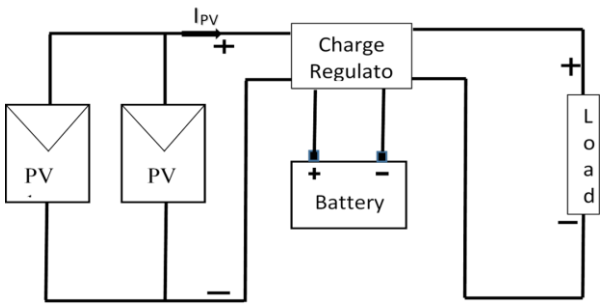


Figure 4.6 Small SAPV System

Tableau 4-1 Electrical experimental Characteristics of SAPV System

Component	Electrical characteristics
PV modules	Pmax=180 Wp (2×90) Vmpp=18.25 V,Impp=9.86 A, Vsc=21.98 V, Isc=11.08 A
Battery	70 Ah (C20) AGM Battery VS=12 V
Charge Regulator	30 A PWM Charge Regulator
Load	50 W Halogen Lamp

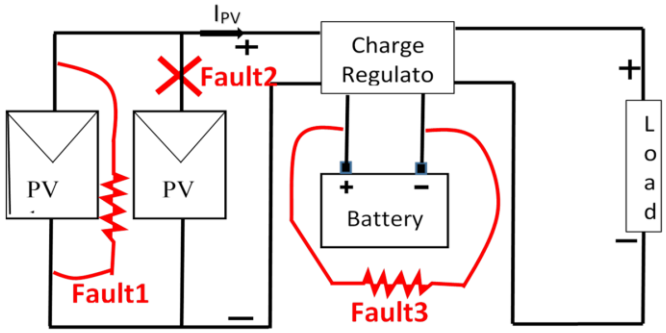


Figure 4.7 Faults Created in SAPV system

4.4.1.2 Data acquisition facilities

DSpace DS 1104 controller board is used to acquire the data from the experimental SAPV system as illustrated in Figure 4.8. This acquisition card offers a Real-Time Interface (RTI) that allows interfacing with the different sensors of the SAPV system. Also, DSpace provides ControlDesk software that allows to monitor and control the measurements in real-time. Finally, the DS 1104 board has 8 ADC channels in total which connect with a computer via a PCI slot.

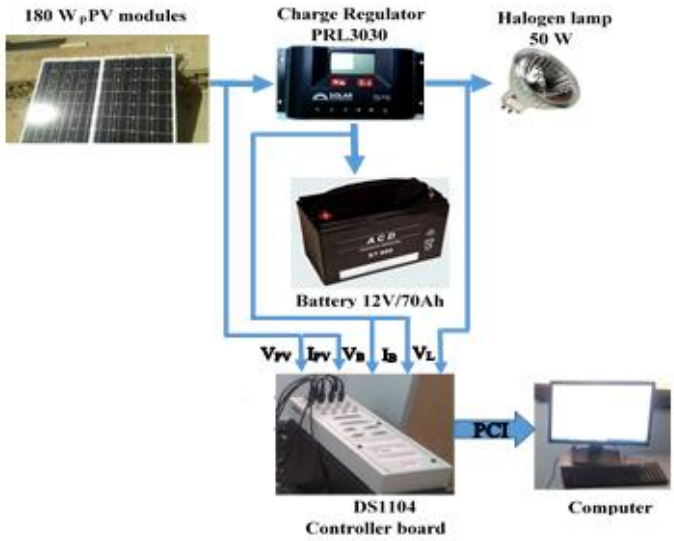


Figure 4.8 Data aquisition facilities from SAPV system

The data acquired consists of the electrical voltage and current of PV modules, battery, and load using the current and voltage sensor Fluke i30s and GW Instek DDP-100, respectively. Figure 4.9 shows the acquisition system facility, in which the acquisition sampling time was set to 1 min to better cover the system operation.



Figure 4.9 Experiment facilities at LREA, Médéa University (Algeria)

4.4.2 Data pre-processing

The data collected from the operation of the SAPV system under Normal and faulty conditions must be pre-treated and cleaned firstly. The total number of data collected is 1746 samples which correspond to their respective class. Data Normalization is applied to speed up the ANN algorithm convergence, this can be done by making the data in the same scale generally between [-1,1] using the formula below:

$$y = \frac{(y_{max} - y_{min})(x - x_{min})}{(x_{max} - x_{min})} + y_{min} \tag{4.20}$$

Where y is the normalized data limited between y_{max}=1 and y_{min}= -1, x is the initial data which has a maximum value x_{max} and minimum value x_{min}.

4.4.3 ANN Configuration

Three layer feedforward ANN is adopted as a structure for ANN FDD in the SAPV system. The input layer contains 6 neurons that correspond to the electrical variable voltage and current of PV modules, battery, and load. The output layer corresponds to the number of faults class together with The Normal class. The hidden layer contains 25 neurons obtained from the trial & error method. The structure of both ANN fault detection and diagnosis is shown in Figure 4.10 and Figure 4.11, respectively. The activation function used is tangent sigmoid (*tansig*) in the hidden layer and log sigmoid (*logsig*) in the output layer that has a binary output (1 or 0) [77]. A binary code at the output layer is resulted to specify each class as indicated in Table 4-2 and Table 4-3.

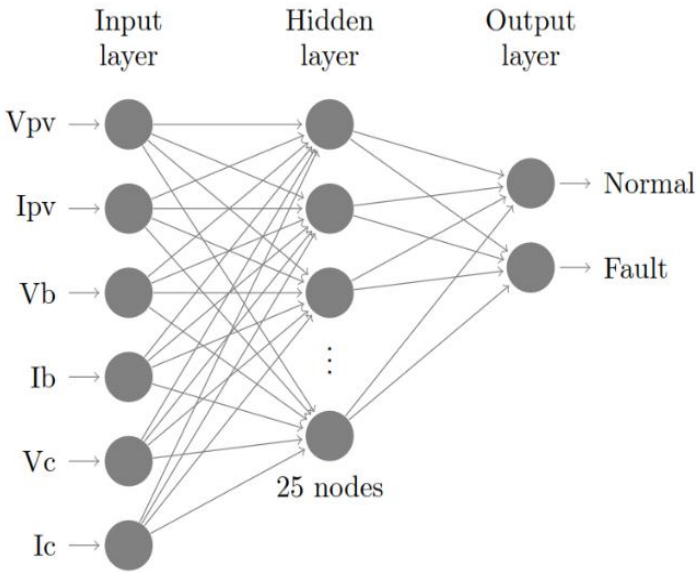


Figure 4.10 ANN structure for fault detection

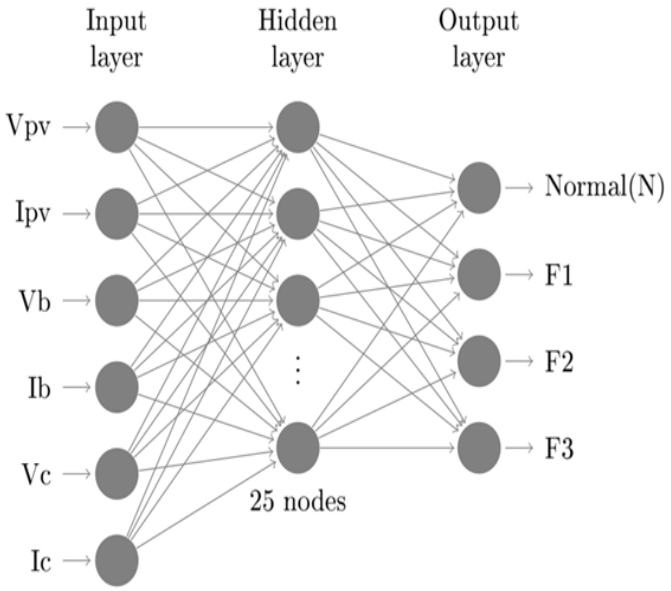


Figure 4.11 ANN structure for fault diagnosis

The size of the training data set is 1397 samples distributed into Normal and faulty operation. Backpropagation with the Levenberg-Marquardt algorithm (BPLM) is used to train both networks, where the value of the error goal is fixed in 0.01 which is sufficient to give a good classification accuracy.

Tableau 4-2 Output vector of ANN fault detection

State of SAPV system	**Specified vector**	
	Y_1	Y_2
Normal	1	0
Fault	0	1

Tableau 4-3 Output vector of ANN fault diagnosis

State of SAPV system	**Specified vector**			
	Y_1	Y_2	Y_3	Y_4
Normal (N)	1	0	0	0
F1	0	1	0	0
F2	0	0	1	0
F3	0	0	0	1

4.4.4 Training, and Test results

To check the performance of training, a learning curve is established for both networks of detection and diagnosis as shown in Figure 4.12 and Figure 4.13 respectively. The result of the ANN detection model in Figure 4.12 achieves the value of the error goal after 26 iterations, whereas the ANN diagnosis model in Figure 4.13 reaches the target after 29 iterations. Both results indicate that the network's parameters (weight and bias) are adopted and the structures are adequately designed.

To evaluate the performance of both networks, a test using the confusion matrix metric is considered as shown in the first test with 394 samples in Figure 4.14 and Figure 4.15. The confusion matrix shows the percentages of correct and incorrect classified data. The rows correspond to the predicted class (Output class) and the columns correspond to the actual class (Target class). The matrix diagonal in green squares corresponds to the correct classified observations. The off-diagonal matrices in the red squares correspond to the incorrect classified observations. Each cell has both numbers of observations and percentages of the total number of observations.

The column on the far right with grey squares shows the percentages of all the examples predicted to belong to each class that is correctly and incorrectly classified. These two metrics correspond respectively to precision (or positive predictive value) and false discovery rate. The row at the bottom with grey squares shows the percentages of all examples belonging to each class that is correctly and incorrectly classified. These two metrics correspond respectively to recall (or true positive rate) and false-negative rate.

The classification accuracy obtained for the first test is 95.1% and 96 % for the ANN fault detection and ANN fault diagnosis respectively. Figure 4.14 shows that the misclassified data (4.9 %) are wrongly distributed into a fault (2.6%) and a Normal (2.3%). Figure 4.15 marked 4% of misclassified data mostly situated in the first class (2%) followed by the second and third class whether by 0.9 %, while the fourth contains the less misclassified data (0.2%).

A confusion matrix of total data (training and test) is performed, in which the results are illustrated in Figure 4.16 and Figure 4.17 for ANN fault detection and ANN fault diagnosis model, respectively. The figures indicate a classification accuracy of 98.3% and 97.4% for the detection and diagnosis model, respectively. The results show the high ability of ANN to predict the faults in

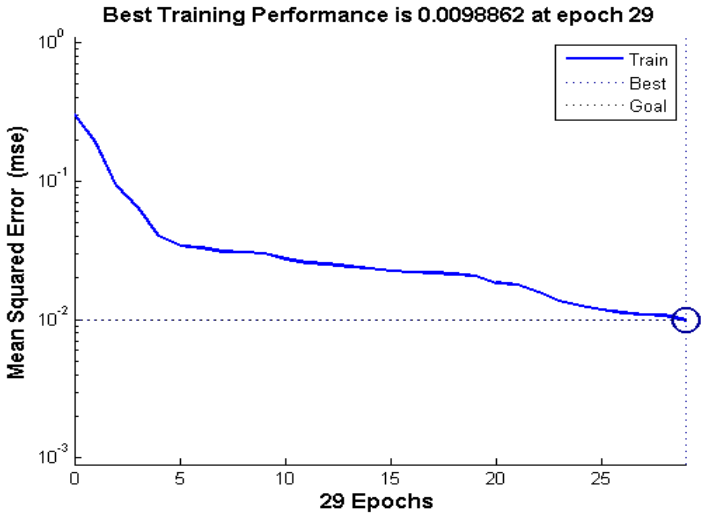


Figure 4.12 Learning curve of ANN fault detection

the SAPV system.

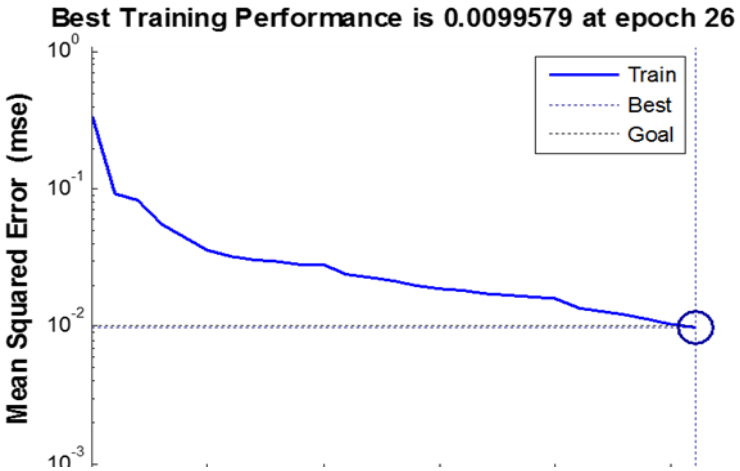


Figure 4.13 Learning curve of ANN fault diagnosis

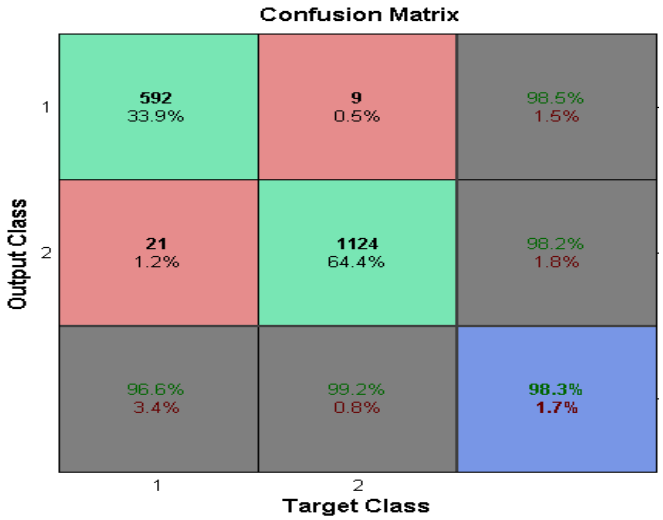


Figure 4.14 Confusion matrix of test ANN detection model

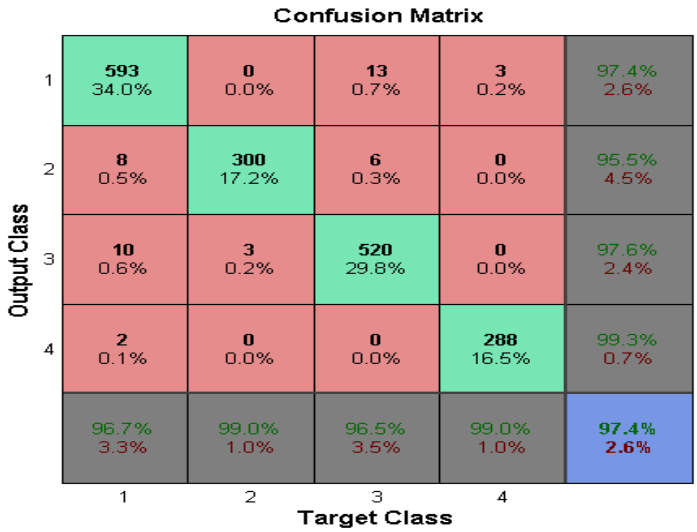


Figure 4.16 Confusion matrix of test ANN diagnosis model

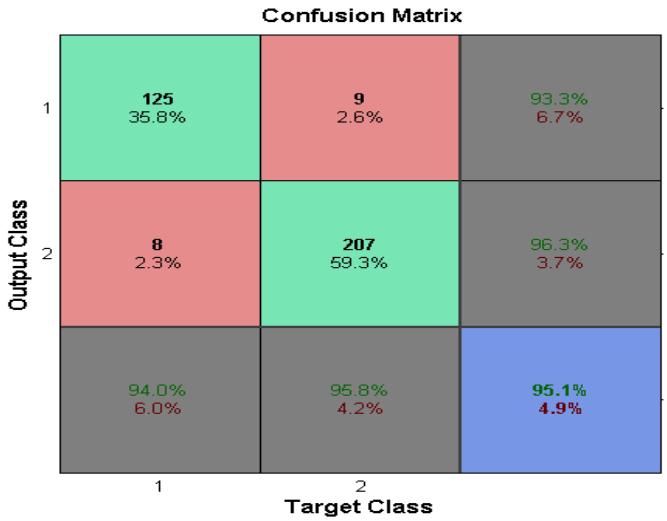


Figure 4.15 General accuracy of ANN detection model

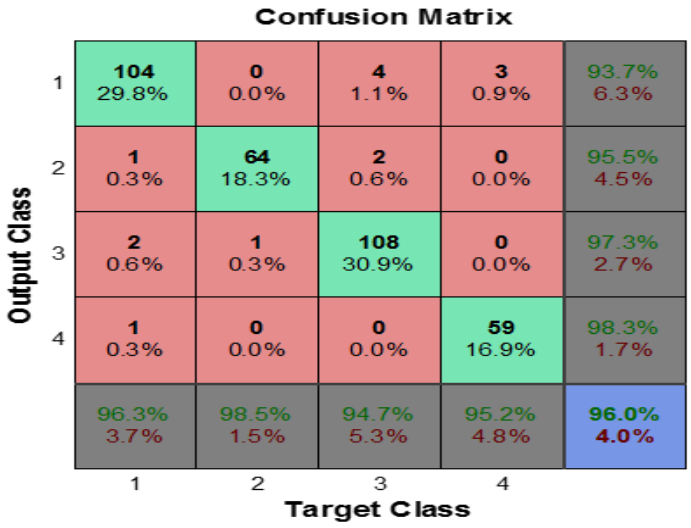


Figure 4.17 General accuracy of ANN diagnosis model

4.4.5 Matlab GUI Integration with the system

A Graphical User Interface (GUI) using Matlab/Simulink is created for predicting the faults in the SAPV system using the trained ANN models. Instead of obtaining directly the ANN output that consists of the binary code, the interface shows the classification result in an easy manner as shown in Figure 4.18. The process of FDD associated with GUI Matlab is described in the flowchart in Figure 4.19. The flowchart proceeds by obtaining and normalizing the data, then a fault detection is executed using ANN. If a fault occured, a classification by ANN is performed and the result is displayed through the interface. Otherwise, the procedure is repeated from obtaining the data.

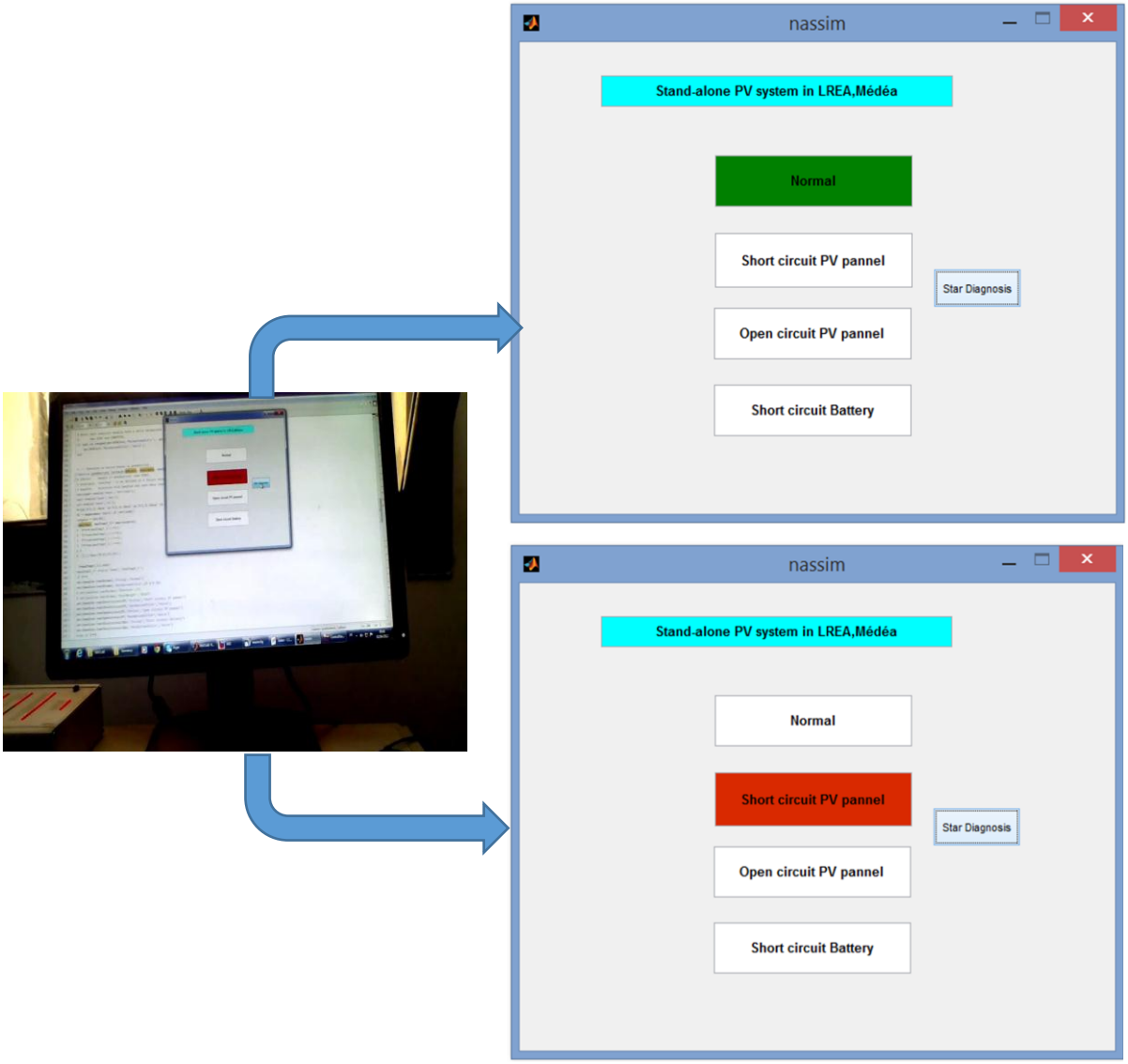


Figure 4.18 Computer implementation of GUI matlab

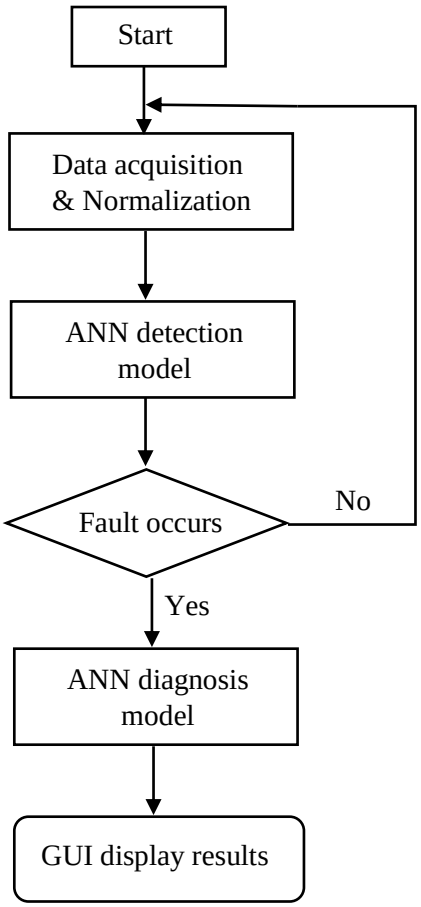


Figure 4.19 Flowchart for fault detection and diagnosis by ANN

4.5 Enhacement of power losses analysis by ANN

4.5.1 Background

Due to the limitations of power loss parameters to determine the fault type in the SAPV system (see Section 1.3.7). ANN is proposed to predict the fault using power loss parameters as ANN inputs. The main advantages of the proposed method are the utilization of two technics: power loss parameters to determine the losses in the system, and ANN to predict the faults. Another benefit is the flexibility of obtaining data from simulation and experimental to build an ANN fault prediction model. Faults data are obtained from simulation which can be more secure and different fault scenarios can be run. Normal data are obtained from the real experiment, in which simplicity and availability are the most common.

4.5.2 Methodology

The supervised machine learning ANN has been used in many research subjects of regression and classification[80]. Regarding the complexity to diagnose the failure in the SAPV system using power loss analysis, ANN is used to remove that uncertainty. The steps to build up the improved ANN fault diagnosis are described in Figure 4.20. First, data extraction is done from the measurements for normal operation of the system, and from the simulation for the created faults. Second, a calculation of the main power loss parameters such as Yr, Ya, Yf, Lc, and Ls for different days. Third, data normalization is applied using equation 4.20 to speed up the ANN convergence. Finally, train the ANN model and test it for validation.

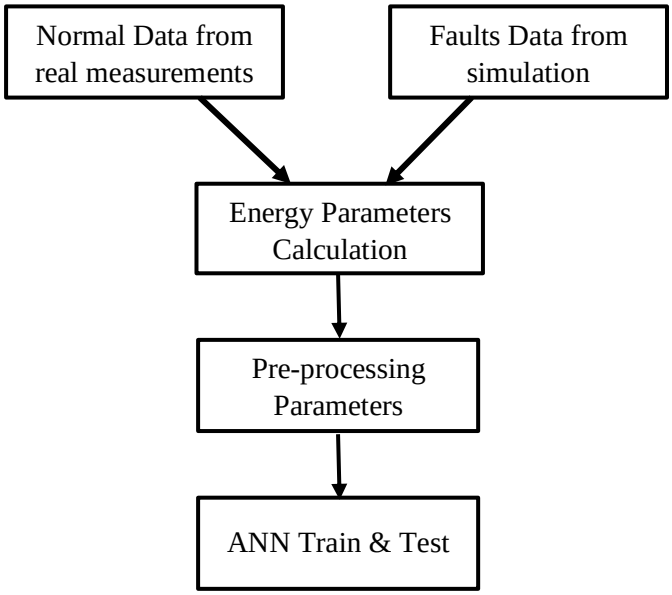


Figure 4.20 Block diagram of construction improved faults daignosis

In addition to the previous studied faults, another fault inside battery has been considered in this section. The fault consists of the unusual battery aging, this fault is generated by increasing the internal resistance of the battery in the order of 100 %, 200%, and 300% of its nominal value. Table 4-4 presents the established faults.

Tableau 4-4 Different faults created in simulation environement

Fault Symbol	Description
F1	Short-circuit of PV module.
F2	Open-circuit of PV module.
F3	Battery External Short-circuit.
F4	Battery aging (Increasing of Internal resistance to: 100% , 200% and 300%).

Three neural network types have been explored for improving the fault evaluation process, MLP, PNN network (Probabilistic Neural Network), and RBFN network (Radial Basis function Network). The most efficient network is chosen after a performance comparison of each network.

4.5.3 Structure design

The MLP network used has a three layer (Figure 4.21a), one input layer that have a number of neurons correspond to the power loss parameters. One hidden layer that contains a number of neurons obtained by trial & error and one output layer that correspond to the faults class. The activation function used is tangent sigmoid in the hidden layer and log sigmoid in the output layer. Levenberg-Marquardt with backpropagation algorithm is used to train the MLP [75], [81], [89]. The training criteria used are given by the value of MSE of 10^{-5}, the number of epochs of 1000 and the minimum gradient of 10^{-8}.

The PNN architecture is similar to the MLP (Figure 4.21b), it consists of one input layer that corresponds to the power loss parameters, pattern layer that has the same number of neurons as the input layer. The summation layer that contains a number of neurons equivalent to the class number, in which they calculate the Probability Density Function of each class. The output layer with only one neuron, decide the high probability class [90], [91]. PNN network uses the exponential function as an activation function, whereas, the spread σ of Gaussian function is obtained by trial & error.

The RBFN structure consists simply of one input layer that corresponds to the power loss parameters, one hidden layer with a number of neurons obtained by trial & error. Finally, one output layer that has a number of neurons corresponding to the class number as shown in Figure 4.21c. The kernel function used is Gaussian function computed in each neuron in the hidden layer, in which the mean and variance parameters are computed by the K-means clustering algorithm.

The method pseudo-inverse matrix is used to compute the weights between hidden and output layer [92].

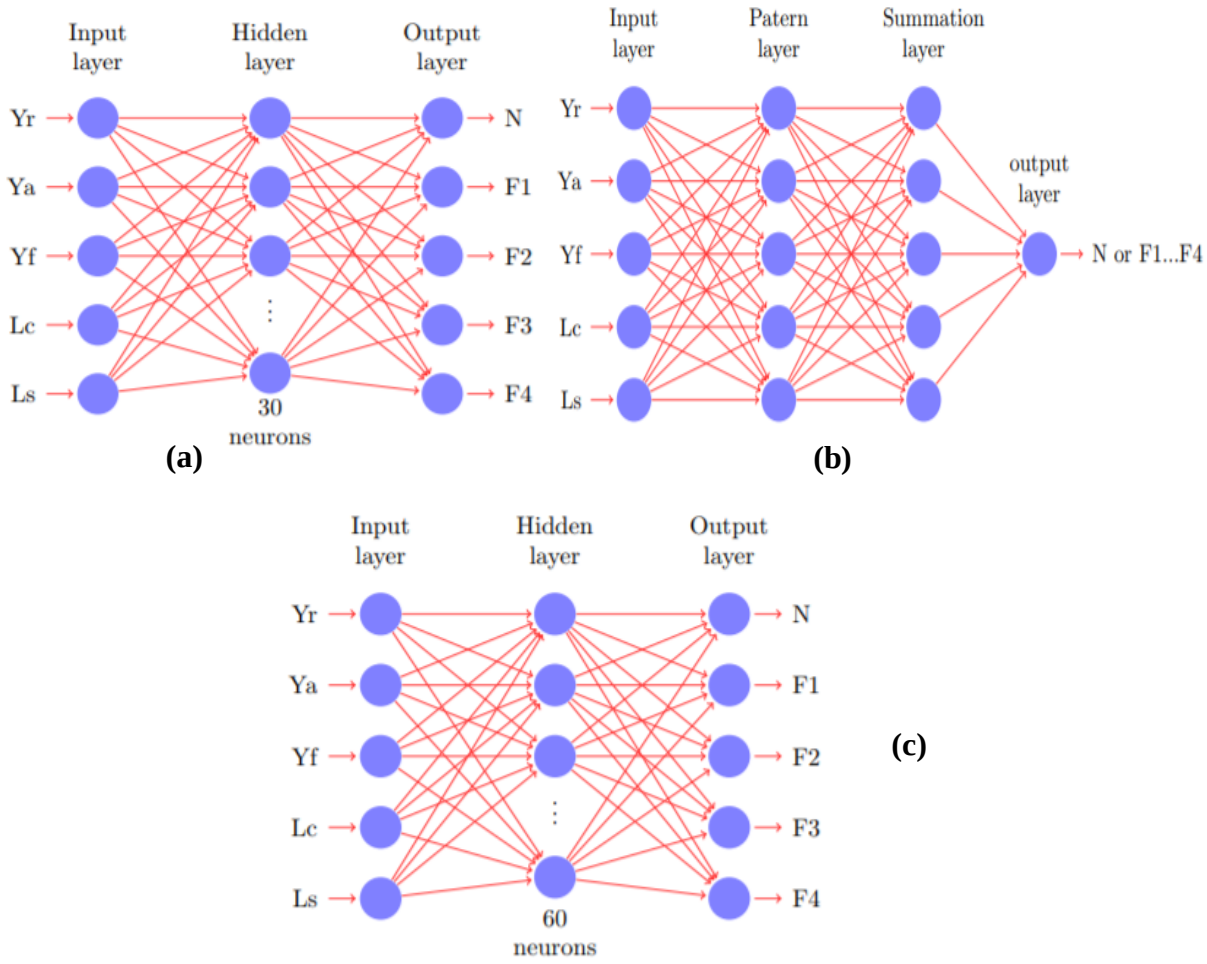


Figure 4.21 ANN structure for : (a) MLP network, (b) PNN network , (c) RBFN network

4.5.4 Network selection

The three network types have been trained and tested using respectively 6727 and 1682 samples. The classification efficiency for each network can be evaluated using the accuracy metric to measure the rate of good classified data, and the prediction quality indices (*PcObs* (*C*) and *Pcpred*(*C*)) metrics [93] defined below.

$$Accuracy = \frac{\neq\ all\ correct\ classified\ Class}{\neq\ all\ data\ class} \times 100 \tag{4.21}$$

$$pcObs(C) = \frac{\neq\ correct\ classified\ Class\ C}{\neq\ observed\ Class\ C\ in\ dataset} \times 100 \tag{4.22}$$

$$pc\,\mathrm{Pr}ed(C) = \frac{\neq\ correct\,classified\,Class\,C}{\neq\ predicted\,Class\,C} \times 100 \qquad (4.23)$$

Predicted (*Pcpred*(*C*)) is the percent of correct classified class C with regard to all predicted class C by ANN.

Observed (*PcObs* (*C*)) is the person of correct classified class C with regard to all observed class C in the data set.

The accuracy results for each network using test data are summarized in Table 4-5. The results indicate that by using MLP architecture, the accuracy achieves 95.9% which is higher than PNN and RBFN. Considering other more fault scenarios, the accuracy of the new trained MLP network could be affected. Nevertheless, the results will not significantly change due to the possibility of obtaining more learning data on related faults.

Tableau 4-5 Test accuracy for MLP, PNN and RBFN network

	MLP	PNN	RBFN
Accuracy (%)	95.9%	76.8%	72.9%

To test the quality of prediction and interpret the obtained accuracy for each network, Figure 4.22, Figure 4.23 and Figure 4.24 shows in a bar graph the correct classified data with respect to observed and predicted (*PcObs* (*C*) and *Pcpred*(*C*)) Class.

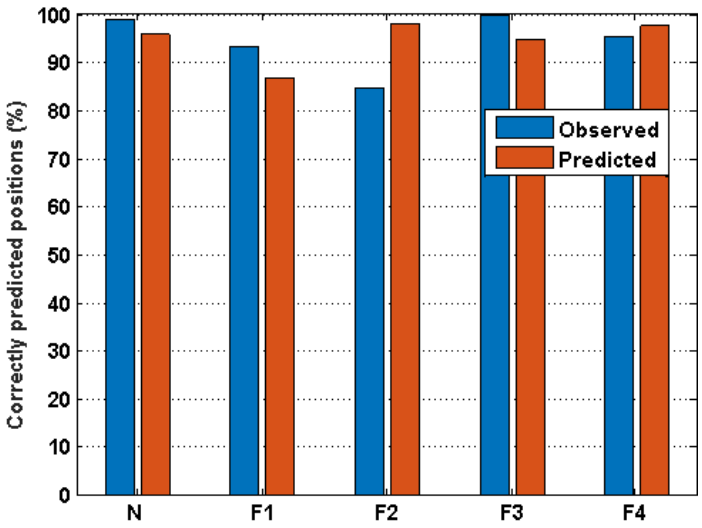


Figure 4.22 Observed, Predicted quality indices for MLP network

Figure 4.22 reveals that by applying the MLP network, the observed and predicted class score more than 85%. These large values justify the best achievable accuracy from the MLP network in Table 4-5. The predicted and observed values are high and close to each other for all classes which increases the MLP chance to properly classify all the faults. However, a little overprediction is noted for the class F2 that has a small influence on the accuracy.

Figure 4.23 shows the results of the predicted and observed class by using PNN, the proportions are about 60% for the class N, F1, and F2 whereas more than 95% for the class F3 and F4. The discrepancy between the two results affects the PNN classification accuracy as given in Table 4-5. The most notable rate of predicted and observed class only lies on one side which leads to an increase in the PNN efficiency to recognize the faults F3 and F4. However, the rest of the faults are not well classified making PNN a partly good classifier.

Figure 4.24 illustrates the results predicted and observed class using RBFN, in which an important difference is noticed (30%) between the percent of observed and predicted for the class F3. The correctly predicted positions are less than 60% of class N, F1, and F2, and reach 0% for the class F4. The results reveal that RBFN has less validity over all the classes compared to MLP and PNN networks.

The results from the test quality indices provide evidence of the inadequacy of PNN and RBFN to identify the faults in the SAPV system. Consequently, the test proves that MLP network is the most accurate to classify all the faults.

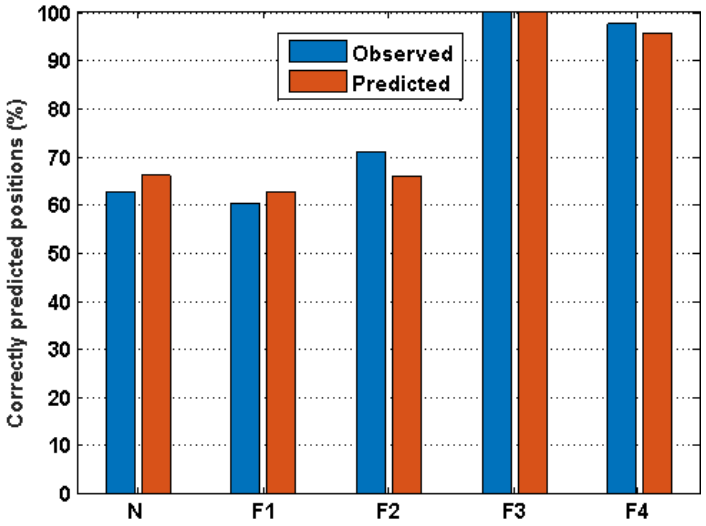


Figure 4.23 Observed, Predicted quality indices for PNN

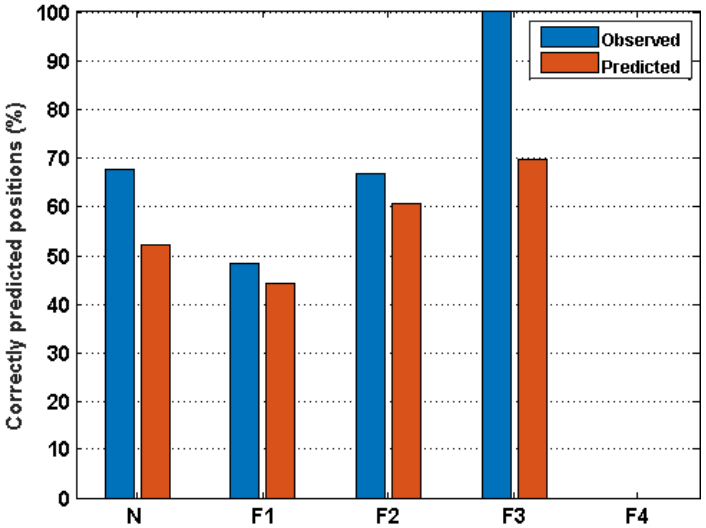


Figure 4.24 Observed, Predicted quality indices for RBFN

4.5.5 Online MLP test

The last test consists to perform some faults in real-time and examine the ability of the best-selected ANN to find these faults in real-time. Noting that, the variation of power loss parameters in real-time due to a failure cannot be appropriately evaluated. However, the trained

ANN fault detection model can determine this abnormality. In this view, some faults have been tested and its class is verified online using simulation fault data.

Figure 4.25 shows the time variation of the Lc parameter and the ANN output in the presence of fault F1. Figure 4.25a illustrates the rise of the simulated Lc curve when the fault F1 occurs and falls when it disappears as illustrated in the shaded region. Figure 4.25b demonstrates that the ANN curve changes according to the fault, in which it rises to F1 and levels off until it disappears. The present test reveals the ability of ANN model to correctly and timely identify the fault F1.

Figure 4.26 shows the variation along time of the Ls parameter and the ANN output when the fault F2 is occurring. Figure 4.26a highlights the change to the simulated Ls curve due to the fault in the shaded region. Figure 4.26b shows the rise of ANN curve to F1 firstly before moving to F2 that maintains it until the fault end. The results indicate that the first sample is misclassified, however, all the rest samples are correctly classified.

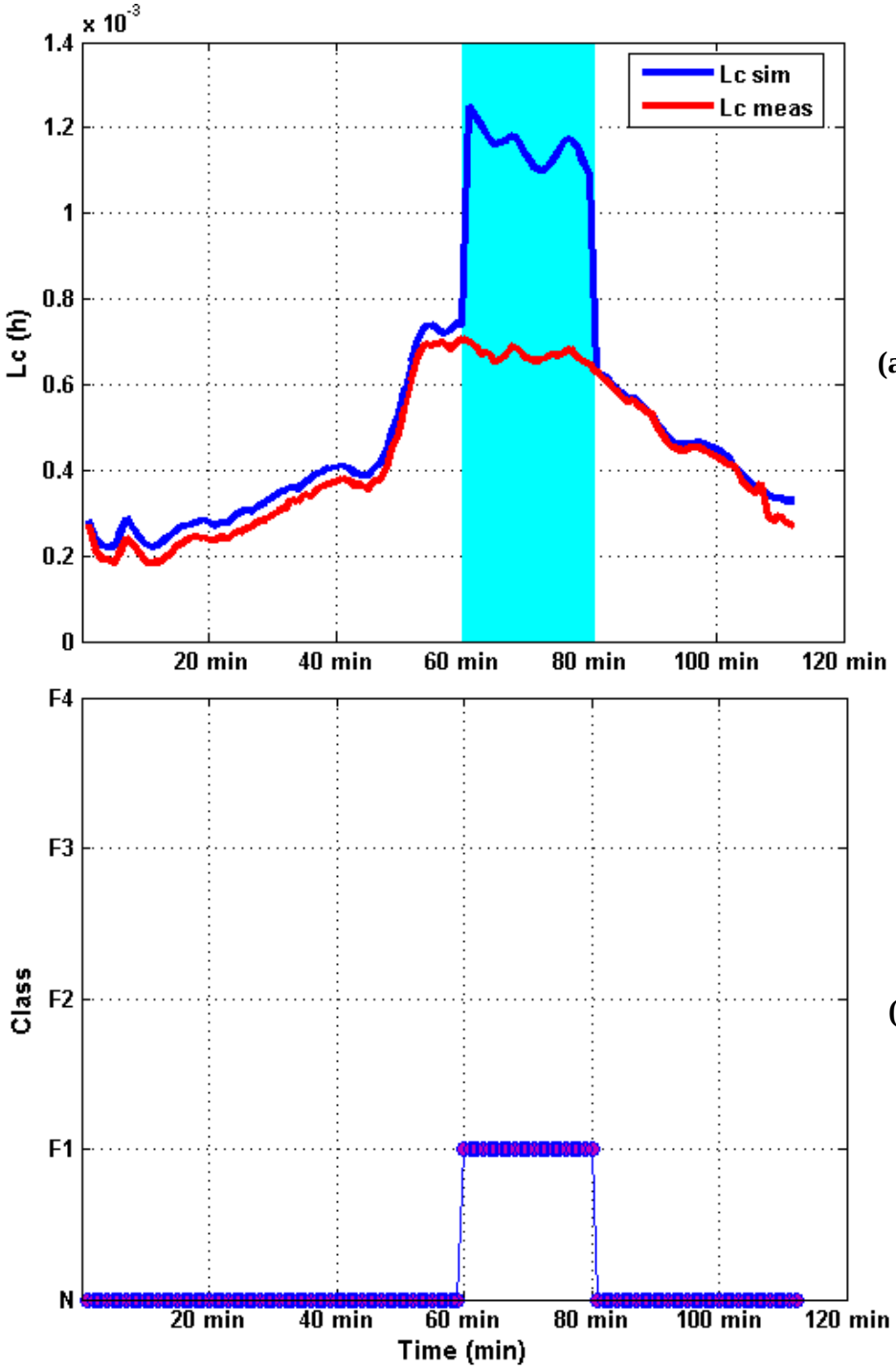


Figure 4.25 Online F1 test (a) Lc variation, (b) ANN output

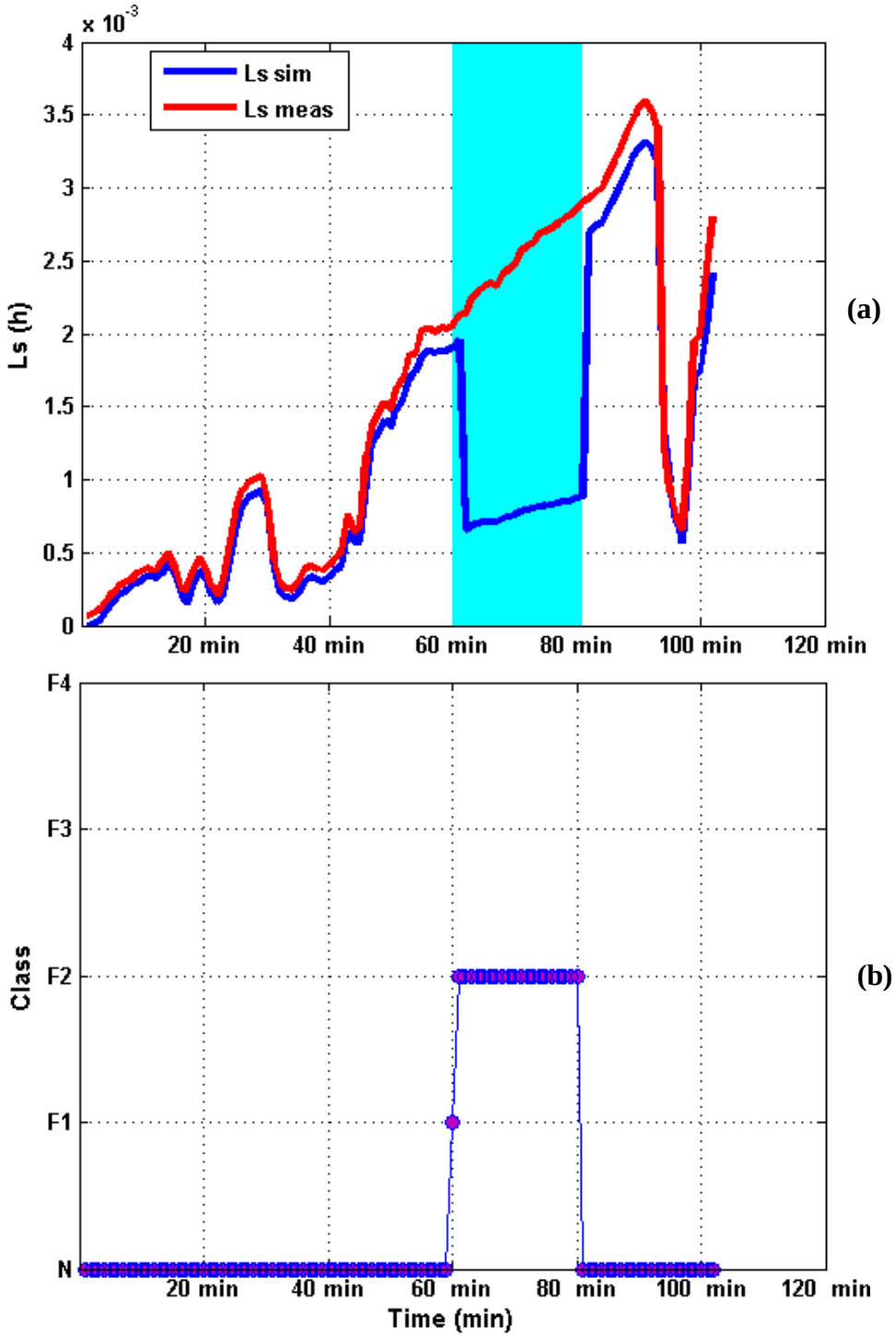


Figure 4.26 Online F2 test (a) Ls variation, (b) ANN output

Figure 4.27 shows the variation in time to the Ls parameter and the ANN response when the fault F3 is developed. Figure 4.27a illustrates the diminish of the Ls parameter during the fault appearance. Figure 4.27b exhibits ANN curve rising to F3 in the shaded region corresponding to the fault. The results from this test clearly show that the fault F3 is properly determined by the trained ANN fault diagnosis model.

The findings from Figure 4.25, Figure 4.26 and Figure 4.27 confirm the ability of the trained ANN model to realize online fault prediction.

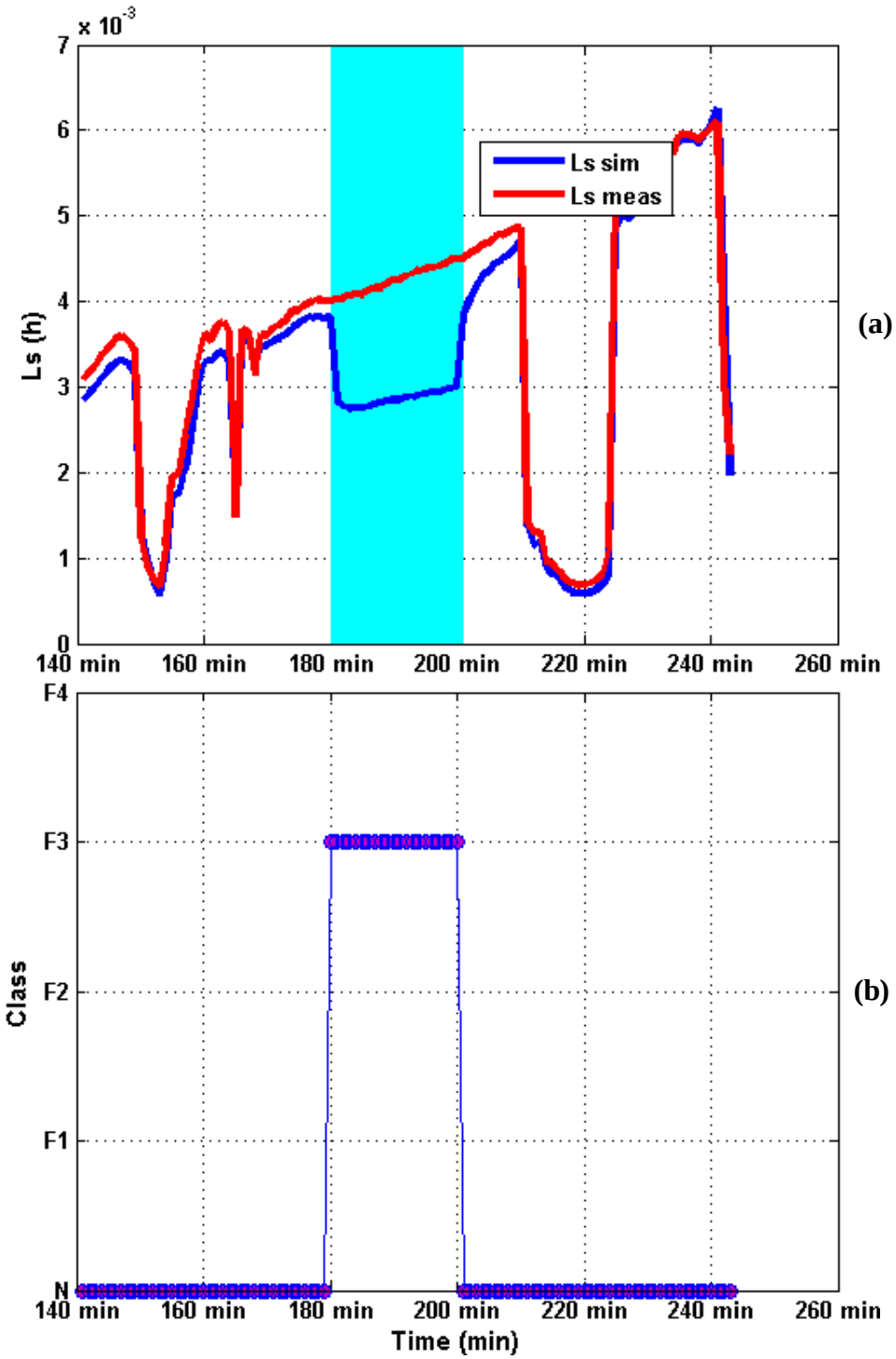


Figure 4.27 Online F3 test (a) Ls variation, (b) ANN output

4.6 Conclusion

This chapter discusses the application of ANN to detect and identify the fault type in the entire SAPV system. First, the fundamental of the ANN approach has been explained in detail, where it is shown that over other training algorithms, BPLM algorithm offers good performance in term of convergence rapidity and precision.

In the second part of the chapter, ANN is directly employed for FDD using SAPV benchmark system data, in which their effectiveness is demonstrated in the separated test set. In addition, a Matlab GUI is created to integrate FDD within the SAPV benchmark system. The proposed method presents the advantages of needing only explicit readily available measurements such as voltage and current to predict the fault. Moreover, the trained ANN could be easily implemented in Hardware (charge regulator) for practical application. However, the supervised ANN method had several drawbacks such as requiring a large amount of learning data that could be difficult to collect in typical fault under real working conditions. Furthermore, the diagnosis is limited to the specified fault in the training.

To overcome the limitations of the previous ANN method as well as the existed fault evaluation using power losses analysis, the last part of the chapter develops new FDD in SAPV system. This new method uses the most relevant power loss parameters and ANN to build-up the FDD, in which the healthy data are gathered from the experimental measurements, while the fault data are obtained from the simulation platform. The improved fault evaluation will bring more security features, accuracy, the generality of ANN fault diagnosis, and save time. Three ANN types have been trained similarly to get the most efficient network, the result reveals that MLP is the most appropriate network to successfully identify the fault. Furthermore, online test monitoring has been realized to check in real-time the effectiveness of the proposed method.

General Conclusion

Nowadays photovoltaic systems are becoming the most popular energy source due mainly to the newly discovered material, improved solar cell efficiency, and reduced cost fabrication. This development of PV panels has driven an increasing interest in the SAPV system as an independent homemade energy source. SAPV system has the advantage to be a silent and free-emission energy source and a good alternative for feeding rural areas, islands, maritime zone, and aerospace applications. However, this system remains without appropriate electrical protection devices, including fuses and circuit breakers.

The fault current in the SAPV system is complicated due to the association of many factors such that the varied environmental condition, fault location, and battery complex internal reactions. As a result, the exact rating of fuse and circuit breaker becomes a pretty complicated task. Faults in the SAPV system have been grouped into two main categories: 1) faults on the PV modules side and 2) faults on the battery side. Both of fault causes a high energy loss and increase the risk of fire hazard and explosion. The main focus of this thesis is to develop efficient fault detection and diagnosis approach for both fault cases.

The data collection under faults and normal operation of the system is quite important to build up the fault diagnosis model. However, the data of fault are hardly and costly obtained from a real SAPV system. To address this issue, an accurate simulation model of the SAPV system is developed under Matlab/Simulink to generate the faulty data. The simulation model is able to take solar irradiance and temperature as inputs to estimate the system output, the model is also flexible to run different fault scenarios in the battery. The simulated output data is tested with the experimental data of the installed SAPV system at CDER, Bouzareah. The irradiance and temperature profile are captured from the CDER site to run the simulation using the same meteorological condition. The results show a good agreement between the simulation and measurement which promotes the study of faults using the developed simulation model.

In order to address the gap in finding the faults in the battery for the photovoltaic system, two machine learning methods have been proposed to supervise the internal short-circuit faults. Anomaly detection has been proposed as fault detection, whereas Support Vector Machine is proposed as fault classification. Both methods present several advantages such that: the high precision and the use of only normal data to train Anomaly detection and a few numbers of fault data to train Support vector machine. The performance of the proposed methods is evaluated using the accuracy metric, in which the results are found to be very accurate for each class. To test the feasibility of the methods to recognize the fault in real-time, several tests are carried out in real-time where the evolution of PDF and the SVM output are plotted separately before and after the

fault occurrence. The monitoring graphs demonstrate the ability of the proposed methods to observe the faults in real-time with some delay that vary greatly with the number of cells infected and the circuit resistance of the fault.

Prediction, investigation, and detection of faults in the whole SAPV system involving PV modules and battery are proposed in the last chapter. Two fundamental approaches of fault detection based on the ANN technique have been introduced in detail, The first fault approach handles experimental data to train and test the ANN FDD. In this case, the ANN input consists of electrical measurements such as voltage and current of PV, battery, and load, in which typical faults experiments have been carried out to extract these measurements under real working conditions. The trained ANN model shows highly accurate results to recognize the fault in test data. The second approach uses simulation and experimental data to train and test the ANN FDD, in which the data of faults are obtained from the simulation, whereas the healthy data are obtained from the experiment. Unlike the first approach, power loss parameters are used as ANN input and three common types of ANN were trained, tested, and compared to choose the most efficient network to predict the faults in the system. The test result reveals that MLP is the most accurate network to recognize the faults, moreover, some fault test has been conducted in real-time to examine their ability to recognize these faults.

Several improvements that result from the introduction of the second approach to detect the fault in the SAPV system: 1) power loss parameters provide relevant information about the losses in the system. 2)The flexibility of obtaining data from the simulation and experimental to build the ANN fault prediction model.3) The high ability to perform real-time monitoring based on power loss parameters and ANN fault prediction.

The findings encourage the application of the proposed method in real-word by an implementation of the ANN into a charge regulator. Also, further research might explore artificial intelligence methods to select the best ANN inputs and other network parameters to allow a more accurate prediction in the SAPV system.

References

[1] IEA-PVPS, *Trends 2018 in Photovoltaics Applications*. 2018.

[2] M. Gaetan, O. Sinead, and R. Manoel, "Global Market Outlook For Solar Power/2018–2022, http://www. solarpowereurope.org/global-market-outlook-2018-2022/ (accessed: Sep 2020).," *EPIA - Eur. Photovolt. Ind. Assoc.*, p. 60, 2018, [Online]. Available: www.africa-eu-renewables.org.

[3] NFPA70, *Article 690-Solar Photovoltaic Systems of National Electrical Code*, Ed. 2011.

[4] R. L. Nailen, "Battery protection-where do we stand?," *IEEE Trans. Ind. Appl.*, vol. 27, no. 4, pp. 658–667, 1991, doi: 10.1109/28.85479.

[5] A. Mellit, G. M. Tina, and S. A. Kalogirou, "Fault detection and diagnosis methods for photovoltaic systems: A review," *Renew. Sustain. Energy Rev.*, vol. 91, pp. 1–17, 2018, doi: https://doi.org/10.1016/j.rser.2018.03.062.

[6] Y. Zhao, "Fault Analysis in Solar Photovoltaic Arrays," Northeastern University, 2010.

[7] D. Stellbogen, "Use of PV circuit simulation for fault detection in PV array fields," in *Conference Record of the Twenty Third IEEE Photovoltaic Specialists Conference - 1993 (Cat. No.93CH3283-9)*, 1993, pp. 1302–1307, doi: 10.1109/PVSC.1993.346931.

[8] M. K. et Al, *Report IEA-PVPS T13-01:2014 "Review of Failures of Photovoltaic Modules."* 2014.

[9] "Corrosion, Shedding and Internal Short - Battery University." https://batteryuniversity.com/learn/article/corrosion_shedding_and_internal_short (accessed Oct. 06, 2019).

[10] "Rising Internal Resistance - Battery University." https://batteryuniversity.com/learn/article/rising_internal_resistance (accessed Aug. 18, 2020).

[11] Thehybridshop.com, "Hybrid Battery Replacement Options."

https://exclusivelyhybrid.com/hybrid-battery-replacement-vs-repair/ (accessed Oct. 14, 2020).

[12] M. A. Munoz, M. C. Alonso-García, N. Vela, and F. Chenlo, "Early degradation of silicon PV modules and guaranty conditions," *Sol. Energy*, vol. 85, no. 9, pp. 2264–2274, 2011, doi: https://doi.org/10.1016/j.solener.2011.06.011.

[13] M. Simón-Martín, A. Diez-Suárez, L.-Á. Prado, A. González-Martínez, Á. de la Puente Gil, and J. Blanes, "Degradation Monitoring of Photovoltaic Plants: Advanced GIS Applications," 2018.

[14] D. Mayer and M. Heidenreich, "Performance analysis of stand alone PV systems from a rational use of energy point of view," *3rd World Conf. Photovolt. Energy Conversion, 2003*, 2003, doi: 10.1109/NPSEC.2005.1532048.

[15] A. Sobirey, H. Riess, and P. Sprau, "Matching factor-a new tool for the assesment of stand-alone systems," *Proceeding Second World Conf. Exhib.*, 1998.

[16] H. Haeberlin and C. Beutler, "Normalized representation of energy and power for analysis of performance and on-line error detection in PV-systems," in *Proc. 13th EU PV Conf., Nice*, 1995, p. 934.

[17] Y. Zhao, "FAULT DETECTION, CLASSIFICATION AND PROTECTION IN SOLAR PHOTOVOLTAIC ARRAYS," 2015.

[18] F. J. Muñoz, G. Almonacid, G. Nofuentes, and F. Almonacid, "A new method based on charge parameters to analyse the performance of stand-alone photovoltaic systems," *Sol. Energy Mater. Sol. Cells*, 2006, doi: 10.1016/j.solmat.2005.10.020.

[19] M. Miwa, S. Yamanaka, H. Kawamura, H. Ohno, and H. Kawamura, "Diagnosis of a Power Output Lowering of PV Array with a (-dI/dV)-V Characteristic," in *2006 IEEE 4th World Conference on Photovoltaic Energy Conference*, 2006, vol. 2, pp. 2442–2445, doi: 10.1109/WCPEC.2006.279703.

[20] A. Abete, E. Barbisio, F. Cane, and P. Demartini, "Analysis of photovoltaic modules with protection diodes in presence of mismatching," in *IEEE Conference on Photovoltaic Specialists*, 1990, pp. 1005–1010 vol.2, doi: 10.1109/PVSC.1990.111769.

[21] P. Hernday, "Field Applications for I-V Curve Tracers," *SolarPro Magazine*, no.

4.5, pp. 77–106, 2011.

[22] S. K. Firth, K. J. Lomas, and S. J. Rees, “A simple model of PV system performance and its use in fault detection,” *Sol. Energy*, vol. 84, no. 4, pp. 624–635, 2010, doi: https://doi.org/10.1016/j.solener.2009.08.004.

[23] A. Drews *et al.*, “Monitoring and remote failure detection of grid-connected PV systems based on satellite observations,” *Sol. Energy*, vol. 81, no. 4, pp. 548–564, 2007, doi: https://doi.org/10.1016/j.solener.2006.06.019.

[24] “International standard IEC 61724: Photovoltaic system performance monitoring{Guidelines for measurements, data exchange and analysis,” 1998.

[25] B. Marion *et al.*, “Performance parameters for grid-connected PV systems,” in *Conference Record of the Thirty-first IEEE Photovoltaic Specialists Conference, 2005.*, 2005, pp. 1601–1606, doi: 10.1109/PVSC.2005.1488451.

[26] A. Chouder and S. Silvestre, “Automatic supervision and fault detection of PV systems based on power losses analysis,” *Energy Convers. Manag.*, vol. 51, no. 10, pp. 1929–1937, 2010, doi: https://doi.org/10.1016/j.enconman.2010.02.025.

[27] L. Schirone, F. P. Califano, U. Moschella, and U. Rocca, “Fault finding in a 1 MW photovoltaic plant by reflectometry,” in *Proceedings of 1994 IEEE 1st World Conference on Photovoltaic Energy Conversion - WCPEC (A Joint Conference of PVSC, PVSEC and PSEC)*, 1994, vol. 1, pp. 846–849 vol.1, doi: 10.1109/WCPEC.1994.520093.

[28] T. Takashima, J. Yamaguchi, K. Otani, T. Oozeki, K. Kato, and M. Ishida, “Experimental studies of fault location in PV module strings,” *Sol. Energy Mater. Sol. Cells*, vol. 93, no. 6, pp. 1079–1082, 2009, doi: https://doi.org/10.1016/j.solmat.2008.11.060.

[29] T. Takashima, J. Yamaguchi, K. Otani, K. Kato, and M. Ishida, “Experimental Studies of Failure Detection Methods in PV Module Strings,” in *2006 IEEE 4th World Conference on Photovoltaic Energy Conference*, 2006, vol. 2, pp. 2227–2230, doi: 10.1109/WCPEC.2006.279952.

[30] C. Cepisca and A. Florin, *ANCUTA,F, CEPISCA,C , Failure Analysis Capabilities for PV Systems*. 2011.

[31] L. Bun, “Détection et localisation de défauts dans un système photovoltaïque,” 2011.

[32] D. Sera, R. Teodorescu, and P. Rodriguez, “Photovoltaic module diagnostics by series resistance monitoring and temperature and rated power estimation,” in *2008 34th Annual Conference of IEEE Industrial Electronics*, 2008, pp. 2195–2199, doi: 10.1109/IECON.2008.4758297.

[33] D. D. Nguyen, B. Lehman, and S. Kamarthi, “Performance evaluation of solar photovoltaic arrays including shadow effects using neural network,” in *2009 IEEE Energy Conversion Congress and Exposition*, 2009, pp. 3357–3362, doi: 10.1109/ECCE.2009.5316451.

[34] D. Riley and J. Johnson, “Photovoltaic prognostics and heath management using learning algorithms,” in *2012 38th IEEE Photovoltaic Specialists Conference*, 2012, pp. 1535–1539, doi: 10.1109/PVSC.2012.6317887.

[35] Syafaruddin, E. Karatepe, and T. Hiyama, “Controlling of artificial neural network for fault diagnosis of photovoltaic array,” in *2011 16th International Conference on Intelligent System Applications to Power Systems*, 2011, pp. 1–6, doi: 10.1109/ISAP.2011.6082219.

[36] A. Massi Pavan, A. Mellit, D. De Pieri, and S. A. Kalogirou, “A comparison between BNN and regression polynomial methods for the evaluation of the effect of soiling in large scale photovoltaic plants,” *Appl. Energy*, vol. 108, pp. 392–401, 2013, doi: https://doi.org/10.1016/j.apenergy.2013.03.023.

[37] Y. Zhao, L. Yang, B. Lehman, J. de Palma, J. Mosesian, and R. Lyons, “Decision tree-based fault detection and classification in solar photovoltaic arrays,” in *2012 Twenty-Seventh Annual IEEE Applied Power Electronics Conference and Exposition (APEC)*, 2012, pp. 93–99, doi: 10.1109/APEC.2012.6165803.

[38] B. Hu, “Solar Panel Anomaly Detection and Classification.” UWSpace, 2012, [Online]. Available: http://hdl.handle.net/10012/6731.

[39] S. Vergura, G. Acciani, V. Amoruso, G. E. Patrono, and F. Vacca, “Descriptive and Inferential Statistics for Supervising and Monitoring the Operation of PV Plants,” *IEEE Trans. Ind. Electron.*, vol. 56, no. 11, pp. 4456–4464, 2009, doi: 10.1109/TIE.2008.927404.

[40] A. Luque and S. Hegedus, “Handbook of Photovoltaic Science and Engineering,” *John Wiley Sons, Ltd*, pp. 92–100, Jan. 2003.

[41] M. Kim and E. Hwang, “Monitoring the battery status for photovoltaic systems,” *J. Power Sources*, 1997, doi: 10.1016/S0378-7753(96)02521-9.

[42] B. Caroline, *A user guide to simple monitoring and sustainable operation of PV-diesel hybrid systems*, Report IEA. IEA, 2015.

[43] M. Tadj, K. Benmouiza, and A. Cheknane, “An innovative method based on satellite image analysis to check fault in a PV system lead-acid battery,” *Simul. Model. Pract. Theory*, 2014, doi: 10.1016/j.simpat.2014.06.010.

[44] Sandia, *Stand-Alone Photovoltaic Systems: A Handbook of Recommended Design Practices*, Sandia Nat. Albuquerque, New Mexico, 1995.

[45] V. Salas, *Stand-alone photovoltaic systems*. Elsevier Ltd., 2016.

[46] A. Keyhani, *Design of smart power grid renewable energy systems*. John Wiley & Sons, 2011.

[47] J. C. Wiles and D. L. King, “Blocking diodes and fuses in low-voltage PV systems,” 2002, pp. 1105–1108, doi: 10.1109/pvsc.1997.654281.

[48] Sandia, *Stand-Alone Photovoltaic Systems: A Handbook of Recommended Design Practices*. Albuquerque, New Mexico: Sandia National Laboratories, 1995.

[49] L. Castaner, S. Silvestre, and L. Castaaner, *Modelling photovoltaic systems using PSpice*. Wiley Online Library, 2002.

[50] X. Luo, J. Wang, M. Dooner, and J. Clarke, “Overview of current development in electrical energy storage technologies and the application potential in power system operation,” *Appl. Energy*, vol. 137, pp. 511–536, Jan. 2015, doi: 10.1016/J.APENERGY.2014.09.081.

[51] E. Koutroulis and K. Kalaitzakis, “Novel battery charging regulation system for photovoltaic applications,” *IEE Proc. - Electr. Power Appl.*, vol. 151, no. 2, pp. 191–197, 2004, doi: 10.1049/ip-epa:20040219.

[52] D. Spiers, “IIB-2 – Batteries in PV Systems,” in *Practical Handbook of Photovoltaics*, Second Edi., Elsevier Ltd, 2012, pp. 721–776.

[53] M. Walid, “Développement d’un régulateur intelligent pour un système PV de faible puissance,” Polytechnical school, Algeria, 2011.

[54] J. R. Woodworth, M. G. Thomas, J. W. Stevens, S. R. Harrington, J. P. Dunlop, and M. Ramu Swamy, “Evaluation of the batteries and charge controllers in small stand-alone photovoltaic systems,” 2002, doi: 10.1109/wcpec.1994.520115.

[55] A. Luque and S. Hegedus, *Handbook of Photovoltaic Science and Engineering*. 2011.

[56] M. G. Villalva, J. R. Gazoli, and E. R. Filho, “Comprehensive approach to modeling and simulation of photovoltaic arrays,” *IEEE Trans. Power Electron.*, 2009, doi: 10.1109/TPEL.2009.2013862.

[57] Y. Mahmoud, W. Xiao, and H. H. Zeineldin, “A simple approach to modeling and simulation of photovoltaic modules,” *IEEE Trans. Sustain. Energy*, 2012, doi: 10.1109/TSTE.2011.2170776.

[58] B. Anderson and R. Anderson, *Fundamentals of Semiconductor Devices*, 1st ed. New York, NY, USA: McGraw-Hill, Inc., 2005.

[59] M. A. Casacca and Z. M. Salameh, “Determination of lead-acid battery capacity via mathematical modeling techniques,” *IEEE Trans. Energy Convers.*, vol. 7, no. 3, pp. 442–446, 1992, doi: 10.1109/60.148564.

[60] O. Tremblay and L. A. Dessaint, “Experimental validation of a battery dynamic model for EV applications,” *World Electr. Veh. J.*, 2009.

[61] N. Thi Minh Phuong, “LEAD ACID BATTERIES IN EXTREME CONDITIONS: ACCELERATED CHARGE, MAINTAINING THE CHARGE WITH IMPOSED LOW CURRENT, POLARITY INVERSIONS INTRODUCING NON-CONVENTIONAL CHARGE METHODS.,” Université Montpellier II -, 2009.

[62] A. Purarjomandlangrudi, A. H. Ghapanchi, and M. Esmalifalak, “A data mining approach for fault diagnosis: An application of anomaly detection algorithm,” *Measurement*, vol. 55, pp. 343–352, 2014, doi: https://doi.org/10.1016/j.measurement.2014.05.029.

[63] Y. Zhao, B. Lehman, R. Ball, J. Mosesian, and J. de Palma, “Outlier detection rules for fault detection in solar photovoltaic arrays,” in *2013 Twenty-Eighth Annual*

IEEE Applied Power Electronics Conference and Exposition (APEC), 2013, pp. 2913–2920, doi: 10.1109/APEC.2013.6520712.

[64] Y. Zhao, F. Balboni, T. Arnaud, J. Mosesian, R. Ball, and B. Lehman, "Fault experiments in a commercial-scale PV laboratory and fault detection using local outlier factor," in *2014 IEEE 40th Photovoltaic Specialist Conference (PVSC)*, 2014, pp. 3398–3403, doi: 10.1109/PVSC.2014.6925661.

[65] S. Marsland, "Novelty Detection in Learning Systems," *Neural Comp. Surv.*, 2003.

[66] M. Markou and S. Singh, "Novelty detection: a review—part 1: statistical approaches," *Signal Processing*, vol. 83, no. 12, pp. 2481–2497, 2003, doi: https://doi.org/10.1016/j.sigpro.2003.07.018.

[67] A. Widodo and B.-S. Yang, "Support vector machine in machine condition monitoring and fault diagnosis," *Mech. Syst. Signal Process.*, vol. 21, no. 6, pp. 2560–2574, 2007, doi: https://doi.org/10.1016/j.ymssp.2006.12.007.

[68] L. Ren, W. Lv, S. Jiang, and Y. Xiao, "Fault Diagnosis Using a Joint Model Based on Sparse Representation and SVM," *IEEE Trans. Instrum. Meas.*, vol. 65, no. 10, pp. 2313–2320, 2016, doi: 10.1109/TIM.2016.2575318.

[69] D. You, X. Gao, and S. Katayama, "WPD-PCA-Based Laser Welding Process Monitoring and Defects Diagnosis by Using FNN and SVM," *IEEE Trans. Ind. Electron.*, vol. 62, no. 1, pp. 628–636, 2015, doi: 10.1109/TIE.2014.2319216.

[70] W. Rezgui, L. H. Mouss, N. K. Mouss, M. D. Mouss, and M. Benbouzid, "A smart algorithm for the diagnosis of short-circuit faults in a photovoltaic generator," in *2014 First International Conference on Green Energy ICGE 2014*, 2014, pp. 139–143, doi: 10.1109/ICGE.2014.6835412.

[71] Z. Li *et al.*, "Online implementation of SVM based fault diagnosis strategy for PEMFC systems," *Appl. Energy*, vol. 164, pp. 284–293, 2016, doi: https://doi.org/10.1016/j.apenergy.2015.11.060.

[72] J. Platt, "Sequential Minimal Optimization: A Fast Algorithm for Training Support Vector Machines," *Adv. Kernel Methods-Support Vector Learn.*, vol. 208, Jul. 1998.

[73] W. S. McCulloch and W. Pitts, "A logical calculus of the ideas immanent in nervous activity," *Bull. Math. Biophys.*, vol. 5, no. 4, pp. 115–133, 1943, doi:

10.1007/BF02478259.

[74] F. Rosenblatt, “The Perceptron: A Probabilistic Model for Information Storage and Organization in The Brain,” *Psychol. Rev.*, pp. 65–386, 1958.

[75] R. P. Lippmann, “An Introduction to Computing with Neural Nets,” *IEEE ASSP Mag.*, 1987, doi: 10.1109/MASSP.1987.1165576.

[76] D. E, J. Mcclelland, and J. L, *Parallel distributed processing: explorations in the microstructure of cognition. Volume 1. Foundations*. 1986.

[77] M. A. Arbib, Ed., *The Handbook of Brain Theory and Neural Networks*, 2nd editio. Madison, wisconsin, 2002.

[78] Y. Murayama, *Progress in geospatial analysis*. 2014.

[79] M. T. Hagan, H. B. Demuth, and M. H. Beale, *Neural Network Design*, 1st ed. USA: PWS Pub, Boston, 1996.

[80] S. Haykin, *Neural networks: a comprehensive foundation*. 1994.

[81] M. T. Hagan and M. B. Menhaj, “Training Feedforward Networks with the Marquardt Algorithm,” *IEEE Trans. Neural Networks*, 1994, doi: 10.1109/72.329697.

[82] R. Isermann, *Fault Diagnosis Systems An Introduction from Fault Detection to Fault Tolerance*. 2006.

[83] A. Rusiecki, M. Kordos, T. Kamiński, and K. Greń, “Training Neural Networks on Noisy Data,” in *Artificial Intelligence and Soft Computing*, 2014, pp. 131–142.

[84] B. Li, C. Delpha, D. Diallo, and A. Migan-Dubois, “Application of Artificial Neural Networks to photovoltaic fault detection and diagnosis: A review,” *Renew. Sustain. Energy Rev.*, p. 110512, 2020, doi: https://doi.org/10.1016/j.rser.2020.110512.

[85] W. Chine, A. Mellit, V. Lughi, A. Malek, G. Sulligoi, and A. Massi Pavan, “A novel fault diagnosis technique for photovoltaic systems based on artificial neural networks,” *Renew. Energy*, vol. 90, pp. 501–512, 2016, doi: https://doi.org/10.1016/j.renene.2016.01.036.

[86] Y. Wu, Q. Lan, and Y. Sun, “Application of BP neural network fault diagnosis in solar photovoltaic system,” in *2009 International Conference on Mechatronics and*

Automation, 2009, pp. 2581–2585, doi: 10.1109/ICMA.2009.5246742.

[87] Z. Li, Y. Wang, D. Zhou, and C. Wu, "An Intelligent Method for Fault Diagnosis in Photovoltaic Array BT - System Simulation and Scientific Computing," 2012, pp. 10–16.

[88] X. Li, P. Yang, J. Ni, and J. Zhao, "Fault diagnostic method for PV array based on improved wavelet neural network algorithm," in *Proceeding of the 11th World Congress on Intelligent Control and Automation*, 2014, pp. 1171–1175, doi: 10.1109/WCICA.2014.7052884.

[89] M. T. Hagan, H. B. Demuth, and M. H. Bealen, *Neural Network Design*. 1996.

[90] D. F. Specht, "Probabilistic neural networks for classification, mapping, or associative memory," vol. 1, pp. 525–532, 2003, doi: 10.1109/icnn.1988.23887.

[91] D. F. Specht, "Probabilistic Neural Networks and the Polynomial Adaline as Complementary Techniques for Classification," *IEEE Trans. Neural Networks*, 1990, doi: 10.1109/72.80210.

[92] J. A. Leonard and M. A. Kramer, "Radial Basis Function Networks for Classifying Process Faults," *IEEE Control Syst.*, 1991, doi: 10.1109/37.75576.

[93] W. Kabsch and C. Sander, "How good are predictions of protein secondary structure?," *FEBS Letters*. 1983, doi: 10.1016/0014-5793(82)80597-8.

Lists of Publications and Conference papers

[P1] **N.Sabri, A.Tlemçani**, **and A.Chouder,** "REAL-TIME DIAGNOSIS OF BATTERY CELLS FOR STAND-ALONE PHOTOVOLTAIC SYSTEM USING MACHINE LEARNING TECHNIQUES", **Revue Roumaine Des Sciences Techniques –Serie Électrotechnique et Énergétique**, vol.66, no.2, pp.105-110, **2021**.

[P2] **N.Sabri, A.Tlemçani, and A.Chouder,** "Battery Internal Fault Monitoring Based on Anomaly Detection Algorithm", **in Advanced Statistical Modeling, Forecasting, and Fault Detection in Renewable Energy Systems,** IntechOpen, **2020**.

[P3] **A.Djalab, M.M.Rezaoui, L.Mazouz, A.Teta, N.Sabri,** "Robust Method for Diagnosis and Detection of Faults in Photovoltaic Systems Using ArtificialNeural Networks", **Periodica Polytechnica Electrical Engineering and Computer Science,** vol.64, no.3, **2020**.

[C1] **N.Sabri**, A.Tlemçani, and A.Chouder, "Faults diagnosis in Stand-Alone photovoltaic system using Artificial Neural Network", **in 2018 6th International Conference on Control Engineering & Information Technology (CEIT)**, pp.1-6, **Istanbul, 2018**.

[C2] **N.Sabri**, A.Tlemçani, and A.Chouder, "Monitoring Tool for Stand-Alone Photovoltaic System Using Artificial Neural Network", **in International Conference in Artificial Intelligence in Renewable Energetic Systems (ICAIRES)**, pp.114-121, **Tipaza, 2018**.

[C3] **N.Sabri**, A.Tlemçani, and A.Chouder, "Intelligent fault supervisory system applied on stand-alone photovoltaic system", **in 2018 International Conference on Applied Smart Systems (ICASS), Médéa, 2018**.

[C4] **N.Sabri,** A.Tlemçani, and A.Chouder, "Internal faults detection of solar battery using anomaly detection algorithm", **in the 2nd International Conference on Applied Automation and Industrial Diagnostics (ICAAID), Djelfa, 2017.**

[C5] A.Djalab, **N.Sabri**, and A.Teta, "Maximum Power Point Tracking (MPPT) for a PV System Based on Artificial Neural Network ANN and Comparison with P&O Algorithm", **in the Fourth International Conference on Electrical Engineering and Control**

Applications (ICEECA), Constantine, 2019.

[C6] A.Djalab, A.Hafaifa, M.M.Rezaoui, A.Teta, and **N.Sabri**, "An Intelligent Faults Diagnosis and Detection Method Based an Artificial Neural Networks for Photovoltaic Array", **in the 3rd International Conference on Applied Automation and Industrial Diagnostics, (ICAAID), Elazig, 2019**.